The Structure of Self-Excited Nonlinear Density Waves in Dusty Plasmas Under Microgravity Conditions

Dissertation
zur Erlangung des Doktorgrades
der Mathematisch-Naturwissenschaftlichen Fakultät
der Christian-Albrechts-Universität zu Kiel

vorgelegt von
Kristoffer Ole Menzel

Kiel
März 2011

Referent: . . . .   Prof. Dr. A. Piel
Korreferent: . . . .   Prof. Dr. R. Wimmer-Schweingruber
Tag der mündlichen Prüfung: . . .   13. Mai 2011
Zum Druck genehmigt: Kiel, den   13. Mai 2011

Der Dekan

Für Tine und Jonte. Für Eure unendliche Liebe.

Kurzfassung

In dieser Dissertation werden Dichtewellen in einem ausgedehnten dreidimensionalen staubigen Plasma unter Schwerelosigkeit in einer Hochfrequenzentladung untersucht. Die Wellen treten bei niedrigen Neutralgasdrücken und hohen Staubdichten in Gegenwart strömender Ionen spontan auf. Sie sind zumeist nichtlinear und das Wellenfeld besitzt eine komplizierte Struktur, die sich beispielsweise durch das Auftreten von sogenannten topologischen Defekten, d.h. Orten, an denen sich Wellenfronten aufteilen oder vereinigen, bemerkbar macht. Ziel der Arbeit ist es, diese raum-zeitliche Struktur der Wellen detailliert zu untersuchen. Die etablierten Methoden, wie z.B. die Fourier-Analyse, sind dafür jedoch aufgrund des transienten Verhaltens der Wellen nur bedingt geeignet. Basierend auf der Hilbert-Transformation ist daher ein neues Verfahren eingeführt worden, welches eine Analyse auf unterschiedlichen, frei wählbaren Zeitskalen erlaubt. Mit dieser Methode lassen sich insbesondere instantane Größen, wie beispielsweise Phase und instantane Frequenz der Welle, definieren. So kann das Wellenfeld für jeden aufgenommenen Zeitschritt rekonstruiert und Position und Bewegung der Defekte bestimmt werden. Außerdem ist es durch eine zeitliche Mittelung der instantanen Größen möglich, die globalen Welleneigenschaften zu untersuchen.

In dieser Arbeit wird primär die räumliche Frequenzverteilung der Wellen untersucht. Dabei zeigt sich, dass die Frequenz in den meisten Fällen räumlich variiert. Überraschenderweise erfolgt der beobachtete Abfall nicht stetig. Stattdessen sind sogenannte Frequenzcluster entdeckt worden. Dies sind Bereiche annähernd konstanter Frequenz, die durch abrupte Frequenzsprünge voneinander getrennt sind. Eine solche Beobachtung wurde in staubigen Plasmen zuvor nicht gemacht. Sie ist nicht mit dem linearen Wellenbild nach Huygens vereinbar, welches lediglich eine variable Wellenlänge zulässt. Weiterhin stellt sich heraus, dass die beiden analysierten Phänomene – Defekte und Frequenzcluster – nicht getrennt voneinander zu beobachten sind. Sie sind vielmehr eng miteinander verknüpft, da sich die Defekte fast ausschließlich entlang der Clustergrenzen bewegen. Eine detaillierte Analyse der instantanen Frequenz gibt ferner Hinweise auf eine unvollständige Synchronisation an den Clustergrenzen, wie es für isolierte, getriebene van-der-Pol Oszillatoren bekannt ist. Dieses Resultat und ein Vergleich der experimentellen Befunde mit numerischen Studien legen nahe, die Wellen als ein System gekoppelter selbsterregter van-der-Pol Oszillatoren zu modellieren. Dafür werden in dieser Arbeit komplementäre numerische Untersuchungen durchgeführt, die insbesondere das Verhalten der Oszillatoren an den Clustergrenzen umfassen. Es zeigt sich, dass sich die Oszillatoren dort gegenseitig durch sogenanntes Frequency-Pulling beeinflussen.

Die Ergebnisse dieser Arbeit führen zu einem modifizierten Bild der Staubdichtewellen, welches die Staubwolke als ein Ensemble miteinander wechselwirkender nichtlinearer und selbsterregter Oszillatoren ansieht, das das instabile, gesättigte Wellenfeld repräsentiert.

Abstract

In this thesis, dust-density waves are investigated in an extended three-dimensional dusty plasma under microgravity conditions in a radio-frequency discharge. The waves emerge spontaneously at low neutral gas pressures and high dust densities in the presence of streaming ions. They are often nonlinear and the wave field comprises a complicated structure, which is reflected, e.g., in the appearance of so-called topological defects, i.e., locations of splitting or merging wave fronts. The aim of the work is to examine this spatio-temporal structure of the waves in detail. For this, the established methods like, e.g., the Fourier analysis are only suitable to a limited extent due to the transient behavior of the waves. Thus, based on the Hilbert transform, a new workflow has been introduced, which allows to analyze the waves on different, individually chosen time scales. In particular, the method can be used to define instantaneous quantities such as the phase or the instantaneous frequency of the wave. With this, the wave field can be reconstructed at each recorded time step and the position and motion of the defects can be determined. Moreover, it is possible to investigate the global wave properties by averaging the instantaneous quantities temporally.

In this work, the spatial frequency distribution of the waves is investigated primarily. It turns out that in most cases the frequency varies in space. Surprisingly, the observed decrease is not constant. Instead, so-called frequency clusters have been discovered. These are regions of almost constant frequency, which are separated by abrupt frequency jumps. Such an observation was not made so far in the field of dusty plasmas. It is not compatible with Huygens' linear wave theory, which involves a constant frequency but a varying wavelength. Furthermore, it has been found that both analyzed phenomena —defects and frequency clusters— cannot be observed independently. Rather, they are closely related to each other since the defects move almost exclusively along the cluster boundaries. A detailed analysis of the instantaneous frequency further reveals hints for an incomplete synchronization at the cluster boundaries as it is typical for isolated driven van-der-Pol oscillators. This result and a comparison with numerical studies suggest to model the waves as a system of coupled self-sustained van-der-Pol oscillators. For this purpose, complementary numerical investigations are realized within the scope of this work, which in particular include the behavior of the oscillators at the cluster boundaries. There, it is found that the oscillators affect each other in terms of so-called frequency pulling.

The results of this thesis lead to a modified picture of dust-density waves, which treats the dust cloud as an ensemble of mutually interacting nonlinear self-sustained oscillators that represents the unstable saturated wave field.

Contents

1 Introduction

A wave is the ubiquitous answer of nature to a perturbation of an otherwise stable system. If the observed system is far from equilibrium, nonlinear waves may occur [1–3]. They are found in everyday life, for instance, as shallow water waves [4], as stop-and-go waves in traffic jams [5] or as transmission of nerve impulses [6]. Nonlinear waves are characterized by the interplay of input energy, dissipation, dispersion and the degree of nonlinearity. They can be excited in different ways. Water waves, for example, can be generated by a single disturbance such as a stone thrown into the water or by means of a periodic force inside a ripple tank [7]. In both cases, the excitation is spatially and temporally localized and one speaks of externally driven waves. However, waves can also emerge in the presence of a global energy source. This is the case for water waves in the ocean, which are fed by the wind blowing over the water surface [4], or for waves in thin fluid layers of ethanol-water mixtures [8], where convection takes place. If the energy source is an intrinsic component of the considered system, the waves are called self-excited.

A complex nonlinear system is the plasma, i.e., an ionized gas consisting of electrons, ions and neutrals. It comprises a multitude of different wave types due to the complicated interaction between the components. A prominent feature of nonlinear systems is synchronization [9, 10], i.e., the mutual adjustment of rhythms between coupled independent oscillators, which is already known since the famous observation of coupled pendulum clocks by Huygens [11]. It is also a well-known feature in plasmas. There, the so-called van-der-Pol oscillator [12] has reached a paradigmatic character for studying synchronization processes. It was applied to numerous externally driven instabilities as, for instance, in gas discharges [13, 14], thermionic diodes [15], weakly magnetized discharges [16, 17] or to drift waves [18, 19]. Moreover, van-der-Pol behavior was observed in self-sustained systems [20, 21].

A unique laboratory for the investigations of dynamic phenomena in strongly coupled systems is the dusty or complex plasma. Besides the species of a classical plasma, it contains a fourth component, namely macroscopic solid particles, the so-called dust. These particles are nanometer up to micrometer in size, and compared to the ions very heavy. This makes the dynamics of a dusty plasma slow with characteristic frequencies of a few ten to hundred Hertz. The particles are highly charged and interact via a screened Coulomb potential (also called Debye-Hückel or Yukawa potential). Typical interparticle distances are a few hundred microns. Consequently, the system is almost transparent and easy to observe by means of standard video cameras.

Interest in dusty plasmas arose from two different sides as it occurs naturally in the interstellar medium [22–24] and also in industrial process plasmas [25, 26]. Dusty plasmas became an independent field of research at latest in 1994 with the discovery

of crystalline structures, so-called Coulomb solids [27–31], which offer a variety of interesting features, such as melting [31–34] or wave motion [35–37]. The coupling strength between the particles can be controlled over a wide range by adjusting the neutral gas pressure, and thus the dust cloud can reside in the solid, liquid or gaseous phase.

In the following two decades much effort on both sides, theoretical and experimental, was spent on dusty plasmas. Nowadays, challenging issues are studied on a fundamental research level, such as drift waves in magnetized dusty plasmas [38], supersonic projectiles in the presence of streaming ions [39] or spatially extended three-dimensional particle clouds in laboratory rf discharges [40]. For the industry, dust became of interest in fusion devices [41–43].

In the laboratory, dusty plasmas are produced either in direct-current (dc) glow discharges or in radio-frequency (rf) plasmas. In the latter case, the particles sediment into the sheath region due to gravity. Extended three-dimensional particle clouds form either if gravity is compensated by means of additional forces [40, 44] or if nanometer sized particles are used [45, 46] and gravity can be neglected. Moreover, experiments can be performed under weightlessness on sounding rockets [47], aboard the ISS [48–53] or under microgravity conditions on parabolic flights [54–57].

In a dusty plasma, waves can be observed in each of the three phases. Two fundamental wave types are of interest. First, this are waves in crystalline structures, where the potential energy of the particles is large compared to their kinetic energy. Such waves are dominated by the interaction of adjacent particles and appear as dust lattice waves [35–37, 58, 59], Mach cones [60–62] or shear waves [63–67]. They are usually generated by means of an external driver. If the kinetic energy of the particles increases, the dusty plasma resides in a fluid-like state. There, the particle discreteness steps into the background and the collective behavior of the dust ensemble prevails. Consequently, space- and time-averaged quantities like the dust density play the decisive role. These waves are called dust-density waves (DDWs) and represent the second fundamental type. They are usually self-excited and gain energy from streaming ions [68, 69]. The transition between lattices waves and DDWs is fluent and difficult to describe.

After the first prediction of a dust-acoustic wave mode[1] by Rao *et al.* [70] in 1990, dust-density waves were observed experimentally in numerous works in the laboratory [71–80] and under weightlessness [54–57]. Nonlinear density waves are also well known in dusty plasmas. This concerns non-periodic structures such as shock waves [81–83], solitary waves [57, 84, 85] and also nonlinear traveling waves [51, 79, 86–89]

In this thesis, nonlinear self-excited dust-density waves are studied under microgravity conditions on parabolic flights. The waves emerge spontaneously below a critical neutral gas pressure and at high dust densities in the presence of streaming ions. The work is focused on the investigation of general wave attributes, such as

---

[1]In this thesis, the term dust-acoustic is used only for theoretical wave descriptions where no driving mechanism (through ion drifts) is included. Experimentally observed waves are consequently always referred to as dust-density waves. In the literature both expressions are often used synonymously.

amplitude, phase and frequency, concerning two main aspects: First, the transient behavior of DDWs is analyzed. This behavior is particularly reflected in the appearance of bifurcations, i.e., splitting or merging wave fronts. The aim is to understand, how these bifurcations influence the structure of the wave fields. Second, the global time-averaged wave properties are investigated, primarily by determining their spatial frequency distributions. This analysis addresses the question to what extent the self-excited DDWs differ from externally driven waves. Interestingly, it turns out that both aspects, although investigated on different time scales, are closely related to each other by means of so-called frequency clusters. Moreover, the experimental findings give rise to study the waves within a numerical model that is based on the van-der-Pol oscillator. An analysis of this model is undertaken within this work.

The present work is a cumulative thesis and lead to publications in peer reviewed journals [90–92], which are included in Appendix B. It is structured as follows: Chapter 2 gives a general theoretical framework, in which this thesis is embedded. It briefly summarizes the basic concepts of dusty plasmas that are necessary to follow the arguments of this thesis and gives an overview on the current status of research on dust-density waves. Chapter 3 introduces the experimental setup and characterizes the discharge. Moreover, it gives a detailed description of the applied analysis methods. In Chap. 4 the main experimental findings of this thesis are outlined and discussed. Chapter 5 presents the recent results of the numerical studies, which have not yet been published. The key statements of this thesis and a short outlook are provided in Chap. 6.

2 Waves in Dusty Plasmas

The beginning of this Chapter focuses on the question how micrometer-sized dust particles arrange in a discharge under microgravity conditions. For this purpose it is, first of all, inevitable to introduce the general concepts within the context of dusty plasmas. Based on this, the forces acting on single particles can be described.

The discussed principles offer the possibility to place the dust-density waves among other instabilities. Therefore, the second fundamental wave type in dusty plasmas, namely the lattice wave, is introduced and compared with DDWs. Lattice waves are observed in crystalline structures and are usually driven by an external force. In contrast, DDWs occur in fluid systems and are often self-excited, i.e., they obtain energy directly from the system.

After the fundamental properties of the dust-density waves have been described, the current status of research is briefly outlined in order to place the questions of this thesis into a global context. The Chapter closes with possible explanations of the wave excitation mechanism since it contributes essentially to the understanding of the phenomena investigated throughout this work.

The basic properties of dusty plasmas include many different and often sophisticated aspects that cannot be covered within this Chapter. Therefore, the reader should refer to the following textbooks [93–96] in order to study the given concepts in more detail. Several further review articles are mentioned in the corresponding Sections.

2.1 Fundamentals of Dusty Plasmas

This Section describes the behavior of dust particles in a plasma background. The forces acting on isolated particles are discussed with an emphasis on the particular situation in rf discharges under microgravity conditions. Some review articles [97–102] summarize the discussed points.

2.1.1 Basic Notations

A plasma is an ionized gas that consists of electrons, ions and neutral gas atoms. If a fourth species of massive particles with typical diameters of $10^{-9} \ldots 10^{-5}$m is embedded in the discharge, it is called a dusty or complex plasma. The dust grains carry a high electric charge $Q_{\mathrm{d}} = -Z_{\mathrm{d}}e$, where Z_{d} is the total number of elementary charges. Due to the higher mobility of the electrons compared to the ions, Q_{d} is in general negative in laboratory plasmas, where other charging processes as, e.g., photoionization and secondary electron emission [23, 94, 103], can be usually neglected. The collection of elementary charges resembles the behavior of electrostatic

Langmuir probes, which are a fundamental diagnostics for monitoring basic plasma parameters [95, 104, 105]. Hence, the charging currents can be determined in first approximation by the "Orbital Motion Limit" theory [106]. Since the grains can be referred to as spherically symmetric, the most common approach to estimate the dust charge is a capacitor model. There, the particles obtain a floating potential ϕ_{fl} after an equilibrium of the currents has been reached. The charge of a particle of radius r_{d} then reads $Q_{\mathrm{d}} = 4\pi\epsilon_0 r_{\mathrm{d}}\phi_{\mathrm{fl}}$.

One of the basic properties of a plasma is its quasineutrality, which means that the net charge in a sufficiently large volume vanishes. This condition still holds if dust particles are present in the plasma. It is then given by

$$n_{\mathrm{e}} + Z_{\mathrm{d}}n_{\mathrm{d}} - n_{\mathrm{i}} \approx 0, \tag{2.1}$$

where n_{e} is the electron density, n_{i} is the ion density and n_{d} is the dust density.

Since the surrounding plasma background shields electric fields very effectively the Coulomb interaction between the charged particles is reduced. It can be approximated by a Debye-Hückel or Yukawa potential [104]

$$\phi(r) = \frac{Q_{\mathrm{d}}}{4\pi\epsilon_0 r} \exp\left(-\frac{r}{\lambda_{\mathrm{D}}}\right). \tag{2.2}$$

Here, the linearized Debye length λ_{D} determines the screening strength of the plasma. It depends on both, electrons and ions, and can be expressed by the individual Debye lengths of each species by the following relation

$$\lambda_{\mathrm{D}}^{-2} = \lambda_{\mathrm{De}}^{-2} + \lambda_{\mathrm{Di}}^{-2}, \tag{2.3}$$

where

$$\lambda_{\mathrm{De}}^2 = \frac{\epsilon_0 k_{\mathrm{B}} T_{\mathrm{e}}}{n_{\mathrm{e}} e^2}, \tag{2.4}$$

$$\lambda_{\mathrm{Di}}^2 = \frac{\epsilon_0 k_{\mathrm{B}} T_{\mathrm{i}}}{n_{\mathrm{i}} e^2}. \tag{2.5}$$

Besides the density, these quantities depend on the temperature $T_{\mathrm{e,i}}$ of the corresponding species. They describe the lengths after which the electric potential is diminished by a factor of $1/e$.

If not one isolated particle but several dust grains are investigated, the mutual interaction between them must be considered. The force between two particles, denoted as i and j, with spatial distance r_{ij} results from the Yukawa potential of Eq. (2.2) and is in general repulsive. It reads

$$\vec{F}_{ij} = \frac{Q_{\mathrm{d}}^2}{4\pi\epsilon_0 r_{ij}^2} \left(1 + \frac{r_{ij}}{\lambda_{\mathrm{D}}}\right) \exp\left(-\frac{r_{ij}}{\lambda_{\mathrm{D}}}\right) \vec{e}_{ij}. \tag{2.6}$$

In situations, where streaming ions are present, these considerations do not necessarily hold any longer because the ions represent a source of free energy and the system is open. Effects that may arise in such situations are described in the next Subsection.

The most prominent consequence of the mutual interaction between dust particles is the formation of Coulomb crystals in externally confined dust clouds. They were investigated throughout numerous works in two-dimensional [27–31] as well as in three-dimensional systems [107–109]. A detailed overview is given in Refs. [110,111]. The state of a dusty plasma can generally be expressed by the coupling strength Γ. It is defined as the ratio of potential to kinetic energy and is also known as Coulomb coupling parameter. It reads

$$\Gamma = \frac{Q_{\mathrm{d}}^2}{4\pi\epsilon_0 a_{\mathrm{WS}} k_{\mathrm{B}} T_{\mathrm{d}}}. \tag{2.7}$$

Here, T_{d} is the dust temperature and a_{WS} is called Wigner-Seitz radius, defined as $a_{\mathrm{WS}} = (4\pi n_{\mathrm{d}}/3)^{-1/3}$.

A system is called weakly coupled, if $\Gamma < 1$. Strongly coupled systems with $\Gamma > 1$ are typically subdivided into fluid-like ($\Gamma < \Gamma_{\mathrm{C}}$) and solid-like ($\Gamma > \Gamma_{\mathrm{C}}$) states. In general, the transition is observed at $\Gamma_{\mathrm{C}} = 170$ [107]. The coupling strength in experiments can be varied externally. For example, the neutral gas pressure influences the thermal particle motion and thus the dust temperature. Another method that can be used to control the dust temperature is given by means of laser manipulation. There, a strong laser kicks the dust particles randomly and thus heats the system [33,34].

2.1.2 Forces Acting on Dust Particles

Besides the described interparticle forces, there are several other forces, which arise from the complicated environment of the background plasma.

Gravity

In contrast to the electrons and ions, the comparatively large mass of micrometer-sized dust particles causes a significantly large gravitational force $\vec{F}_{\mathrm{g}}$. For a single grain with mass m_{d} and mass density ρ_{d} it reads

$$\vec{F}_{\mathrm{g}} = m_{\mathrm{d}}\vec{g} = \frac{4}{3}\pi r_{\mathrm{d}}^3 \rho_{\mathrm{d}}\vec{g}, \tag{2.8}$$

where $\vec{g}$ is the gravitational acceleration. In rf discharges, gravity causes the particles to sediment into the sheath region[1] in quasi two-dimensional dust clouds. In order to minimize gravitational influences on the dust over the entire discharge, experiments can be performed under microgravity. There, extended three-dimensional dust clouds form. In both cases the particles are affected by electric fields.

Electric Field Force

In the presence of an electric field $\vec{E}$ the particles experience an electric field force, which is given by

$$\vec{F}_{\mathrm{el}} = Q_{\mathrm{d}} \cdot \vec{E}. \tag{2.9}$$

---

[1]For a detailed description of the sheath in rf discharges, see Ref. [112].

The electric fields of an rf discharge are highest in the vicinity of the electrodes, where electrons and ions cannot shield each other effectively. In this strongly inhomogeneous region, a positive space charge exists, the sheath. The resulting force is directed into the plasma and is strong enough to compensate for gravity. The comparably weak electric field inside the plasma bulk plays a decisive role under microgravity conditions, where it pulls the particles towards the discharge center. In addition to the internal fields of the plasma, externally applied fields can also affect the particles. However, the interaction arises not from the described electric force. Rather, the dust is influenced indirectly due to a modified discharge topology.

Neutral Drag

Dust particles that move relative to the plasma neutrals at a velocity v_d experience friction due to collisions between both species. The resulting neutral drag force that acts on the dust is given by

$$\vec{F}_n = -m_d \beta \vec{v}_d. \tag{2.10}$$

This general description was first introduced by Epstein [113]. The friction coefficient $\beta = (8\delta p)/(\pi r_d \rho_d \bar{v}_{th,n})$ depends on the characteristic quantities of the particles as well as the neutral gas pressure p, the mean thermal velocity of the neutrals $\bar{v}_{th,n} = (8k_B T_n/\pi m_n)^{1/2}$ and the dimensionless accommodation coefficient δ. This parameter lies in between 1 for specular reflection and 1.44 for diffuse reflection. The exact value has to be determined experimentally, see, e.g., Ref. [114]. The neutral drag plays a leading role for the onset of self-excited dust-density waves since it controls the energy input of the streaming ions.

Ion-Drag Force

Streaming ions are omnipresent in rf discharges due to the ambipolar electric field arising from a nonuniform ion density distribution, as described in Sec. 3.1. The ion drift is given by $\vec{v}_i = \mu_i \vec{E}$, where μ_i is the ion mobility [115]. It has a non-negligible influence on the dust particles. One aspect is the so-called ion-drag force, which is exerted on each individual dust grain. It arises from the momentum transfer between ions and dust. There, each of the bent ion trajectories is examined individually. The ion drag was studied extensively in analytic models [116–120], in numerical simulations [121, 122] and experimentally [123–125].

The ion-drag force F_i can be divided into two parts. The first one is the collection force F_c, which accounts for those ions that reach the surface and directly impinge on the grain. This holds for such ions with velocity v_s that have impact parameters less than the collection radius $b_c = r_d \left[1 - 2e\phi_{fl}/(m_i v_s^2)\right]^{1/2}$. Ions that do not reach the particle surface interact purely electrostatically with the dust. They contribute to the second part, namely the orbital force F_o. In the early model of Barnes *et al.* [116] the ion-drag force reads

$$F_i = F_c + F_o = n_i m_i v_i v_s \left(\pi b_c^2 + 4\pi b_{\pi/2}^2 \ln \Lambda\right). \tag{2.11}$$

Here, the product $n_i m_i v_i v_s$ represents the total momentum flux density of the incoming ions. The first term in the sum represents the cross section of the collection part and the second term corresponds to the cross section of the orbital part. It incorporates the impact parameter for $90°$ deflection, $b_{\pi/2} = Ze^2/(4\pi\epsilon_0 m_i v_s^2)$. The model assumes an ion velocity $v_s = [v_i^2 + 8k_B T_i/(\pi m_i)]^{1/2}$, which is a combination of ion drift and ion thermal speed. The Coulomb logarithm $\ln\Lambda$ is given as

$$\ln\Lambda = \frac{1}{2}\ln\left(\frac{\lambda_s^2 + b_{\pi/2}^2}{b_c^2 + b_{\pi/2}^2}\right). \tag{2.12}$$

For ions in the plasma bulk, which are usually slower than the Bohm velocity[2] ($v_i < v_B$) the effective shielding length λ_s coincides with the linearized Debye length of Eq. (2.3). For larger ion speeds ($v_i > v_B$) it is better described by a modified screening length [121]. This is of importance especially for the situation in the sheath.

Besides the outlined expression for the orbital part of the ion-drag force, a more precise model has been proposed by Khrapak *et al.* [118–120]. It includes all ion trajectories, which intersect with the Debye sphere around the dust, and leads to a modified expression of the Coulomb logarithm. Moreover, an optimized empirical expression for the orbital part was given by Hutchinson [122] as a result of numerical simulations.

Non-Reciprocal Forces

For the calculation of the ion drag in Eq. (2.11), each ion trajectory was examined individually. However, a self-consistent model, which accounts for the collective interaction of the ions, reveals another feature of the ion flow around a dust grain, namely a wake potential in the downstream direction behind the particle. This leads in particular to an enhanced ion density in the wake, which is also known as ion focus [30,126,127]. A second particle, which is located in downstream direction of the grain, consequently experiences an attractive force. This explains, for example, that the particles can arrange themselves in vertically aligned chains in the sheath region of a plasma [128,129]. It was found that the attractive forces are non-reciprocal, i.e., they violate Newton's third law [130]. This effect was attributed to a sound barrier of the supersonic ions and it was pointed out that the system has a non-Hamiltonian character since the ions introduce a source of free energy [131]. Nevertheless, a wake formation was also found for subsonic ion flows (with Mach numbers $M = v_i/v_B > 0.5$), which incorporates attractive forces as well [132,133]. In addition to the formation of particle chains, the wake field behind the dust can also lead to instabilities, in which the downstream particles are forced to oscillate [127,133]. As a result the crystalline order of dust suspensions in the sheath is destabilized and the solid structure melts. However, the importance of this effect for extended three-dimensional dust clouds is unknown. The formation of wake fields and related issues are still under investigation. In so-called electrorheological plasmas [135] symmetric

---

[2]The Bohm velocity $v_B = (k_B T_e/m_i)^{1/2}$ is identical with the ion sound speed.
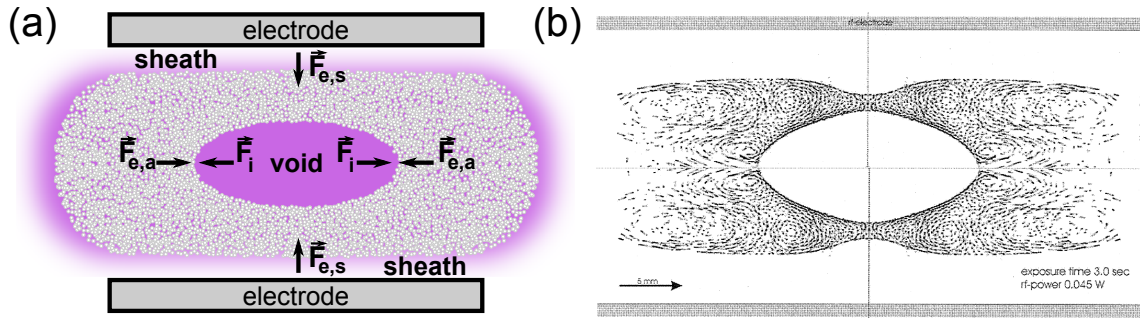
Figure 2.1: (a) Sketch of the forces that act on dust particles in an rf discharge under microgravity conditions. In the center of the plasma the ion-drag force $\vec{F}_i$ pushes the particles radially outwards. At the boundary of the resulting dust-free void the ion drag is compensated by the inward directed electric force $\vec{F}_{e,a}$ arising from the ambipolar electric field. In the vicinity of the electrodes the dust is pushed into the bulk due to the strong electric field force, $\vec{F}_{e,s}$, in the sheath. (b) Example of a recorded dust cloud under microgravity. (From Ref. [145])

time-averaged wake fields with respect to the stream direction were produced by additional alternating electric fields. Furthermore, the influence of wake fields on the particle arrangement in three-dimensional finite systems was analyzed, which lead to a refined definition of Yukawa balls [136].

Compilation of Relevant Forces Under Microgravity Conditions

The experiments conducted within the scope of this thesis were exclusively performed under microgravity conditions. All relevant forces for this distinct situation are illustrated in Fig. 2.1 (a). An experimentally observed dust cloud that forms in the presence of theses forces is shown in Fig. 2.1 (b).

Of course, the gravitational force can be neglected and the dust particles will, in general, fill an extended three-dimensional volume in the discharge. The ionization rate and thus the ion density is highest in the center of the discharge. This causes an outward directed ambipolar ion flow and the corresponding ion-drag force pushes the dust away from the central plasma, resulting in a dust-free region, the so-called void [47]. Outside the center the ion drag is compensated by the electric force of the weak ambipolar field. Hence, the void boundary is given by the equilibrium position, where the net force on the particles vanishes. Much effort has been put into a precise explanation of the void phenomenon from theoretical side and in simulations and the reader is referred to progressive articles for the details [47, 137–141]. The forces at the boundaries were determined using tracer particles [142] and analyzing particle trajectories inside the void [143, 144]. The strongest electric fields arise in the sheath region of a plasma. They are directed towards the electrodes. Since the streaming ions enter the sheath with Bohm velocity, the ion-drag force is considerably small. Thus, the dust particles experience an inward directed force that leads to a dust-free sheath.

In addition to the above mentioned forces, other forces can be considered as well. Nevertheless, they play a minor role in the experiments of this thesis. For example, thermophoresis pushes the particles from hotter into colder regions of a discharge. Since naturally arising temperature gradients in rf plasmas are usually very low, such temperature effects are not significant. Externally generated temperature differences, however, can be used to produce extended dust clouds under laboratory conditions, which are very similar to those observed under microgravity [40, 44].

2.2 Externally Excited Waves in Stable Two-Dimensional Systems

In the previous Section, some static phenomena of dusty plasmas were described, which resulted from the interplay of the acting forces. For example, the coupling between the particles can become sufficiently large to form crystalline structures. This Section focuses to the dynamical behavior in Coulomb crystals that are subject to external disturbances. It turns out that under these conditions several wave structures can be generated.

Experimental observations of dust-lattice waves (DLWs), i.e., compressional modes similar to phonons in a solid, were made for example in one-dimensional linear chains of a few particles [58, 59]. The waves were excited by a chopped laser that periodically pushed the first particle of a chain. The dispersion relation of the waves was obtained by varying the chopping frequency and measuring the corresponding wavelength. The experiments revealed a strong spatial damping of the waves. However, the observation of DLWs was not limited to one-dimensional systems. Similar works showed that it is also possible to generate these waves in extended two-dimensional monolayers [35–37]. Moreover, in such systems also other, more complicated wave types occur, as for example shear waves [63, 64]. There, the particles oscillate inside the crystal plane but perpendicular to the wave motion. In contrast to experiments on DLWs, a short and narrow laser pulse was shot into the particle arrangement in order to excite the waves. Further works investigated this phenomenon in more detail [65–67].

If the externally generated initial disturbance moves faster than the local acoustic speed in the medium, a Mach cone is generated. The corresponding shock wave front propagates away from the disturbance at a certain angle, which indicates the ratio of acoustic to disturbance velocity. Samsonov *et al.* [60, 61] used supersonic particles below the crystal in order to generate Mach cones while Melzer *et al.* [62] perturbed the system with a strong focal laser spot that was moved by a scanning mirror. Due to the dispersive nature of the crystal the wave fronts, which naturally consist of multiple wavelengths, form an interference pattern similar to that of the ion-induced wakes behind a particle. A theoretical investigation of Mach cones in dusty plasmas is, for example, presented in Ref. [146].

To summarize, lattice waves were so far observed in almost perfect crystalline structures. In the solid phase of a dusty plasma, the potential energy of the particles is large compared to their kinetic energy. The behavior of the waves is then

dominated by the interaction between adjacent particles. Consequently, the particles can hardly pass each other and the wave amplitudes are small compared to the interparticle distance and have an almost sinusoidal shape. In most cases, DLWs were excited externally by the radiation pressure of a laser. Due to the strong coupling between the particles the waves usually arise at very low neutral gas pressures ($p \lesssim 10$ Pa). Since the waves propagate into otherwise stable dust clouds, they are damped away immediately by the neutral drag after the driver is turned off.

2.3 Self-Excited Dust-Density Waves

Experiments show that in spatially extended three-dimensional dust clouds dust-density waves can emerge spontaneously if the gas pressure is sufficiently low ($p \lesssim 35$ Pa). In contrast to the previously discussed lattice waves, DDWs are observed if the dust cloud resides in a fluid-like state, i.e., the particles are supplied with significantly more kinetic energy than in the solid phase. Inside DDWs the oscillation amplitudes of individual particles are usually much larger than the inter-particle spacing. Thus, the collective behavior of the particles prevails their mutual interaction and in a description of the wave motion macroscopic measures like the dust density replace microscopic quantities as the interparticle spacing. Due to the high mass of the dust grains, the dust-density wave represents a low-frequency and long-wavelength type compared to waves in conventional plasmas. Typical frequencies are $(5 - 40)$ Hz and the wavelengths lie in between $(1 - 10)$ mm. The waves are usually self-excited and gain their energy from streaming ions. Nevertheless, in some previous works [48–50] DDWs were generated externally. In this case the excitation was of a global type, i.e., no driver excited the cloud periodically at a distinct position. Rather, the whole system was excited parametrically. Surprisingly, the self-excited waves exist at gas pressures where neutral drag is so strong that the waves should be damped after a few wavelengths. The growth rates at the onset are very high and the waves become saturated within approximately one wavelength. Moreover, dust-density waves are often nonlinear. This is reflected in large modulation depths and strongly non-sinusoidal wave shapes.

Status of Research

The first experimental observation of dust-density waves was made by Chu *et al.* [71] in 1994. A correct interpretation of the phenomenon was primary given later in a comment [147]. Dust-density waves are observed in the laboratory in front of the anode of dc glow discharges [72–78, 148–151] or in the sheath region of rf discharges [79,80,88,89,152]. Moreover, they have been investigated in Q-machines [72], hot-filament plasmas [153] and inductively coupled rf discharges [154]. A typical example of dust-density waves in the anode glow of a dc discharge is given in Fig. 2.2 (a), which shows a vertical section through the dust cloud. The wave motion is observed as a strong periodical modulation of the recorded light intensity. The waves propagate in the direction of the local ion flow, i.e., away from the anode. A
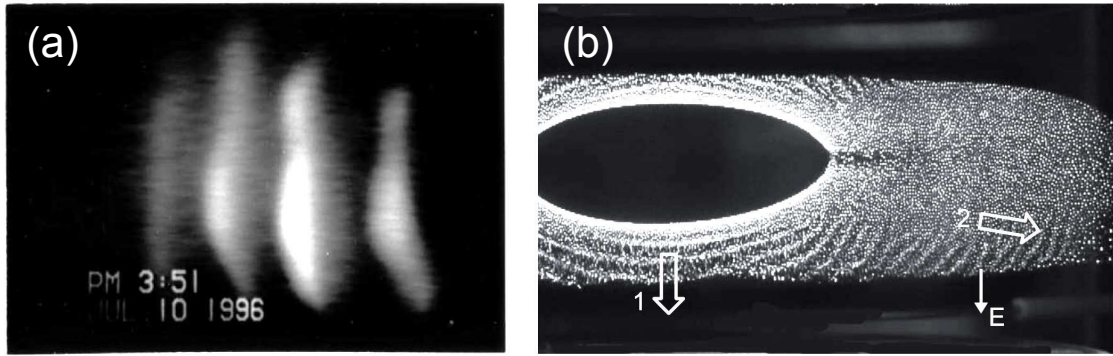
Figure 2.2: Typical examples of dust-density waves. The waves are reflected in strong modulations of the recorded light intensity. (a) In a dc discharge the waves propagate away from the anode (located at the right side) in the direction of the streaming ions. (From Ref. [73]) (b) In rf discharges under microgravity conditions, extended three-dimensional DDWs can be observed. The corresponding wave pattern is usually more complex. The waves propagate at different angles with respect to the discharge electric field, i.e., the ion flow, as indicated by the arrows. (From Ref. [55])

summary of dust-density waves in dc plasmas can be found in the review article of Ref. [155].

Waves in significantly larger dust clouds can be studied in the laboratory if gravity is compensated by thermophoresis [40, 87] or in experiments under weightlessness, as for example on sounding rockets [47], on parabolic flights [54–57] or aboard the ISS [48–53]. The complicated nonlinear wave fields that are observed on parabolic flights were investigated by Piel *et al.* [55, 100] in great detail. It was found that, in the setup used within the context of this thesis, the waves emerge below a critical gas pressure of approximately 35 Pa first at the outer edges of the dust cloud. If the pressure is lowered successively, the wave field extends into the dust cloud and finally covers the entire volume. An example of the wave pattern is shown in Fig. 2.2 (b). Here, the waves propagate radially outwards from the dust-free void to the discharge edges and hit the sheath at different angles.

The dispersion properties of DDWs were investigated by synchronizing the spontaneously emerging waves by an external alternating electric field at a chosen frequency [49, 73, 76, 78, 148, 149]. This technique was also used in order to study the dynamic response of small dust clouds [78]. The synchronization phenomenon itself was investigated recently in Ref. [150]. In complementary experiments the dispersion relation was obtained by varying the discharge parameters [74, 156]. In Refs. [149, 151, 157] it was pointed out that the dispersion properties can be influenced significantly by a finite dust temperature. The linear growth rates inside the wave field were determined in Refs. [76, 77, 80, 154].

Besides measurements of purely linear wave attributes, the nonlinear properties were studied throughout numerous works. Nonlinear waves occur either as traveling periodic waves [79, 86–89] or as localized structures. The latter includes, e.g., solitary waves [57, 84, 85] and shock waves [81–83]. Recently, the development of nonlinearity at the onset of the waves was studied [89]. The observations of resonant

particles [79, 87] and wave breaking [88] provide useful hints for the nonlinear saturation mechanism of the waves. Moreover, it was found that the plasma glow can be strongly modulated by DDWs, which suggested a nonlinear interaction between plasma and waves [158].

On the theoretical side much effort was made in order to expand the early model of Rao *et al.* [70], who made the first prediction of dust-acoustic waves in 1990. This model was based on fluid equations for the dust and treated linear as well as nonlinear cases. Accordingly, various further fluid models [159–163] and kinetic models [164–166] were introduced. They cover a variety of different aspects, such as dust-ion collisions [68, 167], dust-density inhomogeneities [159] or grain charge variations [74, 156, 161, 168–171]. Furthermore, variable dust-size distributions [172] and boundary effects caused by finite cloud sizes [160, 162, 163] were taken into account and the effect of finite dust temperatures was investigated [166]. An overview on specific nonlinear aspects is given, for example, in Refs. [173, 174].

One particular feature of dust-density waves becomes apparent if the streaming ions are treated in two dimensions. This was done in a kinetic approach [68] as well as in a fluid model [55, 100]. It turned out that the wave propagation is not necessarily aligned with the ion flow, i.e., the discharge electric field. In contrast, the fastest growing wave mode propagates obliquely with respect to the electric field if the ions approach Bohm velocity. These two different modes were observed under microgravity [55, 100]. The situation is illustrated in Fig. 2.2 (b) by arrows. The regular mode (arrow '1') is found below the void, where the waves propagate in the direction of the electric field (thin arrow). In the outer regions of the dust cloud, the oblique mode (arrow '2') can be observed.

Excitation Mechanism

As outlined above, the properties of dust-density waves in saturation are well understood theoretically and experimentally, in particular in the linear case. Nonetheless, the details of the mechanism that drives the spontaneously emerging waves is still under debate. Different proposed explanations shall be briefly introduced in the following. By far, the most accepted explanation is given in terms of an ion-dust streaming instability where an ion flow introduces energy into the system. This energy has to overcome dissipation by dust-neutral collisions, which is omnipresent in weakly ionized plasmas. Therefore the critical neutral gas pressure, below which waves can be observed, is determined by the balance between the instability and the damping from neutral drag. It was found that the energy of the ions is indeed sufficiently large to drive the wave [69]. Experimental studies at the instability threshold were carried out in Refs. [80, 87, 175]. Theoretical descriptions of the instability were given either by a Vlasov model [68] or within a fluid description [55, 56, 176]. Both variants treated the ions and the dust particles as streaming and interacting populations with a relative velocity to each other. This situation is different from the conventional beam plasma instability, since neither of the species can be regarded as a collimated beam with a narrow velocity distribution. It is rather attributed to

the so-called Buneman-instability [177]. For this type the wave is e-folded within one period, which is in agreement with most experimental observations.

In addition to this approach, it was found that instabilities can arise in the wake potential behind a dust particle [127,133]. It is consequently reasonable to conjecture that particles, exposed to streaming ions, begin to oscillate, which finally results in wave-like structures. Moreover, it was proposed that charge variations within the dust cloud may lead to a parametric excitation of DDWs [74,161].

Besides the discussed internal excitation mechanism, one could also argue that energy is provided by external sources. For dust-density waves under microgravity on parabolic flights two sources are possible. First, the waves might be triggered initially by fluctuations of residual gravity, which is always present due to the imperfect parabolic maneuver. Second, it is known that the dust cloud can be subject to a low-frequency resonance that leads to a periodically expanding and collapsing void boundary. This phenomenon is often observed for dust clouds if the rf voltage reaches the 'plasma-off' limit and is called 'heartbeat instability' [178].

Like the excitation mechanism itself, the mechanism of amplitude saturation is still unclear. It was proposed that trapping of plasma ions could limit the amplitude growth [68,179]. The trapping of dust particles [79] and a mode coupling between fundamental and higher harmonics [180] were also discussed.

2.4 Summary

In this Chapter it was described how dust particles arrange themselves under microgravity conditions. The observed dust clouds reveal two characteristics: First, since the micrometer-sized particles are influenced mainly by the electric field force and streaming ions but not by gravity, a three-dimensional cloud forms, which can be observed in laboratories only if an additional force is introduced that compensates for gravity. Second, due to the interplay of the forces, a dust-free region in the center of the discharge is generated, the void.

The described dust cloud resides in a fluid-like state, in which dust-density waves can emerge spontaneously at sufficiently high dust densities and low gas pressures. These waves are dominated by the collective behavior of the dust particles. Consequently they are best described in fluid models, which include space- and time-averaged quantities like the dust density. DDWs are most often found self-excited since they gain energy from streaming ions, most likely due to a Buneman-type instability. A second fundamental wave type in dusty plasmas, namely the lattice waves, occur in crystalline structures, where the mutual interaction between the particles becomes dominant. The oscillation amplitudes of individual particles in DLWs are consequently significantly smaller. They are usually excited by an external driver. Nevertheless, other excitation mechanisms such as a particle beam are generally possible [181]. The transition between the described extreme cases of waves in dusty plasmas is fluent and difficult to describe. There are several approaches proposed to meet the fact that strong coupling effects contribute to the description of DDWs [80,176,182–184].

The investigations of dust-density waves in the last two decades revealed various interesting features. This includes in particular those properties of the waves that can be interpreted within the context of linear theories like the dispersion behavior or growths rates. Recently, the focus turned towards nonlinear phenomena. These investigations covered nonlinear structures, such as solitons or shocks, but also traveling periodic waves.

For the examination of these issues, advanced technologies like new classes of high-speed cameras, are necessary. They allow, for example, to track individual particles inside the wave field at a high temporal resolution. Furthermore, in such situations the established methods of analysis reach their limits. Thus, alternative techniques are required to provide more detailed insight. One possibility is introduced in the next Chapter.

3 Generation and Analysis of Dust-Density Waves

After describing the particle arrangement inside a plasma under microgravity conditions, now the distinct experimental setup is introduced that was used for the measurements of this thesis. Besides a brief introduction of the applied diagnostics and the discharge topology, the peculiarities of the complex experiments on parabolic flights are outlined since they influence the recorded data.

For the analysis of the waves, several methods are available. With the space-time diagram and the Fourier analysis the most common ones are introduced in this Chapter. They are mainly used to determine the basic wave characteristics such as wavelength and frequency. However, the observed DDWs often have a strongly nonlinear character and comprise transient phenomena as splitting or merging wave fronts. For the description of such features, the aforementioned methods are only suitable to a limited extent. Thus, the concept of the analytic signal is used within the context of this this, which leads to the definition of instantaneous wave attributes like phase or instantaneous frequency. These quantities finally allow to investigate the waves on different, individually chosen time scales. Consequently, an analysis workflow, based on the analytic signal, is developed that reconstructs the complete spatio-temporal structure of the waves.

3.1 Dusty Plasma in the IMPF-K2 Chamber

The dusty plasma is generated in a low-temperature, low-density parallel-plate rf discharge, called IMPF-K2. It is a modification of the chamber prototype from the International Microgravity Plasma Facility (IMPF), which was designed to fly aboard the ISS. It is similar to the chamber[1] described in Refs. [142, 185], which consisted of two independently operated concentric electrodes (center and ring). Sketches of the chamber can be found in Fig. 3.1. The capacitively coupled parallel-plate reactor consists of two transparent indium tin oxide (ITO) electrodes, which allow optical access through the bottom and the top of the chamber but was not used here. The electrodes are 78 mm in diameter and have a vertical gap of 30 mm. Guard rings surround the electrodes and guarantee that the plasma production has its maximum in the center of the discharge. The self-bias is suppressed by means of a shunt resistor. The recipient is filled with argon as working gas. Waves are observed at pressures of $p = (5 \ldots 35)$ Pa.

---

[1]Some of the evaluated data were recorded in this chamber. The corresponding section is noted separately.
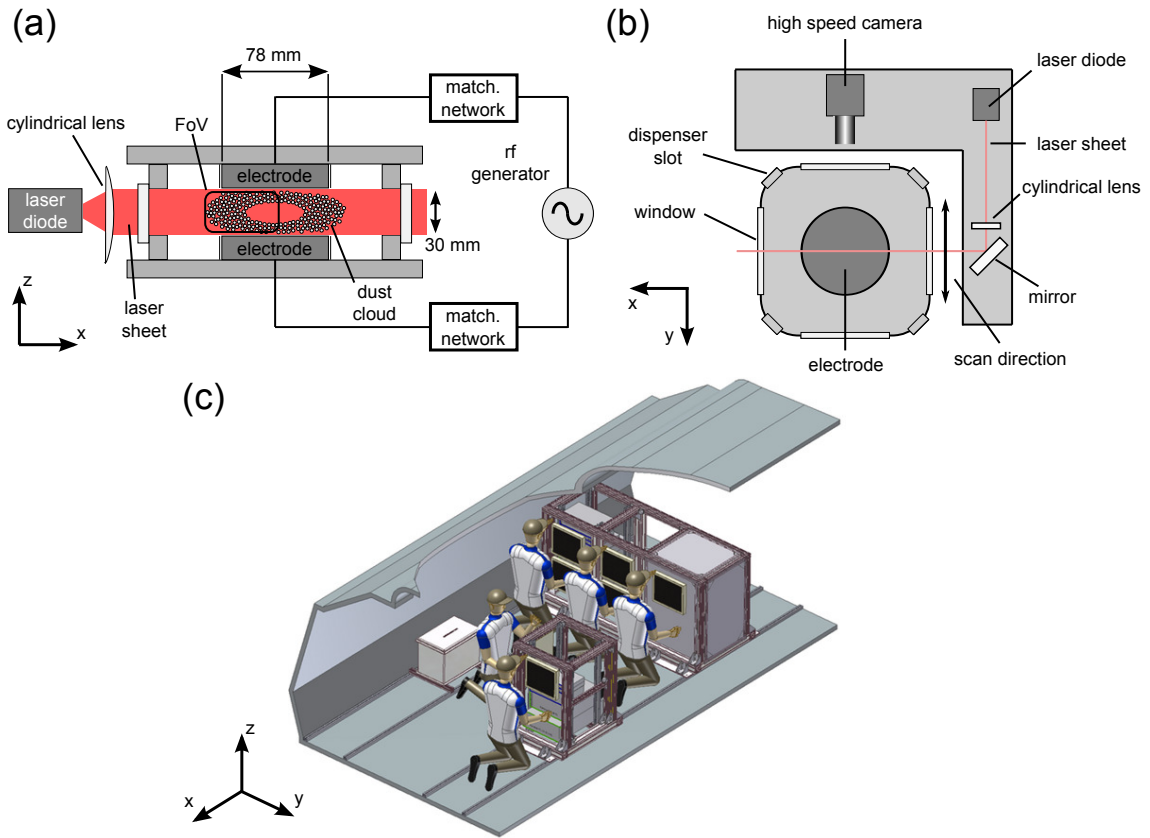
Figure 3.1: (a) Side view of the IMPF-K2 chamber. Particles are illuminated by a laser diode. The field of view (FoV) of the high speed camera is marked with a rectangle. Both electrodes are fed by the same rf generator operating in push-pull mode. (b) The top view of the chamber shows the camera setup. It is mounted on a translation stage, which allows for scans along the y-axis. (c) Sketch of the complete facility installed in the plane. Five crew members sit at two racks to operate the experiment.

A plasma is produced by applying an rf voltage ($f_{rf} = 13.56$ MHz) to the electrodes. Typical peak-to-peak voltages of $U_{rf} = (40\ldots70)$ V_{pp} allow the formation of a stable dust cloud in which waves can emerge. The generator is coupled to the electrodes by matching networks, which match the impedances of the rf generator and the chamber. Since the generator is operated in push-pull mode, i.e., the signals of upper and lower electrode exhibit a constant phase shift of 180°, maximum electric fields are realized. For a detailed discussion of the physics of rf discharges the reader is referred to Ref. [112].

In order to generate extended dust clouds, spherical and monodisperse melamine formaldehyde (MF) particles are injected into the chamber. This is realized by electromagnetically agitated dust dispensers, which are similar to salt shakers. Since dust-density waves only exist at comparably high dust densities, the dispensers have to inject large amounts of dust. Throughout this work, particles with a diameter of 6.8 μm and 9.55 μm were used and only one size was chosen at a time. Typical dust densities of this setup are $n_d \approx 10^{10}$ m^{-3}.

The primary diagnostics for the observation of the dust cloud is a video microscope. Its basic components are a laser and video camera. The red laser diode ($\lambda = 660$ nm and $P = 50$ mW), which is expanded to a vertical sheet of parallel laser light, illuminates a thin section through the center of the dust cloud, see Fig. 3.1 (a). The scattered light from the particles is recorded at right angle by a high-speed CMOS video camera. The chosen frame rate of 97 fps ensures that aliasing effects can be neglected since the waves have frequencies of only a few Hz. The camera has a spatial resolution of 1200×1024 pixels. Different field of views (FoV) were used for the analysis.

As shown in Fig. 3.1 (b) the camera setup is mounted on a movable stage together with the illumination laser. Such an assembly is known as scanning video microscope and allows to record excentric parallel cuts of the cloud. Furthermore, fast camera scans at a speed of several mm/s through the dust cloud are possible and can principally be used for a reconstruction of the three-dimensional structure of the dust cloud.

The experiments of this thesis were exclusively performed on parabolic flights aboard a specially equipped Airbus A-300. For this purpose the plasma chamber and all related items were integrated in a transportable facility, which can be mounted inside the plane. An illustration of the in-flight setup is shown in Fig. 3.1 (c). The complexity of the experiment necessitates that it is operated by a total of five persons. The data of this thesis was recorded on four successive flight campaigns in the years 2007-2010. The campaigns included three flight days with 31 parabolas each. During one parabola approximately 22 s of microgravity can be provided. With the described setup the recorded videos were limited to a duration of 8 s. The residual gravity in a few of the parabolas was so strong that the corresponding measurements could not be evaluated.

An acceleration sensor monitors the mechanical accelerations of the vacuum chamber for all spatial dimensions during the flight with a temporal resolution of 1 kHz. In particular, the device allows to detect any residual gravity during a parabola and can thus be employed to investigate the correlation between mechanical forces and dust-density waves.

Basic Properties of the Discharge

The topology of the discharge can be determined by simulations with the two-dimensional SIGLO fluid code [186]. Figure 3.2 shows simulation results at $p = 30$ Pa and $U_{\mathrm{rf}} = 65$ V$_{\mathrm{pp}}$. It includes two-dimensional maps of the plasma potential $\phi_{\mathrm{p}}(x, z)$ [Fig. 3.2 (a)] and the electron density distribution $n_{\mathrm{e}}(x, z)$ [Fig. 3.2 (b)]. Obviously, the plasma potential is highest at the center of the discharge ($U_{\mathrm{rf,max}} = 70$ V$_{\mathrm{pp}}$) and decays gradually towards the electrodes and the periphery. The sheath region comprises a strong potential drop, which results in the strongest electric fields of the discharge. The electron density is also highest in the center ($n_{\mathrm{e,max}} = 1.8 \times 10^{15}$ m^{-3}). It decreases gradually to the discharge edges. This gradient causes an ambipolar drift of the ions and is, in combination with the ambipolar electric field of the bulk plasma, the reason for the ion streaming discussed above. The
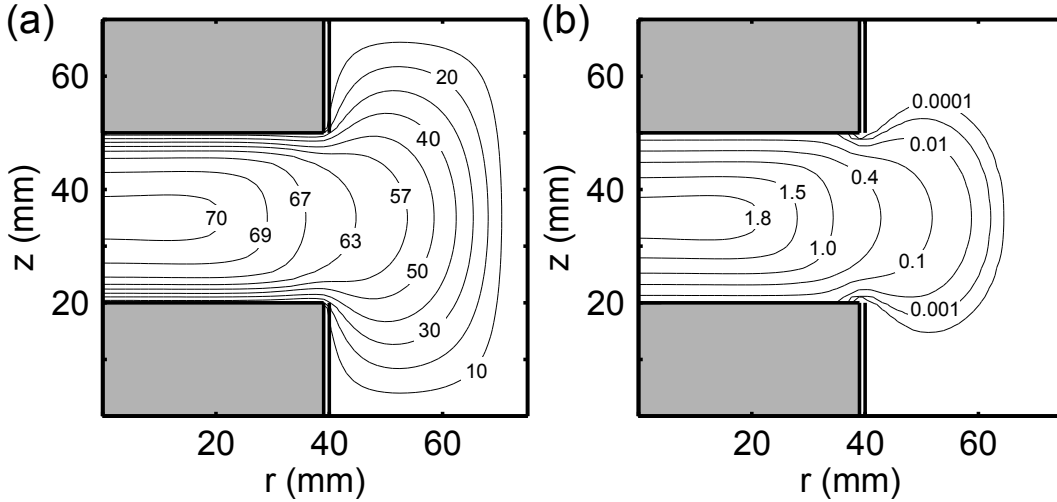
Figure 3.2: SIGLO simulation of the rf discharge in the IMPF-K2 chamber at $p = 30$ Pa and $U_{rf} = 65$ V_{pp}. (a) Plasma potential in Volt and (b) electron density normalized to 10^{15} m^{-3}. Both quantities are highest in the discharge center, which means that ions stream radially outwards from the center to the discharge edges. The electrodes (gray rectangles) and guard rings (vertical bars) are admitted to the sketch for a better orientation.

simulated temperature profile is almost constant between the electrodes ($T_e \approx 6$ eV). However, this value is not in agreement with the measurements of Ref. [185], which give significantly lower temperatures of $T_e = (3-4)$ eV. There, it was also shown that the temperature increases when dust is present. Ions and dust are usually assumed to be at room temperature [56]. The OML model then yields typical particle charges of $Q_d = -(17000\ldots32000)e$, depending on the particle size. Using a model, which accounts for streaming ions [187], leads to significantly lower charges [$Q_d = -(8000\ldots12000)e$]. They are more reliable in the present situation.

The SIGLO simulations did not take into account any influence of the dust particles and are thus only a rough estimation of the plasma parameters. However, several specialized simulations were carried out that modeled dust particles and background plasma simultaneously [139, 141, 188, 189]. Those simulations addressed the particular geometry of the PKE chamber [47], which is quite similar to IMPF-K2, except for smaller electrode diameters. Hence, the results of these investigations can be transferred carefully and allow reasonable comparisons. It was found [188] that the plasma potential in the dusty discharge decreases in the entire discharge but keeps its spatial topology. In contrast, the electron density in the dusty discharge drops significantly in regions of high dust densities. This electron depletion results from the charge competition between the dust grains. The simulations [188, 189] showed that electrons almost disappear inside the dust cloud whereas the density remains constant inside the void. Hence, the topology of the electron density distribution differs markedly from that obtained from SIGLO simulations.

## 3.2 Analysis of the Spatio-Temporal Wave Properties

In this Section, different techniques for the analysis of dust-density waves are introduced. Each method is demonstrated by applying it to the wave field in Fig. 3.3 (a), which was recorded at $p = 30$ Pa and $U_{\mathrm{rf}} = 65$ V$_{\mathrm{pp}}$ ($d = 2r_{\mathrm{d}} = 6.84$ μm). The waves are similar to those of Fig. 2.2 (b) but cover the entire dust cloud. Moreover, the Figure reveals another typical feature of the examined DDWs: The wave field is spatially disordered similar to ripple marks in the sand at shores. The wavelength is spatially varying and bifurcations occur at positions where two wave fronts split or merge.

For the analysis of DDWs, most of the previous investigations evaluated the dust density itself since it can be obtained directly from the primary recorded light intensity. This is due to the fact that both quantities are proportional to each other, see, e.g., Refs. [50, 51, 83, 190]. However, this approximation is only justified if the granularity of the particles can be neglected. To meet this requirement, the raw images are usually blurred with a Gaussian low-pass filter. The dust density is also used as input for the presented analysis but it should be mentioned that other quantities contain information about the waves as well. For example, the velocity of individual dust particles allows to determine wave frequencies and derived parameters [77].

3.2.1 Space-Time Diagram

The easiest way to determine the main wave properties is given in terms of a space-time diagram. It transforms the intensity evolution along a selected line in the wave field into a two-dimensional map, where the abscissa represents the time and the ordinate represents the spatial dimension. Since space-time diagrams can be analyzed without any complicated preprocessing they are widely used for the analysis of DDWs [51, 80, 87, 150]. A typical example of such a diagram, compiled for the dashed line in the wave field of Fig. 3.3 (a), is shown in Fig. 3.3 (b). For a better visualization, a closeup of the black rectangle is displayed in Fig. 3.3 (d). Single wave fronts can be tracked over time as oblique lines of maximum intensity. Obviously, this spatio-temporal illustration of the waves also contains bifurcations (green circle), which were found in the raw data as pure spatial events. In the diagram, a wave frequency can be defined very intuitively as the inverse time lag between characteristic wave features. This can be the distance between two wave troughs or wave crests, respectively, as illustrated in Fig. 3.3 (d) by a red horizontal bar. The wavelength is measured analogously by corresponding distances parallel to the abscissa (blue vertical bar) and the phase velocity can be detected as the slope of a tangent to the wave fronts (oblique orange line). The presented diagram reveals that the frequency (and also the wavelength) for a fixed spatial position is temporally almost constant, except for positions in the vicinity of a bifurcation. There, the frequency changes dramatically for a short time.

Unfortunately, these events cannot be analyzed precisely in space-time diagrams since they are restricted to the chosen line. In addition, the diagrams yield erroneous
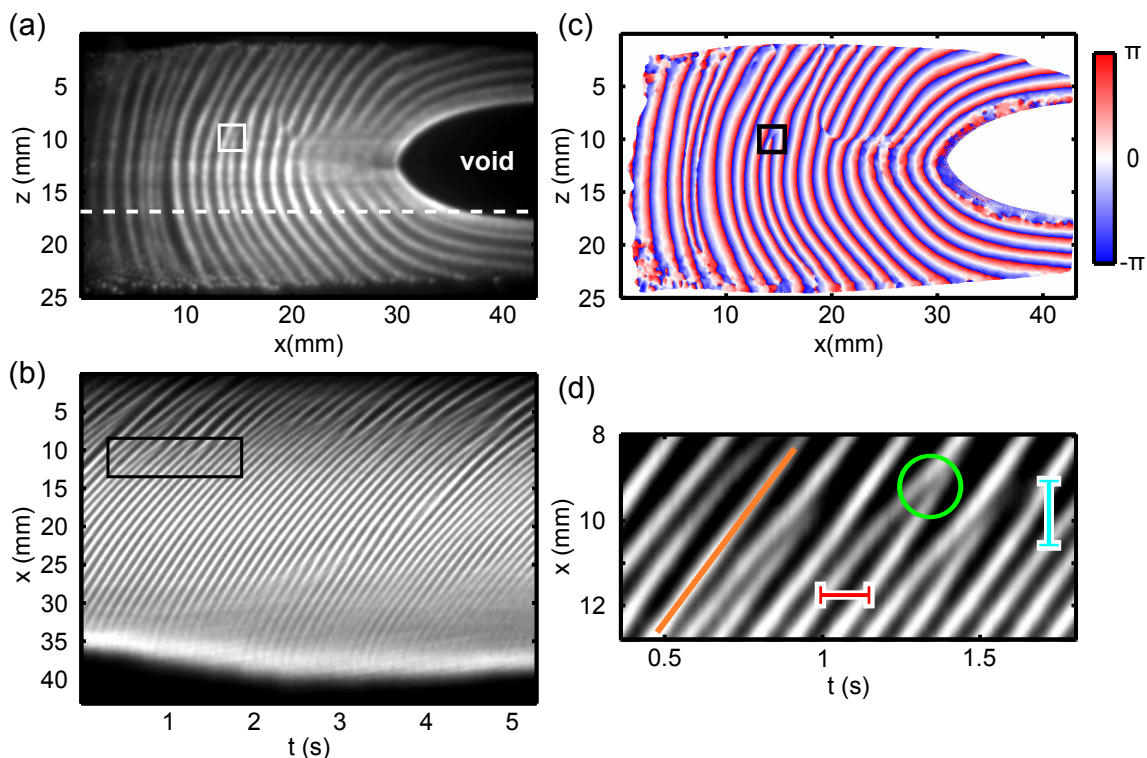
Figure 3.3: (a) Blurred raw image of a typical wave field under microgravity conditions. The waves propagate radially outwards from the void to the discharge edges. A bifurcation of two merging or splitting wave fronts can be observed in the white square. It is called a topological defect. (b) Space-time diagram for the dashed line in the wave field. (c) Phase map of the wave field. It clearly resembles the raw data and depicts wave activity in regions of low dust density, which is not detected visually in the raw data. (d) Closeup of the space-time diagram. The bars indicate wavelength (vertical bar), wave period (horizontal bar) and phase velocity (oblique line). (Adapted from Appendix B.3)

wave properties if this line does not coincide with the direction of wave propagation. In the presented example this leads to too large wavelengths near the void. As a consequence, space-diagrams are mainly used for the analysis of systems with one preferred direction as in the sheath of rf discharges, see, e.g., Ref. [80].

3.2.2 Fourier Analysis

The most obvious method to investigate the frequency content of the waves in more detail is a spectral analysis by means of a Fast Fourier Transform (FFT). A typical power spectrum is shown in Fig. 3.4 (d). It was determined for the time series in Fig. 3.4 (a), which was recorded at the center of the white square in Fig. 3.3 (a). It consists of a dominant peak at $f \approx 8.7$ Hz and a slightly asymmetric sideband structure.

The FFT represents a standard technique within the context of wave analysis and was applied to DDWs in numerous works [51, 78, 89, 150, 190]. Since the intensity is recorded at each position of the camera sensor, one obtains two-dimensional fre-
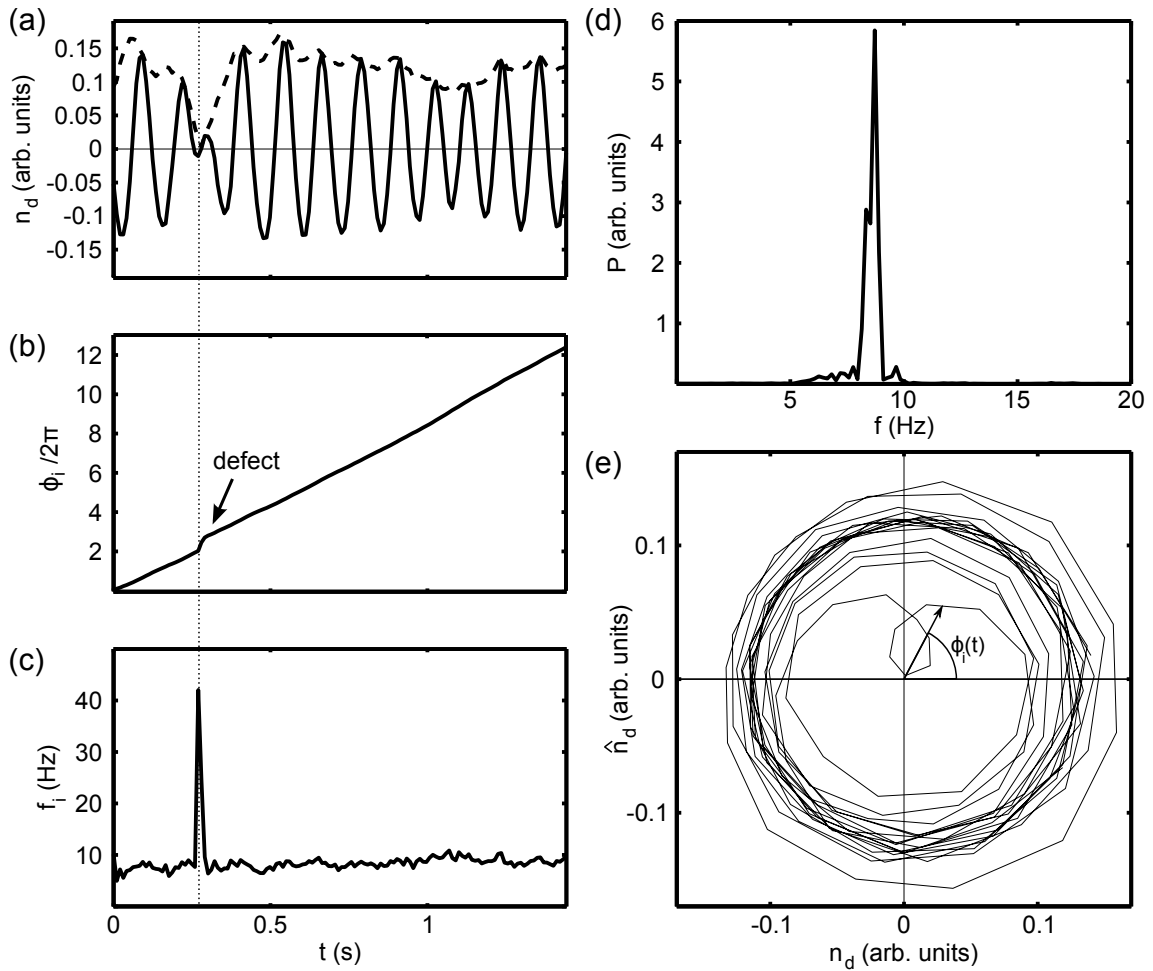
Figure 3.4: (a) Sample time series of the zero-mean dust-density evolution $n_d(t)$. The envelope function $E(t)$ is marked by a dashed line. (b) Corresponding instantaneous phase evolution $\phi_i(t)$. (c) Corresponding instantaneous frequency $f_i(t)$. (d) Power spectrum. (e) Analytic signal $A(t)$ in the complex plane. (Panels (a)-(c) adapted from Appendix B.3)

quency distributions [150]. The method is also feasible to examine the behavior of higher harmonics in the signal. Recently, this information was used to analyze the development of nonlinearity at the onset of wave motion [89]. The FFT can be further used to determine the dispersion relation of the self-excited waves directly, i.e., without synchronizing with an external signal, if the Fourier transform is performed in the space and in the time domain simultaneously [190].

Although the Fourier analysis offers a lot of advantages, it is not able to describe the spatio-temporal behavior of the waves and, in particular, that of the bifurcations adequately. This is due to the fact that the FFT is an integrating technique with a time-averaging character. Signals that include transient phenomena with a temporally varying frequency exhibit broad spectra. Consequently, the identification of the wave frequency as the maximum peak in the spectrum, as widely used, is not reasonable for the examined nonlinear DDWs. Even a refined definition using the weighted spectral intensity [150] is not suitable to capture all features of the waves.

3.2.3 Analytic Signal

It was described in Sec. 3.2.1 that the space time diagram is, in principle, able to resolve the spatio-temporal behavior of the dust-density waves. Nevertheless, it only provides information for one spatial dimension. The Fourier analysis allows to evaluate the frequency content of the waves at each position of the wave field but is not able to describe transient phenomena. A possibility to combine both aspects is given by the analytic signal. So far this concept was not applied within the context of dusty plasmas and should thus be introduced in the following. The derived wave attributes will be described in detail.

The analytic signal at an arbitrary position (x, z) in the wave field reads

$$A(t) = n_\mathrm{d}(x, z, t) + i \cdot \hat{n}_\mathrm{d}(x, z, t) \tag{3.1}$$

and is an expansion of the original time series $n_\mathrm{d}(x, z, t)$ into the complex plane. It was first introduced by Gabor [191]. The imaginary part $\hat{n}_\mathrm{d}(x, z, t)$ of the new signal is determined by shifting the original time series $n_\mathrm{d}(x, z, t)$ by $T/4$, i.e., a quarter of the wave period. Mathematically, this operation is called Hilbert transform $H\{n_\mathrm{d}(x, z, t)\}$ and is defined as

$$\hat{n}_\mathrm{d}(x, z, t) = H\{n_\mathrm{d}(x, z, t)\} = \frac{1}{\pi} \int_{-\infty}^{+\infty} \frac{n_\mathrm{d}(x, z, \tau)}{t - \tau} \mathrm{d}\tau. \tag{3.2}$$

The integral corresponds to a convolution of $n_\mathrm{d}(x, z, t)$ with $(\pi t)^{-1}$ and discards the negative frequency components from the spectrum, which are included in any real-valued signal. The Hilbert transform represents a standard technique in digital signal processing since it allows to derive modulation techniques [192]. The analytic signal can be interpreted as a vector that rotates in the complex plane. It is then better expressed by an angle, the so-called instantaneous phase $\phi_\mathrm{i}(t)$, and a corresponding length, the so-called envelope function $E(t)$. Both quantities can be calculated from the original components of $A(t)$ by rewriting it using Euler's notation as $A(x, z, t) = E(x, z, t) \cdot \exp\left[i \cdot \phi(x, z, t)\right]$. Hence, one obtains

$$E(x, z, t) = \left[n_\mathrm{d}(x, z, t)^2 + \hat{n}_\mathrm{d}(x, z, t)^2\right]^{1/2} \tag{3.3}$$

and

$$\phi_\mathrm{i}(x, z, t) = \mathrm{atan2}\left[\hat{n}_\mathrm{d}(x, z, t), n_\mathrm{d}(x, z, t)\right]. \tag{3.4}$$

There, the function atan2 is a variation of $\arctan(\hat{n}_\mathrm{d}/n_\mathrm{d})$ that measures the angle of a vector for the full range $-\pi < \phi_\mathrm{i} < \pi$.

The analytic signal of the sample time series in the complex plane is illustrated in Fig. 3.4 (e). It rotates (counterclockwise) around the origin, except for a distinct time step, where the trajectory intersects itself. Since the length of the vector also represents the amplitude of the time series, it is added in Fig. 3.4 (a) as a dashed line. One clearly sees that the amplitude is strongly modulated: The modulation within one period results from nonlinearity and the modulation on a larger time scale is due to non-stationarity. The evolution of the corresponding unwrapped instantaneous

24

phase[2] is shown in Fig. 3.4 (b). It increases monotonically but deviates slightly from a linear function due to nonlinearity. This means, however, that the analytic signal does not rotate at a constant velocity and the well-known definition of the angular frequency, $\omega = (2\pi)/T$, where T is the oscillation period, does not hold for the depicted time series. This leads to a modified definition, which accounts for such a nonlinear temporal behavior. It reads

$$\omega_{\mathrm{i}}(x, z, t) = \left.\frac{\partial \phi_{\mathrm{i}}(x, z, t')}{\partial t'}\right|_{t'=t} \tag{3.5}$$

and is called instantaneous angular frequency[3]. The corresponding evolution is shown in Fig. 3.4 (c). Here, the fluctuations due to nonlinearity are even more pronounced than in the amplitude and phase evolution. Since phase and frequency are determined for each time step of the originally recorded dust density, their temporal resolution coincides with the frame rate of the camera.

Due to the fact that the wave attributes are affected by temporal modulations on different time scales, it is useful to average the instantaneous frequency over a carefully selected time interval ΔT depending on the specific purpose of the data analysis. No averaging gives the instantaneous properties of the wave. Averaging over a complete wave period ($\approx$ 10–20 frames) discards effects of nonlinearity and improves the signal-to-noise ratio. The resulting frequency then matches the inverse time lag between characteristic wave features, i.e., the frequency definition for space-time diagrams. Averaging over several wave periods (> 100 frames) yields global wave properties and corresponds to a time averaged frequency of the space-time diagram. This variant is used to define a time-independent frequency for each spot in the wave field as $f_{\mathrm{m}}(x, z) = \langle f_{\mathrm{i}}(x, z, t)\rangle_{\Delta T}$, which corresponds to a spatial frequency distribution.

3.2.4 Defect Detection

The most prominent feature in the analyzed time series of Fig. 3.4 (a) is found at $t \approx 0.3$ s. There, the amplitude of the signal almost vanishes. At the same time step, the phase suddenly jumps and the instantaneous frequency increases drastically. This special event is known as phase or topological defect or simply as dislocation. The influence of these defects on the global frequency distribution is addressed in Sec. 4.3. It is found that defects are no pure temporal features, which appear in dust-density evolution. They are rather spatio-temporal events and coincide with the above mentioned bifurcations in the wave fields.

The instantaneous phase of Eq. (3.4) can be used to reconstruct the recorded two-dimensional sections through the dust cloud. Figure 3.3(c) shows the phase map of the raw image of Fig. 3.3 (a). It clearly resembles the wave field and consequently

---

[2]Note, that two definitions of the instantaneous phase are common: The wrapped phase accounts for the rotation in the complex plane and is restricted to the interval $\phi_i \in [0, 2\pi)$. The unwrapped phase is not restricted and thus has no 2π-periodicity.

[3]In the literature, instantaneous angular frequency and instantaneous frequency are often used synonymously, although the latter is defined as $f_{\mathrm{i}} = \omega_{\mathrm{i}}/(2\pi)$.
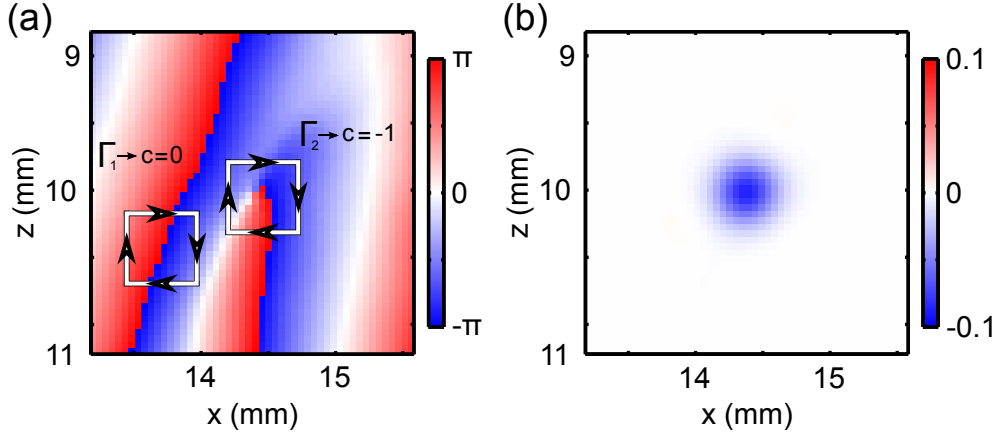
Figure 3.5: (a) The spatial phase information in the vicinity of a defect. Two paths, according to Eq. (3.6), are drawn. One path (Γ_1) is located on a wave front and the other one (Γ_2) encircles a defect. Only the latter contributes to the topological charge. (b) Topological charge density $c_d(x, z)$, according to Eq. (3.7), for the same image. (Adapted from Appendix B.3)

includes also the position of all occurring topological defects. Other methods have been introduced that also determine the phase at a high temporal resolution, either within the context of dusty plasmas [80] or in other fields [8]. Nevertheless, those approaches include comparably complicated calculations and the evaluated time series are subject to strict requirements. The defect positions can be extracted from the phase map with the aid of the topological charge

$$c(x, z, t) = \frac{1}{2\pi} \oint_{\Gamma} \vec{\nabla} \phi_i(x, z, t) \cdot \mathrm{d}\vec{l},$$ (3.6)

which was originally established by Nye and Berry [193] for the analysis of singularities in ultrasonic waves. It was subsequently applied in numerous studies [8,194–196]. The definition is in analogy to the Burgers vector that characterizes defects in solids and is well known in crystallography [197]. In Eq. (3.6), infinitesimal phase differences $\vec{\nabla} \phi_i$ are summed up along a closed path Γ. Consequently, only those paths contribute to the topological charge which encircle a defect. The method is illustrated in Fig. 3.5 (a), which shows a closeup of Fig. 3.3 (c) in the vicinity of a defect, marked by a black square. Two paths are drawn. Path Γ_1 has its center on a wave front. The other path, Γ_2, has its center on a defect. Thus only the charge that is assigned to Γ_2 differs from zero.

Applying Stokes's theorem on Eq. (3.6) allows to further define the topological charge density as [198]

$$c_d(x, z, t) = \frac{1}{2\pi} \left[\vec{\nabla} \times \vec{\nabla} \phi_i(x, z, t) \right].$$ (3.7)

This conversion allows to determine the topological charge with a significant reduction of computation time. The result for the phase map in Fig. 3.5 (a) is shown in Fig. 3.5 (b). Since the vector field $\vec{\nabla} \phi_i$ was initially blurred with a Gaussian filter

the resulting profiles of $c_d(x, z, t)$ are very smooth. The charge that is assigned to a defect is given by the sum of all corresponding pixels. It takes values of $+1$ or -1, where the sign is given by the sense of rotation of the phase. In principle defects of higher order, i.e., higher integers, are possible, if three or more wave fronts merge into a single one. This was not observed in the analyzed wave fields.

For the actual detection of a topological defect, standard particle detection algorithms [61, 199] can be applied to the calculated charge density maps. They work with a high accuracy since the defects are several interparticle distances from each other apart and the charge density of a defect is almost Gaussian distributed.
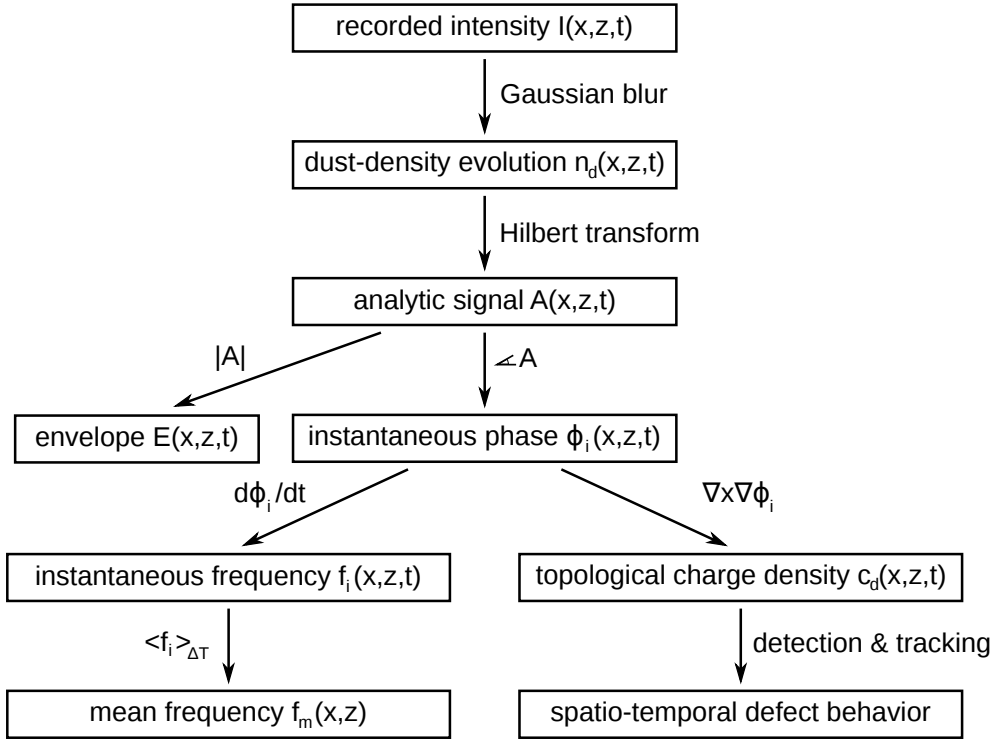
3.3 Concluding Remarks

In this thesis, dust-density waves were observed in the IMPF-K2 chamber, a capacitively coupled rf reactor. The specific experiment parameters, at which DDWs can be observed, are similar to those of previous investigations in rf discharges [55, 56]. Since the experiments were carried out under microgravity on parabolic flights, the number of recorded video sequences and the length of each video were limited. The basic topology of the discharge was characterized with the aid of a SIGLO simulation, which estimated the plasma potential and electron density profiles. Although other simulations, which included dust particles as additional species, revealed that the discharge parameters change significantly, if dust is present, the SIGLO simulation allowed to explain the appearance of streaming ions, which are made responsible to excite the waves.

For the analysis of the observed waves, a large number of mathematical methods exist. Within the context of dusty plasmas, the space-time diagram and the Fourier analysis are the most common ones. Further approaches have been used in previous works, as for example the singular value decomposition [76] or a phase sensitive method, described in Ref. [80]. They also provide useful information on the wave characteristics but cannot be further described here.

The DDWs in extended three-dimensional dust clouds comprise a very complicated spatio-temporal behavior, covered by transient phenomena like topological defects. In this case, the Fourier analysis is not able to describe the waves adequately since it has a time-averaging character. Such description is generally possible with the space-time diagram. However, detailed conclusions concerning the defect behavior cannot be drawn either since the temporal resolution of the diagrams is of the order of a wave period. Moreover, the diagram is suitable for one-dimensional processes only.

Consequently, it is necessary to expand the group of well-established techniques. For this purpose, the Hilbert transform has been introduced as a complementary method. It expands the measured time series into the complex plane, generating the so-called analytic signal. This concept is widely used in various different research fields, such as physiology, biology and nonlinear dynamics [9] but has not been applied to dust-density waves so far. Its main advantage is that it facilitates to investigate the waves on individually chosen time scales similar to the Wavelet

```
                    ┌──────────────────────────┐
                    │  recorded intensity I(x,z,t)  │
                    └──────────────────────────┘
                                │  Gaussian blur
                                ▼
                  ┌─────────────────────────────┐
                  │  dust-density evolution n_d(x,z,t) │
                  └─────────────────────────────┘
                                │  Hilbert transform
                                ▼
                     ┌───────────────────────┐
                     │  analytic signal A(x,z,t)  │
                     └───────────────────────┘
                    |A|                    ∡A
              ▼                                  ▼
   ┌──────────────────┐   ┌──────────────────────────┐
   │ envelope E(x,z,t) │   │ instantaneous phase φ_i(x,z,t) │
   └──────────────────┘   └──────────────────────────┘
               dφ_i/dt                  ∇×∇φ_i
          ▼                                      ▼
┌─────────────────────────────┐   ┌──────────────────────────────┐
│ instantaneous frequency f_i(x,z,t) │ │ topological charge density c_d(x,z,t) │
└─────────────────────────────┘   └──────────────────────────────┘
        <f_i>_{ΔT} │                    detection & tracking │
                   ▼                                         ▼
   ┌─────────────────────────┐   ┌─────────────────────────────┐
   │  mean frequency f_m(x,z)  │   │  spatio-temporal defect behavior │
   └─────────────────────────┘   └─────────────────────────────┘
```

Figure 3.6: Schematic of the developed analysis workflow, which is based on the analytic signal.

transform, which also allows an adaptive control of the temporal resolution. Within the context of this thesis, a workflow has been developed, which is based on the analytic signal and captures the complete spatio-temporal behavior of the DDWs. The schematic of Fig. 3.6 summarizes the corresponding steps.

The analytic signal allows to derive instantaneous wave properties, as, e.g., the envelope function or the phase of a wave. Here, instantaneous means that the temporal resolution of each of this quantities coincides with the frame rate of the camera. The spatial resolution is given by the resolution of the camera sensor. The instantaneous phase information can be used to reconstruct the wave field at each time step. This in turn leads to a very accurate detection of the defects by means of the topological charge.

The analysis further provides mean wave properties if the instantaneous quantities are averaged over a sufficiently long time interval: Averaging over one wave period discards any nonlinear features and choosing a time interval of several wave periods suppresses effects from non-stationary situations. This is of interest for the mean frequency since the method allows to compile the global frequency content of a wave field. However, this definition of a wave frequency is not unambiguous and other approaches are possible. The most intuitive one concerns the counting of characteristic wave features as, e.g., wave crests or troughs, and the subsequent averaging over an appropriate time interval. This method can be applied to space-time diagrams or the original time series. Nevertheless, this definition coincides with that of an averaged instantaneous frequency and was not used in this work since the

numerical effort is comparably high.

The Fourier analysis also allows the definition of a mean frequency, commonly given by the maximum peak of the spectrum. This approach is restricted to one spectral component and disregards the information of other components. It is thus less reliable than the averaged instantaneous frequency. Moreover, the spectra of the conducted experiments have a rather poor resolution due to the limited recording time during the parabolas. For a critical discussion of the complex problem of a frequency definition the interested reader is referred to further literature as, e.g., the comprehensive articles of Refs. [200, 201].

In the following Chapter the spatial frequency distribution of the waves and the spatio-temporal behavior of the defects, which are both analyzed using the analytic signal, are first investigated separately and afterwards the relationship between the results is discussed.

4 Self-Excited Dust-Density Waves Under Microgravity

The presented examples of dust-density wave fields under microgravity conditions comprised a complicated wave pattern, especially due to the amount of topological defects. At the beginning of this Chapter it is shown that DDWs exist that contain almost no such defects. These waves exhibit a strong spatial coherence and allow to reconstruct the three-dimensional structure of the dust cloud. In order to investigate the differences between the coherent and incoherent wave states, the frequency content of the wave fields is analyzed using the previously introduced methods. It turns out that the frequency distribution of the incoherent waves is spatially not constant. Instead, regions of different but almost constant frequency occur, so-called frequency clusters. This observation is new within the context of dusty plasmas. Since the investigated wave states differ in particular in the amount of appearing defects, a detailed study of the spatio-temporal behavior of the defects is performed. It reveals that the defects appear at the boundaries between adjacent clusters and, moreover, that DDWs show similarities with relaxation oscillators.

4.1 Global Wave Structure

In this Section the global structure of dust-density wave fields is investigated. For this purpose, the recorded sections through the dust clouds are analyzed. The problem of how far the evaluated two-dimensional information is representative for the behavior of the waves is clarified by means of a reconstruction of the three-dimensional wave using the scanning video microscope.

Wave States

A first insight into the global behavior of the DDWs is gained from a direct look at single video frames. Two examples[1] are shown in Figs. 4.1 (a) and (b), recorded at $U_{\rm rf} = 70$ $V_{\rm pp}$ for particles with a diameter of $d = 6.8$ μm and at gas pressures of $p = 15$ Pa and $p = 30$ Pa, respectively. In both cases, the waves propagate radially outwards from the void boundary, as expected. The first wave field exhibits a very high spatial and temporal coherence. It shows no defect structures. The spatial coherence perpendicular to the wave propagation is even so strong that the wave

---

[1]The DDWs in this Sections were recorded during the parabolic flight campaign 2007, i.e., in the IMPF-K chamber and not in the IMPF-K2 chamber. The ring electrode was biased at $U_{\rm rf} = 50$ $V_{\rm pp}$.
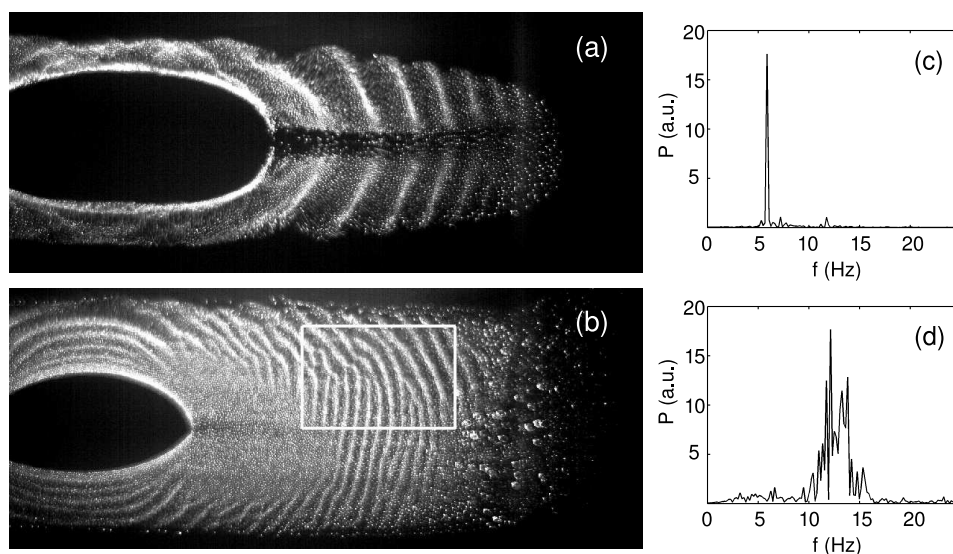
Figure 4.1: Specific states of dust-density wave fields. (a) Coherent situation and (b) polychrome situation. The large particles in the dust cloud periphery in both figures are dust agglomerates. (c) Power spectrum of the coherent wave field and (d) power spectrum of the polychrome wave field. (Adapted from Appendix B.1)

fronts in the upper and lower part of the cloud are correlated to each other over the dust free region in the equatorial plane. A similar behavior is found in the wave field of Fig. 3.3 (a). There, the wave fronts seem to be connected beyond a region of low dust density in the vicinity of the void boundary, in which no wave activity can be observed visually. In this example another advantage of the phase map becomes obvious as it clearly depicts that the wave fronts are indeed connected [see Fig. 3.3 (c)]. The second wave field in Fig. 4.1 (b) shows a completely different situation: A defect structure is clearly visible. Single wave fronts split or merge at various positions in the wave field. Since the defects obviously diminish the coherence in the system, the total number of defects can be interpreted as a measure for the coherence. This is similar to Ref. [8], where the defects were introduced as a measure of disorder.

The difference between the exposed wave fields is even more pronounced in their Fourier spectra. Figure 4.1(c) shows a typical power spectrum inside the coherent waves. Only one sharp peak exists at $f = 5.9$ Hz. Moreover, the shape of this spectrum is similar for all locations in the dust cloud and the corresponding frequency of the maximum peak deviates only by a few tenths percent from the mean of the entire wave field. The spectrum of the second wave field in Fig. 4.1 (d) differs significantly from the first case: It is broadband and consists of multiple peaks. This implies that the number of wave fronts that passes a fixed point per time varies temporally, which means that the temporal coherence is low. Furthermore, the frequency of the maximum peak deviates much stronger over the dust cloud.
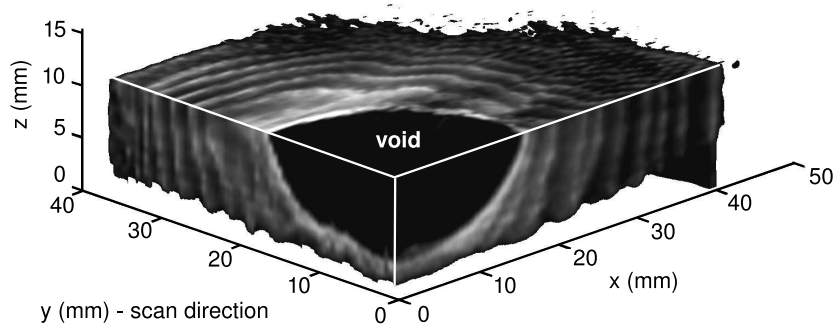
Figure 4.2: Octant of a reconstructed three-dimensional dust-density wave field obtained from a camera scan through the dust cloud. The recorded images lie in the xz-plane. The scan was performed along the y-axis. Potential irregularities are due to fluctuations of residual gravity. (Adapted from Appendix B.1)

Three-Dimensional Structure

As mentioned above, the dust-density waves exhibit an extended three-dimensional structure. In order to verify that the two-dimensional diagnostics provides representative data, it is necessary to get a general idea of this structure. Although there are several methods, which allow to detect three-dimensional particle positions [202–206], none of them could be applied on dust-density waves so far due to the high dust density inside the wave crests. In addition the observed volumes were very small, including at most one wavelength, which prevents the analysis of extended wave fields.

However, the existing scanning video microscope, which was introduced in Sec. 3.1, allows camera scans through the dust cloud perpendicular to the recorded sections. This in turn can be used in combination with the high global coherence of some of the waves to reconstruct a still image of a three-dimensional wave field. Since a successful reconstruction assumes a high degree of coherence, first a correlation analysis between different locations in the wave field is performed to assure this requirement. Afterwards, the images with a constant phase relation to each other are selected from a complete sequence recorded during a scan. This means that the time lag $\Delta T = n/f_{\mathrm{rec}}$ between two chosen frames is an integer multiple of the reciprocal reconstruction frequency f_{rec}, which is identified as the maximum of a spectrum taken during a scan. Since the velocity of the translation stage ($v = 3.15$ mm/s) is of the order of the phase velocity of the waves, the reconstruction frequency does not coincide with the frequency of the waves but is Doppler-shifted to a higher value. After the images have been selected they are combined to a three-dimensional data set since they can be treated as if they were recorded at the same time. The different spatial resolutions along the spatial axes are adjusted by linear interpolation. The result of a reconstruction can be seen in Fig. 4.2. For a better illustration only one octant of the dust cloud is shown. The scan was performed along the y-axis and the recorded images lie in the xz-plane. The reconstruction clearly reveals the shape of single wave fronts, which concentrically surround the void. It substantiates the presumption of a rotational symmetry. Hence, the realized reconstructions allow the

conclusion that the recorded two-dimensional sections through the dust cloud are representative in the sense that the wave field has no preferred direction. Nevertheless the presented method is not able to describe transient wave phenomena since they would inevitably break the rotational symmetry of the dust cloud.
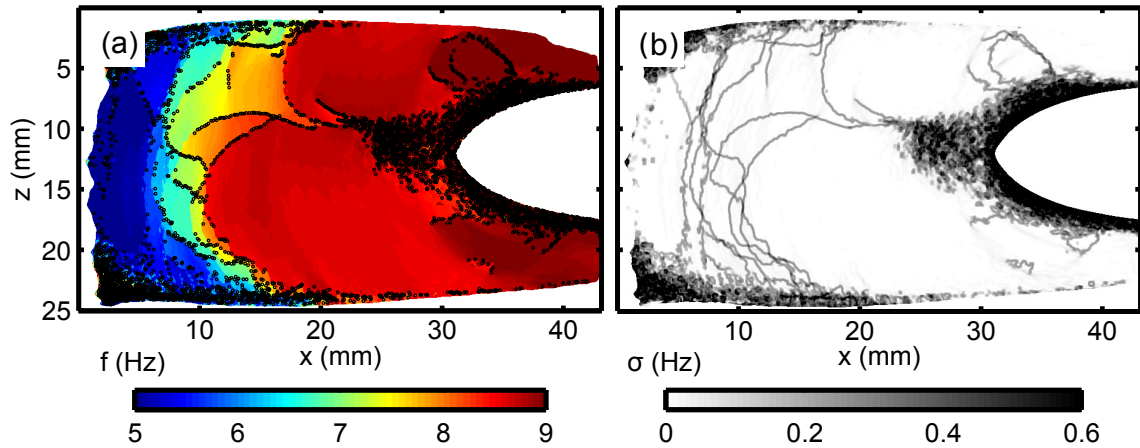
4.2 Frequency Distributions of the Waves

The last Section showed that, according to the discharge parameters, the waves show different behaviors: They reside either in a coherent state or in a polychrome state. The differences become especially apparent in the Fourier spectra. In this Section the spatial frequency content of the wave fields is determined in order to investigate the wave states in more detail and find hints for a possible explanation of their appearance. For this purpose, the developed procedure, which is based on the analytic signal, is applied to the waves. Since the waves are found in the polychrome wave state in the majority of measurements, this state is examined first.

Frequency Clusters

The schematic of the workflow in Fig. 3.6 shows that the analytic signal leads to a time-averaged spatial frequency distribution $f_{\mathrm{m}}(x, z)$. For the exposed measurements the time series are averaged over 10–20 wave periods. The distribution for the wave field in Fig. 3.3 (a) is shown in Fig. 4.3 (a). Suprisingly, the frequency is not spatially constant but decreases from the void boundary to the discharge edges, i.e., the waves propagate from higher to lower frequencies. This result cannot be understood within Huygens' linear wave model. There, one would expect that the wavelength adjusts to any parameter variations in system and the frequency remains constant. The obtained distribution is even more remarkable since the frequency decay is not continuous, which might have been expected from the fact that the plasma parameters vary gradually, as was shown in Fig. 3.2. Instead, regions of almost constant frequency form, which are separated by boundaries of abrupt frequency jumps. These distinct domains are called frequency cluster or frequency cells. The largest clusters in the exposed example have frequencies of $f_1 = 5.2$ Hz, $f_2 = 7.8$ Hz and $f_3 = 8.6$ Hz. The effect of frequency clustering has been observed in dust-density waves for the first time within the scope of this thesis. Only a few experimental studies in other systems were reported previously. This applies for vortex streets behind cylinders, where the shedding frequency was found to vary stepwise with water height although the stream velocity decreases gradually [207,208]. Furthermore, it was shown that sections of the small intestine of mammalians agree on a common oscillation frequency [209,210]. Both cases treated purely one-dimensional systems.

As explained in Sec. 3.3, space-time diagrams also allow to determine wave frequencies and can be used in principle to determine spatial frequency distributions. Corresponding results are described in Appendix B.3. They also suggest the formation of clusters. However, the analysis cannot resolve fine structures and is not

Figure 4.3: (a) Frequency distribution for the wave field of Fig. 3.3 (a), obtained from the time-averaged instantaneous frequency. Clusters of constant frequency form. They are separated by distinct frequency jumps at the boundaries. Topological defects (black dots) occur almost exclusively at these locations. (b) The spatial standard deviation of the frequency distribution shows that almost no variation is found inside the clusters. Pixels with no wave activity were removed from both maps. (Adapted from Appendix B.3)

able to provide a two-dimensional distribution as obtained from the analytic signal. Nevertheless, this complementary method substantiates the described finding.

To further verify the idea of frequency clustering, the standard deviation of the spatial frequency variations is calculated in a (5×5) vicinity at each position in the wave field. The resulting map is displayed in Fig. 4.3 (b). It reveals well-defined cluster boundaries at locations where the standard deviation is sufficiently large. In contrast only small deviations are found inside the clusters. The cluster boundaries can be obtained in a similar way by using the so-called effective diffusion coefficient as introduced in Ref. [211].

Comparison With Numerical Simulations

Besides experimental studies, there are several numerical investigations of frequency clusters. They examined the influence of varying system parameters on the cluster behavior. In the following, these simulations are briefly introduced and their results are compared with the measurements of dust-density waves.

Interestingly, all of the numerical investigations contain the same basic ingredients, namely a network of mutually coupled self-sustained nonlinear oscillators, which is subject to a spatial dispersion of natural frequencies. The simulations mainly differ in the choice of the distinct oscillator. They cover van-der-Pol oscillators [208, 210, 212–214], circle maps [215], Rössler oscillators [216], Ginzburg-Landau systems [211, 217–219] and Luo-Rudy heart cells [220]. A review on most of these works can be found in Ref. [221]. The investigations yielded three tendencies concerning the dependence of the cluster size on the variation of system parameters: The cluster size, i.e., the number of corresponding oscillators, increases with the
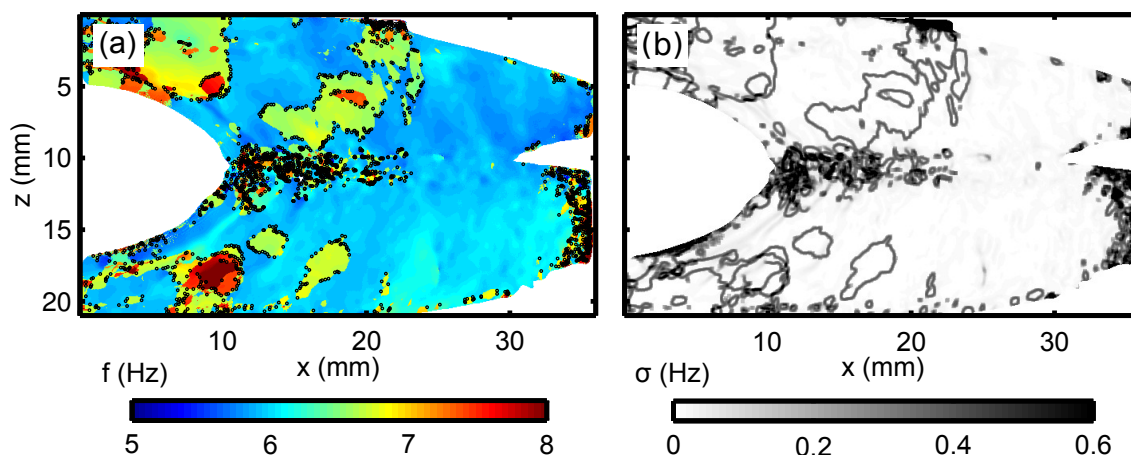
Figure 4.4: (a) Frequency distribution for the wave field of Fig. 4.1 (a), obtained from the time-averaged instantaneous frequency. The distribution comprises one large cluster. Topological defects are marked by black dots. (b) Spatial standard deviation of the frequency distribution. Pixels with no wave activity were removed from both maps. (Adapted from Appendix B.2)

coupling strength [210–212, 217, 218] or with the degree of nonlinearity [217, 218] or if the gradient of natural frequencies decreases [217, 218].

In order to find hints for these tendencies in the experimentally observed dust-density waves, the presented frequency distribution is compared with the distribution of the highly coherent waves of Fig. 4.1 (a). The compiled frequency map and the corresponding map of standard deviations are shown in Figs. 4.4 (a) and (b). They reveal a significantly different topology in that the wave field consists of one large cluster with only few rather small embedded cells. This result could already be expected from the fact that the maximum peak of the power spectra varied only slightly over the entire wave field, as mentioned in Section 4.1.

The degree of nonlinearity is estimated for both wave fields. It can be identified as the asymmetry of the zero-mean dust-density evolution with respect to the time axis, averaged over all positions in the cloud where a sufficiently high wave activity is detected. This asymmetry is determined from the ratio of signal maxima to signal minima. The given definition is reasonable since it describes the deviation of a signal from a sinusoidal function, which would result in a value of 1. The analysis shows that the coherent wave field has a markedly larger asymmetry (1.62) as the polychrome wave field (1.42). This agrees with the aforementioned simulations because the wave field with smaller clusters reveals a lower degree of nonlinearity.

Moreover, an analysis of the dust-density distribution, as described in Appendix B.3, disclosed that the dust density decreases gradually from the void to the discharge edges in each measurement. Since the frequency distribution shows a similar decrease —except for the clustering— this observation allows to identify the natural frequencies in the systems in first approximation with the local dust density. A comparison between the exposed situations showed that the density gradients in the coherent wave field are 2-3 times lower than for the polychrome waves. This

leads to the conclusion that the cluster size increases with a decreasing gradient of the natural frequency, as was found in the numerical simulations.

The influence of the coupling strength on the clusters size is not investigated since the coupling cannot be varied externally in a controlled manner in fluid dust clouds.
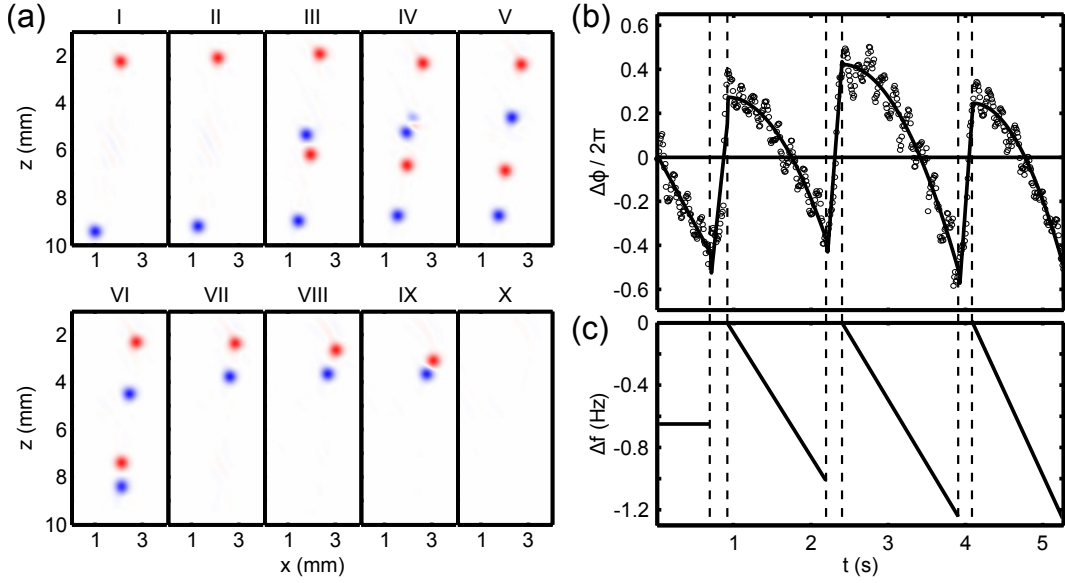
4.3 Topological Defects

The appearance of topological defects results in incoherent wave fields that comprise frequency clusters. In contrast, wave fields without defects consist of one cluster and are consequently monochromatic. In this Section the influence of defects on the cluster formation is investigated in more detail. For this purpose, the spatio-temporal behavior of the defects is studied and the phase and frequency evolutions at the cluster boundaries are analyzed.

Spatio-Temporal Behavior of Defects

The defect positions inside the dust cloud are determined by using the topological charge density as introduced in Sec. 3.2. Their temporal evolution can be obtained from suitable particle tracking algorithms, see Ref. [199]. The analysis shows that the defects neither rest at a fixed position in the dust cloud nor move together with the 'underlying' wave field. Instead, they move with 70–90% of the local phase velocity. Moreover, videos of the phase maps reveal that, at a bifurcation, the wave front that lags behind in moving direction is ruptured and caught up by the subsequent front. This in turn causes a new rupture and so forth. In accordance to previous investigations [195, 222], the defect velocity is split into a part that is perpendicular to the local phase velocity (climb motion) and an additional parallel part (glide motion). It is found that in most measurements, the glide motion exceeds the climb motion. The difference between defect velocity and wave velocity can be explained by the fact that a defect represents a spot of vanishing amplitude in the wave field. Thus, a defect results as a consequence of destructively interfering waves and it is therefore reasonable that the defect moves with the local group rather than the phase velocity.

The investigations also reveal that the defects often occur not isolated but they move together as pairs of opposite topological charge. The lateral distance between both defects can almost reach the height of the wave field. In Fig. 4.5 (a) such a pair is followed over ten successive frames. The lag between two steps is given by the frame rate of the camera as approximately 0.01 s. Two typical features can be seen in the sequence. In frame III, an additional pair of defects is created, which results in four defects of alternating charge. These pairs move together until the lower one annihilates at frame VII and the upper pair at frame X. This behavior is well known from other systems that contain defects, as for example ethanol-water mixtures [8] or inclined fluid layers [195].

To investigate the relationship between the occurrence of defects and the formation of frequency clusters, first, the defect positions in the frequency distributions are

Figure 4.5: (a) Motion of a defect pair with opposite topological charge. An additional pair is created in frame III, resulting in four defects of alternating charge. The lower pair is annihilated in frame VII and the upper one in frame X. The colorbar is the same as in Fig. 3.5 (b). (b) Temporal evolution of the phase difference $\Delta\phi(t) = \phi(t) - \bar{\phi}(t)$ (circles) at a cluster boundary. Parabolic functions were piecewise fitted to the data (straight line). (c) Frequency difference $\Delta\omega(t)$ derived from the temporal derivative of the fitted curve. Two different time scales are obvious. A slow evolution between two defects and a fast evolution when a defect occurs. (Adapted from Appendix B.2)

examined. The influence of the spatio-temporal evolution of individual defects on the cluster formation is discussed afterwards. In Figs. 4.3(a) and 4.4(a), each defect that appeared in the analyzed video sequence, is plotted on top of the determined frequency map. Obviously, the defects occur almost exclusively at the boundaries between two adjacent clusters. Only at the void boundary and the cloud edges, a high amount of defects can be observed. Hence, it stands to reason to make the defects responsible not only for a wavelength matching but also for the establishment of abrupt frequency jumps in the frequency distributions.

Similar results were also found in the aforementioned simulations. There, the defect occurred periodically and the step height between the clusters was proportional to the repetition rate [217]. However, this periodicity cannot be expected in the case of dust-density waves. This is due to the fact that waves are characterized by their three-dimensional topology and the clusters are three-dimensional objects, which are surrounded by boundary surfaces rather than lines. The defects occur on these surfaces along so-called nodal lines [196] and can enter or leave the plane of observation randomly. Hence, not all defects that form a cluster can be detected. Furthermore, temporal variations of the system parameters and noise lead to a broadening of the cluster boundaries [211], which causes that the defects do not appear repeatedly at the same position. An indication for this behavior in the measurements is the fact that some tracked defects suddenly disappear for one or two frames.

Phase Evolution at the Cluster Boundaries

The detection of the defects and the tracking of their motion allowed to investigate the relationship between defects and clusters. However, the analysis does not provide information on the defects at a microscopic level. For this purpose, the temporal evolutions of the instantaneous phase and frequency are investigated directly. Both quantities reveal significant variations from linear functions only at the cluster boundaries. The phase evolution can be studied even better if the phase difference, defined as $\Delta\phi(t) = \phi_i(t) - \bar{\phi}(t)$, is examined. There, the averaged phase evolution $\bar{\phi}(t)$, determined from a linear fit, is subtracted from the instantaneous phase $\phi_i(t)$ in order to elucidate the evolution on a smaller time scale. An example is displayed in Fig. 4.5 (b), indicated by circles. It shows a periodic pattern, in which three defects occur, each indicated by an abrupt phase changes. Since $\Delta\phi(t)$ is governed by fluctuations in between two defect events due to the nonlinear wave character, parabolic functions are fitted piecewise to the data (solid line). A differentiation of this curve translates the phase difference into a frequency difference $\Delta\omega(t)$. The resulting time series is displayed in Fig. 4.5 (c). It reveals a sawtooth-like evolution, i.e., a linear decrease followed by a sudden increase. This implies that the interference phenomenon that leads to the appearance of topological defects has a nonlinear character, which is a typical feature of relaxation oscillators. In the linear case, a sinusoidal fluctuation of the frequency around its mean would be expected. Other measurements showed phase evolutions with opposite slope and an opposite sign of the phase jump. However, the presented example is typical in that it reveals an alternating linear and parabolic phase evolution on two markedly different time scales.

4.4 Discussion

In this Chapter, extended dust-density wave fields under microgravity conditions were investigated experimentally. In Sec. 4.1 it was shown that the waves can be found either in a highly coherent and almost monochromatic state or in polychromatic state, which reveals broad spectra and the occurrence of topological defects. The high coherence was used to reconstruct a still image of the three-dimensional wave field with scanning video microscopy, which comprised a rotational symmetry of the wave field. The method shows therefore that the recorded two-dimensional data sets have a representative character. A reconstruction of waves that contain defect structures, which would inevitably break the symmetry, is not possible with the presented technique since such waves have no time-independent phase relation.

Due to significant differences in the Fourier spectra of the wave states the frequency content of the DDWs was analyzed in detail using the analytic signal and derived quantities. The analysis revealed the formation of frequency clusters, which was unexpected. As mentioned above, this finding is not compatible with linear wave theories, where the frequency is constant over the entire wave field. This can be understood in terms of conservation of wave crests, which holds only for linear waves [1, 4]. It states that the number of wave fronts that enter a region in the
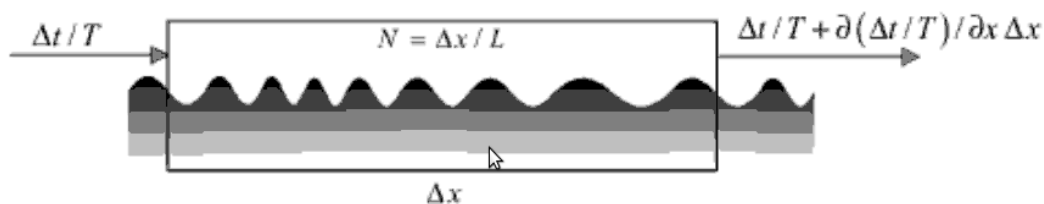
Figure 4.6: Illustration of the conservation of wave crests. The averaged temporal rate, at which wave fronts enter a region in the wave field (left side of the rectangle) must coincide with the rate, at which they leave this region (right side of the rectangle). Otherwise, wave fronts have to be created or annihilated. This is not possible for linear waves. (From Ref. [4])

wave field per unit time must coincide with the number of wave fronts that leave this region per unit time, see Fig. 4.6. Consequently, frequency variations are only possible if the number of crests is not conserved and wave fronts are added to or removed from the system, i.e., if a topological defect occurs. The observation of frequency clusters in dust-density waves was not reported so far. However, Pilch *et al.* [150] presented an analysis of the spatial frequency content of DDWs in small dust clouds of anodic plasmas. They found that the frequency of self-excited waves decays gradually. Separated regions of different but constant frequency were observed when the waves are synchronized with an external driver. In contrast to the presented situation, this behavior was explained by a synchronization of the waves with higher harmonics or subharmonics of the driving frequency.

Besides dust-density waves, frequency clusters were found in few other experimental investigations of one-dimensional systems. The work of Ref. [208] showed similar results concerning the frequency variations within one cluster and between adjacent clusters. Furthermore, a comparison between the frequency distributions of the different wave states revealed similarities with numerical studies of mutually coupled nonlinear oscillators in that the cluster sizes depend on the degree of nonlinearity and the spatial topology of a system parameter. Besides the adjustment of their frequencies, the simulations further showed that the oscillators adjust their phases, leading to the appearance of wave patterns in one- [217] and also two-dimensional systems [220]. In particular, it was found for integrate-and-fire oscillators [223] that the waves propagate from higher to lower frequencies, which is in agreement with the dust-density wave fields. Consequently, the results of the frequency analysis and a comparison with numerical studies give valuable hints for an explanation of the existence of markedly different wave states.

Since frequency clusters are observed in wave fields with a significant amount of defects, in Sec. 4.3 the relationship between defects and frequency clusters was studied. It was found that the concept of the topological charge, as presented in Sec. 3.2, allows the precise detection of defects and the analysis of their spatio-temporal behavior. The analysis revealed that the defects move almost exclusively along the cluster boundaries and can thus be understood as the building blocks for the formation of frequency clusters. Nevertheless, the defects do not occur repeatedly at the boundaries, in contrast to numerical simulations, since they move inside a three-

dimensional wave field and may be missed by the two-dimensional diagnostics. The investigation of the instantaneous phase and frequency at the cluster boundaries showed a temporal evolution on two different time scales, which is typical for relaxation oscillators. The frequency decreases or increases linearly between two defect events. This behavior resembles the periodic pulling effect of driven van-der-Pol oscillators, where the oscillator frequency is pulled toward the driving frequency but entrains only for a short time until it jumps back [224].

The experimental findings give reason to describe the waves with the aid of a numerical model. The analysis of this model is presented in the following Chapter.

5 Numerical Analysis of Coupled Van-der-Pol Oscillators

At the end of the previous Chapter, it was shown that the dust-density waves at the cluster boundaries resemble the behavior of relaxation oscillators. The van-der-Pol equation represents the archetype for self-sustained nonlinear oscillations near a limit-cycle. It plays a pivotal role as the Korteweg-de Vries equation for solitons [1,2] or the Rankine-Hugoniot equation for shock waves [3]. In this Chapter a model, based on the van-der-Pol oscillator, is introduced that emulates the behavior of DDWs numerically. Different from detailed simulations, the aim of this approach is to identify similar elementary structures in model and experiment. The search for analogies between different systems is a guiding theme in the field of nonlinear dynamics. This becomes particularly apparent in the introduction of Haken's fundamental textbook on synergetics [225], where he points out that

> "... we are searching for such analogies which show up in the essential gross features of our system."

This in turn means that the microscopic characteristics of the compared systems as, e.g., the exact shape of the measured and simulated signals, may differ. Haken concludes:

> "When each system is analyzed in more and more detail down to the subsystems, quite naturally more and more differences between these may show up."

Although there are several calculations, which already examined the phenomenon of frequency clustering, it lacks a detailed analysis of the cluster boundaries. Such analysis was realized in complementary numerical studies within the scope of this thesis. In the following, the applied model is described and the fundamental properties are analyzed. Afterwards, the behavior of individual oscillators at the boundaries and their relationship to neighbors in adjacent clusters are examined and finally compared with the experiments on dust-density waves.

5.1 Description of the Model

Due to the similarities between self-excited dust-density waves and relaxation oscillators it is justified to describe the waves as an ensemble of mutually interacting relaxation oscillators. Such models were also proposed for other experimental studies of frequency clusters [208, 210, 212–214]. There, the oscillator was of the van-der-Pol

type. This choice is also reasonable for the examined DDWs. First, the van-der-Pol oscillator is self-sustained, i.e. it is independent from external forces and second, it has a nonlinear amplitude saturation. Furthermore, the van-der-Pol oscillator has a paradigmatic character for various wave types in gas discharges. It can for example successfully describe oscillations in thermionic diodes [15] or weakly magnetized plasmas [16,17,226]. Moreover, it was applied to self-excited and to driven ionization waves [14, 20] and also to drift waves [18, 19].

The presented studies of a chain of mutually coupled van-der-Pol oscillators are governed by the following equation:

$$\ddot{x}_i - \epsilon(1 - \beta x_i^2)\omega_{0i}\dot{x}_i + \omega_{0i}^2 x_i = g[\dot{x}_{i-1} + \dot{x}_{i+1} - 2\dot{x}_i]. \tag{5.1}$$

Here, x_i describes the elongation of the i-th oscillator in the chain. The natural frequency of each oscillator reads $\omega_{0i} = 2\pi f_{0i}$. It is not constant but depends on the position in the chain. The spatial dispersion is chosen to be linear and is given by $\omega_{0i} = 1 + i \cdot \Delta$, where Δ is the constant frequency mismatch between two adjacent oscillators. The nonlinear damping term $\omega_{0i}\dot{x}_i$ is characterized by the degree of non-linearity ϵ and the amplitude saturation β. The latter is a fundamental characteristic of the van-der-Pol oscillator since it is the reason that the oscillator stabilizes its amplitude autonomously. It includes first a condition for self-excitation since small amplitudes $(x_i^2 < \beta^{-1})$ are amplified, and second a condition for amplitude saturation since large amplitudes $(x_i^2 > \beta^{-1})$ are damped. The coupling between the oscillators is measured by the coupling constant g. It is diffusive, i.e., it incorporates only nearest neighbor interactions, and it is viscous, which means that the neighbors are coupled through their velocities. The boundary conditions correspond to free ends, i.e., the outermost oscillators are coupled to their sole neighbor.

The system (5.1) is solved numerically for a chain of $N = 100$ oscillators using a fourth-order Runge-Kutta scheme with an adaptive step size control. The amplitude saturation is set to $\beta = 1.0$. The total number of simulation steps is $T = 10000$. In order to eliminate transients and guarantee that the oscillators are only studied on their limit-cycle, the first third of each time series is initially discarded. The analysis of the main oscillator characteristics is the same as for the DDWs in order to allow a comparison between simulation and experiment: The evolutions of instantaneous phase and instantaneous frequency are determined according to Eqs. (3.4) and (3.5) and the averaged frequency of an oscillator is calculated by $\bar{\omega}_i = \langle\omega_i\rangle_T$.

5.2 Basics Results

The frequency distribution $\bar{\omega}_i$ for the free parameters $g = 0.15$, $\epsilon = 1.4$ and $\Delta = 0.002$ is shown in Fig. 5.1 by a solid line. The results can be summarized as follows: The distribution is not linear but frequency clusters occur, in which the oscillators share a common frequency. If the internal stress between two adjacent oscillators becomes too strong, the frequency-locked group breaks up and a new cluster forms. It is further found that the frequencies are always slower than in the linear case (dotted line), i.e., the distribution of ω_{0i}. Furthermore, they are faster than in
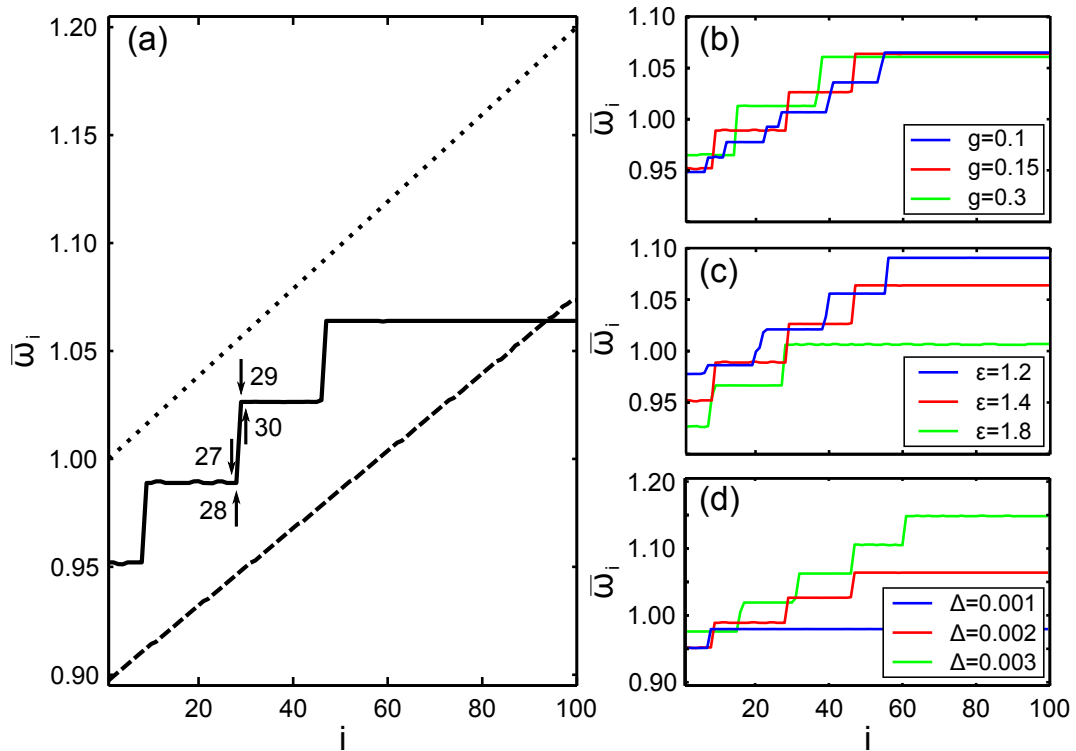
Figure 5.1: Results of the numerical investigations of a chain of 100 mutually coupled van-der-Pol oscillators. (a) Distribution of the averaged instantaneous frequency $\bar{\omega}_i$ for $g = 0.15$, $\epsilon = 1.4$ and $\Delta = 0.002$ (solid line) in comparison to the linear natural frequencies ω_{0i} (dotted line) and the nonlinear uncoupled case ($g = 0$, dashed line). (b) Distributions for different values of coupling coefficient g ($\epsilon = 1.4$ and $\Delta = 0.002$). (c) Distributions for different values of degree of nonlinearity ϵ ($g = 0.15$ and $\Delta = 0.002$). (d) Distributions for different values of frequency mismatch Δ ($g = 0.15$ and $\epsilon = 1.4$).

the uncoupled nonlinear case ($g = 0$, dashed line), except for the high-frequency end ($i > 93$). In addition, the distribution comprises an asymmetric shape with respect to the chain position. The size of a cluster decreases from higher to lower frequencies. This is in accordance with Ref. [212]. Due to the nonlinear damping, the difference between the linear and the nonlinear uncoupled distribution increases with the degree of nonlinearity. A similar result was found in Ref. [213] although the functional relationship is different. A previous analysis of Ginzburg-Landau systems [219] showed that the relative position of the distribution with respect to the linear case depends on the coupling scheme, which was not investigated here.

The frequency distribution for three different coupling strengths are shown in Fig. 5.1 (b). One can see that the cluster size increases with the coupling strength. The behavior of the clusters for three different degrees of nonlinearity are presented in Fig. 5.1 (c). As expected, the cluster size increases with ϵ and the whole distribution is shifted to lower frequencies. The frequency clustering is further studied under a variation of frequency mismatches in Fig. 5.1 (d). Obviously, the difference between lowest and highest oscillator frequency increases with increasing Δ, whereas the size of the clusters diminishes. The asymmetry depends critically on

each of the three quantities. It increases with increasing coupling strength, with increasing nonlinearity and with decreasing frequency mismatch.

It turns out that the proposed model of coupled van-der-Pol oscillators shows the expected behavior. The performed numerical studies reveal frequency clustering and the same tendencies concerning a variation of the system parameters as found in previous works, see Sec. 4.2. In the following, the distinct behavior of oscillators in the vicinity of a cluster boundary is studied.

5.3 Cluster Boundaries

The elongations $x_i(t)$ for four representative oscillators of the chain are shown in Figs. 5.2 (a)-(d). The oscillators are located at different sides of the same cluster boundary, see arrows in Fig. 5.1. The first two oscillators ($i = 27$, $i = 28$) sit at the low-frequency side of the cluster and the others ($i = 29$, $i = 30$) at the high-frequency side. For all signals an amplitude modulation is observed. The amplitude of the outer oscillators [Figs. 5.2 (a)+(d)] decreases gradually until it suddenly increases very rapidly and returns to the maximum value. For the oscillators in the immediate vicinity of the boundary [Figs. 5.2 (b)+(c)] the gradual decrease is even stronger and the amplitude abruptly drops down. In both cases, the behavior repeats periodically.

The instantaneous phase is also modulated temporally. It is in general a monotonically increasing function but comprises deviations from this evolution when the amplitude drops drown. As mentioned in Sec. 3.2 this event can be identified as a topological defect. Consequently, the instantaneous frequency [Fig. 5.2 (e)-(h)] varies on two different time scales. On the low-frequency side of the cluster boundary, the frequency increases slowly (apart from the high-frequent modulations due to nonlinearity) until it changes quickly to a smaller value. For the high-frequency side the situation is found reverted. This behavior can be interpreted as an incomplete synchronization between the mutually interacting oscillators. It was not reported for coupled self-sustained oscillators but is typical for systems of isolated relaxation oscillators [9]. There, it is referred to as periodic pulling or frequency pulling [16, 227, 228]. The analysis further reveals that inside a cluster the amplitude and phase of the oscillators are not modulated and consequently no pulling effect is observed.

The simulated elongations allow to determine the frequency spectra of the oscillators. They are obtained from a Fast Fourier Transfrom (FFT) after a Hanning window was applied to the time series. The results are presented in Figs. 5.2 (i)-(l). Obviously, the spectra comprise only odd higher harmonics besides the fundamental. The spectra give further hints for periodic pulling: The fundamental is governed by a sideband structure. This feature is even more pronounced for the higher harmonics. The sidebands reveal a strong asymmetry since one of them is significantly suppressed. This is caused by the simultaneous amplitude and frequency modulation. For an externally driven single van-der-Pol oscillator, always the sideband on the side of the driver is suppressed [14, 15, 17, 20, 224]. Here, the sideband cancellation occurs in panels (i) and (j) on the high-frequency side whereas in panels (k)

and (l) the sidebands on the low-frequency side become weaker. Hence, the coupling across the cluster boundary can be interpreted as the driver that is responsible for the sideband cancellation. Since the limited time during one parabola does not allow to record long time series, the frequency resolution of the Fourier spectra is rather poor, see Fig. 4.1 (d), and a reliable identification of a sideband structure is consequently not possible.

5.4 Comparison With Experiments

In order to compare the numerical findings with the results of the experiments, two positions in the frequency distribution of Fig. 4.3 (a) are investigated. They are located at the vicinity of a cluster boundary where periodic pulling can be observed, see positions '1' and '2' in the closeup of Fig. 5.3 (i). First, the deviation $\Delta\phi(t)$ of the instantaneous phase from its averaged evolution is calculated as defined in Sec. 4.3. Results for the numerical studies and the experiment are shown in Figs. 5.3 (a),(c) and Figs. 5.3 (b),(d), respectively. It is seen in both situations that in the low-frequency cluster [panels (a)+(b)], the phase difference gradually increases and suddenly drops down before it increases again. In the high-frequency cluster [panels (c)+(d)], the evolution is vice versa: $\Delta\phi(t)$ first decreases, then rapidly increases to a higher value and decreases again afterwards. In both cases, the abrupt changes can be identified as a defect event.

In addition, the deviation $\Delta\omega(t)$ of the instantaneous frequency from its average is determined as the temporal derivative of $\Delta\phi(t)$. A reasonable comparison of absolute values for $\Delta\omega(t)$ is not possible and thus the resulting evolutions are normalized to the average frequency $\bar{\omega}$. The results are presented in Figs. 5.3 (e)-(h). As expected, the frequency difference varies only slightly until a strong variation is observed when a defect occurs. This behavior is observed in both cases.

In the numerical simulations the temporal evolutions of phase and frequency difference show periodic modulations, which are owing to the nonlinearity of the system. Hints for such a feature are also found in the experimental data but cannot be identified unambiguously due to comparably low temporal resolution.

To summarize, in this Chapter, a chain of mutually coupled van-der-Pol oscillators was studied numerically in order to understand the behavior of the dust-density waves at the boundaries of frequency clusters in more detail. The obtained results lead to the conclusion that the model indeed shows topological structures that are similar to the experimentally observed DDWs: Accordingly, groups of oscillators inside the chain agree on a common frequency. Further, the interacting oscillators at a cluster boundary reside in a state of incomplete synchronization, which is well known from isolated driven systems but which has not yet been reported for self-sustained coupled oscillators. The study showed that this feature is more pronounced on the low-frequency side of each cluster, which attributes a leading role to the higher-frequency oscillators.

The model discussed here is different from simple models of dust-lattice waves [37, 229] although both consist of a network of coupled oscillators. However, in the present case the individual oscillators cannot be associated with a single dust particle, which interacts electrostatically with its neighbors. Rather, an oscillator includes the quorum of particles that exhibit the local system behavior at the position of the oscillator in the dust cloud. This is due to the fact that the examined DDWs occur in the fluid state of a dusty plasma, where the collective behavior of the particles dominates over their microscopic interactions. In this sense, the proposed model can be understood as a discretization of a continuous process.

The presented results and derived conclusions of the previous Chapters give rise to a higher-ranking discussion, which leads to a modified view on the phenomena of self-exited dust-density waves. The following Chapter is dedicated to this discussion.
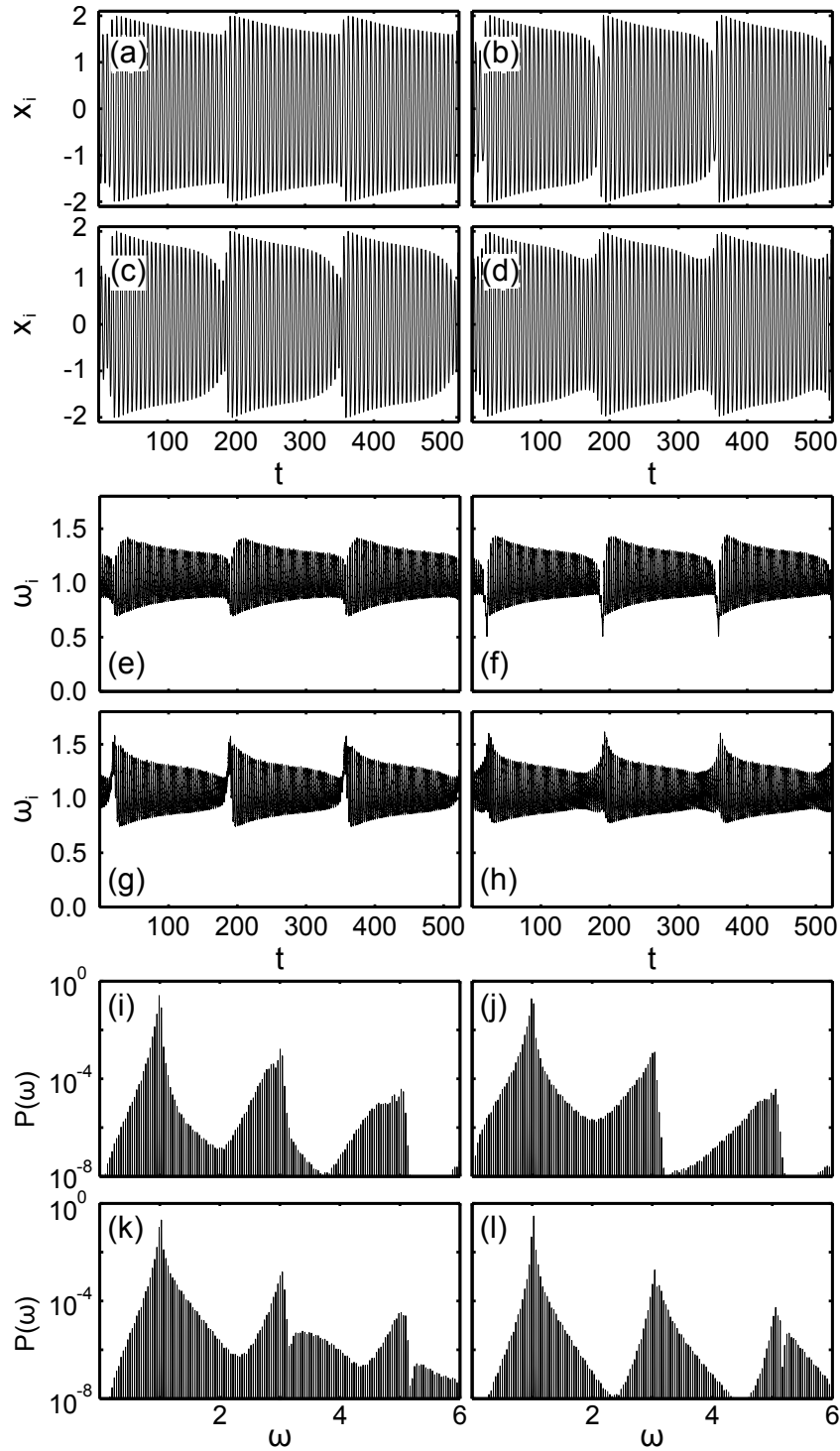
Figure 5.2: (a)-(d) Temporal evolutions of the oscillator elongations at a cluster boundary, marked by arrows in Fig. 5.1 (a). The observed periodical variation of the amplitude is a clear hint for periodic pulling. (e)-(h) Corresponding evolution of the instantaneous frequency. (i)-(l) Power spectra of the oscillators. A sideband suppression can be clearly seen. The asymmetry changes at the cluster boundary between (j) and (k).
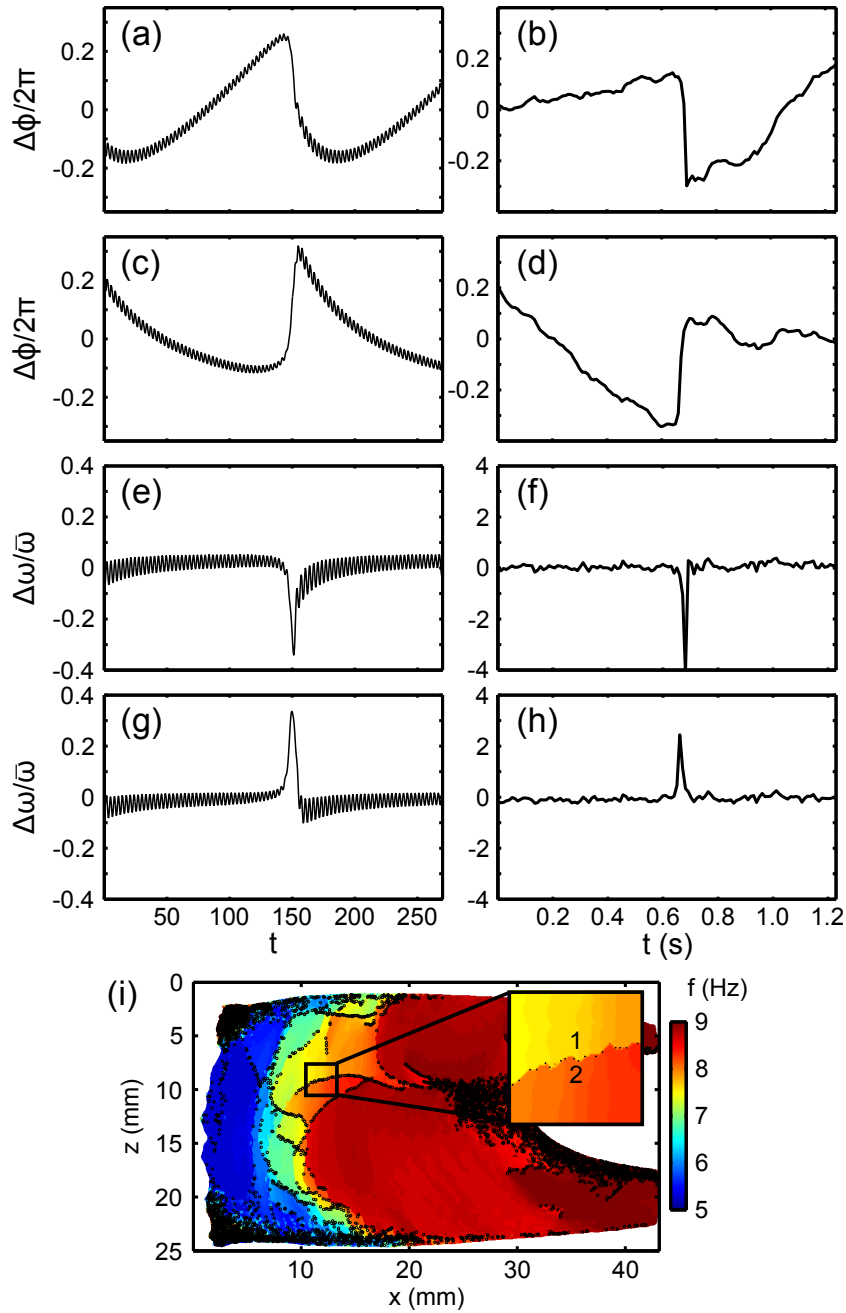
Figure 5.3: Comparison between numerical and experimental results at a cluster boundary. The evolutions of the phase difference $\Delta\phi(t)$ are shown for oscillators at $i = 28$ (a) and $i = 29$ (c). The same is calculated for the experiment at the locations '1' and '2' in panel (i). In both situations a variation on two time scales is observed. The evolutions of the corresponding frequency differences $\Delta\omega(t)/\bar{\omega}$ also reveal a similar behavior in simulation (e)+(g) and experiment (f)+(h).

6 Summary and Conclusions

In this thesis, self-excited dust-density waves were investigated in extended three-dimensional dust clouds under microgravity conditions. In order to analyze the complicated spatio-temporal structure of the waves, refined data analysis techniques by means of the Hilbert transform were introduced. They allow to study the waves on different time scales. The presented investigations were focused on two different wave features. The spatial frequency content of the waves was determined from the time-averaged instantaneous frequency. This analysis led to the discovery of so-called frequency clusters, i.e., regions of almost constant frequency that are separated by abrupt frequency changes. Additionally, phase defects were investigated using the concept of topological charge. It was found that both aspects, frequency clusters and defects, are intimately related to each other, although observed on significantly different time scales. A detailed study of the waves at the cluster boundaries revealed similarities between DDWs and isolated driven van-der-Pol systems. This finding resulted in the idea of modeling the waves as a chain of mutually coupled self-sustained nonlinear oscillators. The main results of this thesis lead to the following key statements:

The determination of instantaneous wave attributes accounts fundamentally for the understanding of the wave mechanism

The observed DDWs show a nonlinear behavior, which manifests in a non-sinusoidal wave shape and a high degree of modulation. Moreover, they reveal transient features like the appearance of topological defects. Both phenomena lead to modulations of the measured time series within a wave period. The established methods, such as space-time diagram and Fourier analysis, are insufficient to analyze this special behavior. Thus, the Hilbert transform and the resulting analytic signal were used within this thesis. They are adapted from digital signal processing and allow to determine the wave attributes like phase or frequency for each time step of the recorded time series. As a result, it is possible to reconstruct the complete spatio-temporal behavior of the waves, which, of course, includes the positions of the defects as well. This analysis is of importance since the defects occur in the majority of measurements and are an essential part of the wave fields.

The observed dust-density waves in saturation are self-excited and fundamentally different from driven linear waves in a passive medium

The presented investigations showed that DDWs exist in a pressure regime (15–35 Pa), where any disturbance of the system should be damped completely within a few millimeters [80]. This observation contradicts the idea of a wave that propagates

through the dust cloud, excited at a distinct position, which might be given, e.g., by the 'heartbeat instability' [178]. A parametric excitation by the system due to mechanical forces arising from residual gravity can be excluded since the measured fluctuations are significantly higher (> 50 Hz) than the wave frequencies.

Consequently, the DDWs must gain energy at each position in the system. Streaming ions, which arise due to the ambipolar electric field in the discharge, are such an energy source. They are able to excite waves most likely by a Buneman-type instability. In this sense, the dust cloud can be interpreted as an active medium, similar to an amplifying laser medium.

Linear waves, which are excited by means of a localized driver, usually exist at lower gas pressures (< 10 Pa). They were so far observed as lattice waves in almost perfect one- and two-dimensional monolayers and were mostly generated by the radiation pressure of strong lasers.

The observed dust-density waves cannot be explained in terms of Huygens' linear theory

It is known from simulations that the plasma conditions inside an rf discharge are nonuniform. Further, additional measurements showed that also the dust-density is not constant over the dust cloud. This is reflected in spatially varying wave attributes. In particular, it was found that the frequency, which was defined as the time-averaged instantaneous frequency, decreases from the void boundary to the discharge periphery. This decay is not compatible with the linear wave picture of Huygens, which involves a constant frequency and a variable wavelength. A simple reason therefore is given in terms of conservation of wave crests, which holds for linear waves and means that the number of wave fronts entering a region in the wave field per unit time must match the number of wave fronts leaving this region per unit time.

The appearance of frequency clusters in the wave fields indicates that the dust cloud can be understood as an ensemble of mutually coupled, nonlinear and self-sustained oscillators

The observations showed that the spatial frequency decay is not continuous but frequency clusters occur. These clusters were investigated extensively in numerical studies, see, e.g., Refs. [208, 211, 212, 217]. All proposed models consisted of a network of mutually coupled nonlinear oscillators. These oscillators were not excited by means of an external driver but they were self-sustained. Moreover, the individual oscillators were subject to a spatial gradient of their natural frequencies. Similar conditions apply also for DDWs. First, the dust cloud is an active medium, in which the waves emerge spontaneously. Second, a frequency gradient can be assumed as well. This can be understood as follows: The high growth rates of the Buneman instability [68] ensure that the fastest growing mode determines the wave frequency. The latter is given by the local plasma parameters, i.e., particle mass, particle charge and dust density. As mentioned above, these quantities are distributed non-uniformly in

the dust cloud (except for the particle mass), which suggests a decrease of the natural frequencies in the system from the void to the discharge edges. Consequently, it is reasonable to assume that a model of the dust-density waves consists of the same ingredients as the numerical simulations. This conclusion is substantiated by the fact, that a synchronization of the oscillator phases, which leads to the propagation of waves, was also observed in the aforementioned works. Moreover, a variation of the system parameters revealed similar tendencies concerning the cluster size for DDWs and simulations.

Adjacent clusters match their frequencies via topological defects

The analysis of defect trajectories by means of the topological charge and a standard particle tracking algorithm revealed that the defects move almost exclusively along the cluster boundaries. This behavior can be explained from the aforementioned conservation of wave crests, which is obviously violated at the cluster boundaries due to the appearing frequency variation. This in turn is only possible if wave fronts are added to or removed from the system, i.e., if a topological defect occurs. Since the frequency is almost constant inside the clusters, wave crest conservation holds and no defects are found.

This behavior is known from other systems, which comprise frequency jumps. For example, defects were observed at mode transitions in ionization waves [230,231] and they were also found between regions of harmonic and subharmonic synchronization for DDWs in anodic plasmas [150].

Of course, the previous simulations of frequency clusters also showed defects at the cluster boundaries. It was reported [217] that they occur periodically. In the experiment such periodicity at a distinct position is rare, which is a consequence of observing only a two-dimensional section of a three-dimensional wave field.

The van-der-Pol oscillator is a suitable system to model dust-density waves

The simple fact that the examined waves are self-excited and saturated indicates a certain relationship between DDWs and the van-der-Pol oscillator. Moreover, the determined temporal evolution of the instantaneous frequency revealed a characteristic development on two different time scales, namely a long linear variation between two defect events and an abrupt increase or decrease when a defect occurs. Obviously, the oscillators at a cluster boundary are not able to synchronize each other like those inside a cluster and one consequently speaks of a process of incomplete synchronization. This behavior is typical of isolated driven van-der-Pol systems for distinct values for driving amplitude and frequency mismatch between driver and oscillator [9, 10]. There, the oscillator is pulled towards the driver, entrains for a short moment and then changes abruptly. Thus, it is reasonable to assume that the individual oscillator in the ensemble, which represents the dust cloud, is of the van-der-Pol type.

The interaction of adjacent clusters is determined by the oscillators at the cluster boundary

The performed numerical studies of a chain of mutually coupled van-der-Pol oscillators revealed a general agreement with the experimental studies of dust-density waves. Besides the expected formation of frequency clusters, the analysis showed similar variations in the temporal evolutions of instantaneous phase and instantaneous frequency. Furthermore, the studies depicted an asymmetric sideband structure of the Fourier spectra for oscillators in the vicinity of a cluster boundary, which could not be resolved in the measurements due to the comparably poor spectral resolution. The observed features at the cluster boundary are characteristic for the frequency-pulling phenomenon. They were not found inside the clusters. In the numerical investigations the pulling effect was more pronounced on the low-frequency side of each boundary. This suggests a leading role of higher-frequency oscillators on their low-frequent neighbors. In that sense the observations differ from those of driven van-der-Pol systems, where no such asymmetry was found.

The presented conclusions, which resulted from the experimental and numerical studies of this thesis, draw a modified picture of nonlinear self-excited dust-density waves in saturation. They can be interpreted as an ensemble of mutually coupled nonlinear and self-sustained oscillators. This ensemble is embedded in an active medium, which feeds the oscillators internally with energy. A phase synchronization of the oscillators leads to a periodic wave pattern.

An unsolved problem is the question why the oscillators often synchronize over large distances, even beyond regions of low dust density. In particular, the measurements showed that the waves on opposite sides of the void are correlated to each other. This leads to the assumption that, besides the direct coupling between the oscillators, a global interaction of the oscillators with the background plasma might play an important role. First indications for this interplay were found in complementary investigations in the IMPF-K2 chamber [158], which revealed a significant increase of the overall plasma glow after dust was injected and, moreover, a modulation of the glow by the dust-density waves.

Further advanced measurements could bring useful hints to solve this question. The following improvements and extensions of the presented investigations will be certainly helpful:

- **Refined glow diagnostics:** First hints on a correlation between plasma glow and DDWs were obtained from a simple setup, which simultaneously recorded glow and dust. Further refined investigations with improved optical components might clarify these preliminary observations.

- **Three-dimensional diagnostics:** The experimental setup allowed to observe two-dimensional sections through the dust cloud in the equatorial plane and also off-axis by using a translation stage. Nevertheless, the wave field reveals a complicated three-dimensional spatio-temporal behavior that could

not be reconstructed with the current setup, except for highly coherent waves. In particular, the three-dimensional defect trajectories could not be analyzed. Thus, a true three-dimensional diagnostics of the waves is desirable.

- **Laboratory experiments:** The maximum recording time on parabolic flights is limited by the duration of a parabola. Thus, complementary laboratory experiments may provide useful additional information since they allow to record time series of arbitrary length. In particular, the recently developed IMPF-KT chamber [40] might be a suitable alternative to the presented microgravity experiments. It facilitates to generate extended three-dimensional dust clouds by means of thermophoretic levitation. Moreover, the experimental setup is almost identical with that of IMPF-K2.

- **Three-dimensional simulations:** The realized numerical studies included a one-dimensional chain of mutually coupled oscillators. An extension of this model to three dimensions could bring new insight into the complicated motion of the defects in the dust clouds.

- **Investigations on a microscopic level:** The presented investigations analyzed the dust-density information and were able to determine the global frequency content and the defect motion. However, the experiments could not provide the individual particle trajectories, which might elucidate the formation of defects in more detail.

A Bibliography

[1] G. B. Whitham, *Linear and Nonlinear Waves* (Wiley-Interscience, New York, 1974).

[2] E. Infeld and G. Rowlands, *Nonlinear Waves, Solitons and Chaos* (Cambridge Univ. Press, Cambridge, 2000).

[3] J. Billingham and A. C. King, *Wave Motion* (Cambridge Univ. Press, Cambridge, 2001).

[4] L. H. Holthuijsen, *Waves in Oceanic and Coastal Waters* (Cambridge Univ. Press, Cambridge, 2007).

[5] D. Helbing, *Traffic and related self-driven many-particle systems*, Rev. Mod. Phys. **73**, 1067 (2001).

[6] B. Katz, *Nature of the Nerve Impulse*, Rev. Mod. Phys. **31**, 466 (1959).

[7] G. Kuwabara, T. Hasegawa, and K. Kono, *Water waves in a ripple tank*, Am. J. Phys. **54**, 1002 (1986).

[8] A. La Porta and C. M. Surko, *Phase Defects as a Measure of Disorder in Traveling-Wave Convection*, Phys. Rev. Lett. **77**, 2678 (1996).

[9] A. S. Pikovsky, M. Rosenblum, and J. Kurths, *Synchronization: A Universal Concept in Nonlinear Science* (Cambridge Univ. Press, Cambridge, 2001).

[10] A. Balanov, N. Janson, D. Postnov, and O. Sosnovtseva, *Synchronization: From Simple to Complex* (Springer, Berlin, 2008).

[11] C. Huygenii, *Horologium Oscilatorium* (Parisiis, France, 1673).

[12] B. van der Pol, *On oscillation hysteresis in a triode generator with two degrees of freedom*, Philos. Mag. **43**, 700 (1922).

[13] T. Klinger, A. Piel, F. Seddighi, and C. Wilke, *Van der Pol dynamics of ionization waves*, Phys. Lett. A **182**, 312 (1993).

[14] K. D. Weltmann, M. Koepke, and C. A. Selcher, *Spatiotemporal laser perturbation of competing ionization waves in a neon glow discharge*, Phys. Rev. E **62**, 2773 (2000).

[15] T. Klinger *et al.*, *Van der Pol behavior of relaxation oscillations in a periodically driven thermionic discharge*, Phys. Rev. E **52**, 4316 (1995).

[16] T. Gyergyek, M. Čerček, N. Jelić, and M. Stanojević, *Mode suppression of a two-dimensional potential relaxation instability in a weakly magnetized discharge plasma*, Phys. Lett. A **177**, 54 (1993).

[17] T. Klinger, A. Piel, I. Axnäs, and S. Torvén, *The bifurcation structure of periodically forced current disruptions*, Phys. Scripta **56**, 70 (1997).

[18] D. Block, A. Piel, C. Schröder, and T. Klinger, *Synchronization of drift waves*, Phys. Rev. E **63**, 056401 (2001).

[19] C. Brandt, O. Grulke, and T. Klinger, *Nonlinear interaction of drift waves with driven plasma currents*, Phys. Plasmas **17**, 032304 (2010).

[20] M. E. Koepke, T. Klinger, F. Seddighi, and A. Piel, *Periodic nonlinear wave–wave interaction in a plasma discharge with no external oscillatory driving force*, Phys. Plasmas **3**, 4421 (1996).

[21] H. Klostermann, A. Rohde, and A. Piel, *Van der Pol behavior of virtual anode oscillations in the sheath around a grid in a double plasma device*, Phys. Plasmas **4**, 2406 (1997).

[22] C. K. Goertz and G. E. Morfill, *A model for the formation of spokes in Saturn's rings*, Icarus **53**, 219 (1983).

[23] C. K. Goertz, *Dusty plasmas in the solar system*, Rev. Geophys. **27**, 271 (1989).

[24] M. Horányi, *Charged dust dynamics in the solar system*, Annu. Rev. Astron. Astrophys. **34**, 383 (1996).

[25] D. M. Manos and D. L. Flamm, *Plasma Etching: An Introduction* (Academic Press, San Diego, 1989).

[26] G. S. Selwyn, J. Singh, and R. S. Bennett, *In situ laser diagnostic studies of plasma–generated particulate contamination*, J. Vac. Sci. Technol. A **7**, 2758 (1989).

[27] J. H. Chu and L. I, *Coulomb lattice in a weakly ionized colloidal plasma*, Physica A **205**, 183 (1994).

[28] H. Thomas *et al.*, *Plasma Crystal: Coulomb Crystallization in a dusty plasma*, Phys. Rev. Lett. **73**, 652 (1994).

[29] Y. Hayashi and K. Tachibana, *Observation of Coulomb-Crystal Formation from Carbon Particles Grown in a Methane Plasma*, Jpn. J. Appl. Phys. **33**, 804 (1994).

[30] A. Melzer *et al.*, *Structure and stability of the plasma crystal*, Phys. Rev. E **54**, R46 (1996).

[31] H. M. Thomas and G. E. Morfill, *Melting dynamics of a plasma crystal*, Nature **379**, 806 (1996).

[32] H. Totsuji, *Structure and melting of two-dimensional dust crystals*, Phys. Plasmas **8**, 1856 (2001).

[33] M. Wolter and A. Melzer, *Laserheating of particles in dusty plasmas*, Phys. Rev. E **71**, 036414 (2005).

[34] V. Nosenko, J. Goree, and A. Piel, *Laser method of heating monolayer dusty plasmas*, Phys. Plasmas **13**, 032106 (2006).

[35] J. B. Pieper and J. Goree, *Dispersion of Plasma Dust Acoustic Waves in the Strong-Coupling Regime*, Phys. Rev. Lett. **77**, 3137 (1996).

[36] M. Zuzic, H. M. Thomas, and G. E. Morfill, *Wave propagation and damping in plasma crystals*, J. Vac. Sci. Technol. A **14**, 496 (1996).

[37] A. Homann *et al.*, *Laser-excited dust lattice waves in plasma crystals*, Phys. Lett. A **242**, 173 (1998).

[38] P. Manz and F. Greiner, *Linear study of the nonmodal growth of drift waves in dusty plasmas*, Phys. Plasmas **17**, 063703 (2010).

[39] O. Arp, D. Caliebe, and A. Piel, *Cavity dynamics and particle alignment in the wake of a supersonic projectile penetrating a dusty plasma*, Phys. Rev. E., accepted (2011)

[40] C. Schmidt, O. Arp, and A. Piel, *Spatially extended void-free dusty plasmas in a laboratory radio-frequency discharge*, Phys. Plasmas **18**, 013704 (2011).

[41] J. Winter, *Dust in fusion devices—a multi-faceted problem connecting high- and low-temperature plasma physics*, Plasma Phys. Control. Fusion **46**, B583 (2004).

[42] A. W. Kleyn, W. Koppersa, and L. Lopes Cardozoa, *Plasma-surface interaction in ITER*, Vacuum **80**, 1098 (2006).

[43] B. M. Annaratone, W. Jacob, C. Arnas, and G. E. Morfill, *Critical Review of Complex Plasma (Dusty Plasma) Diagnostics and Manipulation Techniques for the Fusion Community and Others*, IEEE Trans. Plasma Sci. **37**, 270 (2009).

[44] H. Rothermel *et al.*, *Gravity Compensation in Complex Plasmas by Application of a Temperature Gradient*, Phys. Rev. Lett. **89**, 175001 (2002).

[45] G. Praburam and J. Goree, *Experimental observation of very low-frequency macroscopic modes in a dusty plasma*, Phys. Plasmas **3**, 1212 (1996).

[46] M. Mikikian and L. Boufendi, *Experimental investigations of void dynamics in a dusty discharge*, Phys. Plasmas **11**, 3733 (2004).

[47] G. E. Morfill *et al.*, *Condensed Plasmas under Microgravity*, Phys. Rev. Lett. **83**, 1598 (1999).

[48] S. A. Khrapak *et al.*, *Compressional waves in complex (dusty) plasmas under microgravity conditions*, Phys. Plasmas **10**, 1 (2003).

[49] V. V. Yaroshenko *et al.*, *Electrostatic modes in collisional complex plasmas under microgravity conditions*, Phys. Rev. E **69**, 066401 (2004).

[50] S. V. Annibaldi *et al.*, *Dust-acoustic dispersion relation in three-dimensional complex plasmas under microgravity*, New J. Phys. **9**, 0327 (2007).

[51] M. Schwabe *et al.*, *Nonlinear waves externally excited in a complex plasma under microgravity conditions*, New J. Phys. **10**, 033037 (2008).

[52] M. H. Thomas *et al.*, *Complex plasma laboratory PK-3 Plus on the International Space Station*, New J. Phys. **10**, 033036 (2008).

[53] S. K. Zhdanov *et al.*, *Auto-oscillations in complex plasmas*, New J. Phys. **12**, 043006 (2010).

[54] M. Thoma *et al.*, *Parabolic flight experiments with PK-4*, Microgravity Sci. and Technol. **18**, 47 (2006).

[55] A. Piel *et al.*, *Obliquely Propagating Dust-Density Plasma Waves in the Presence of an Ion Beam*, Phys. Rev. Lett. **97**, 205009 (2006); A. Piel *et al.*, *Erratum: Obliquely Propagating Dust-Density Plasma Waves in the Presence of an Ion Beam*, Phys. Rev. Lett. **99**, 209903 (2007).

[56] A. Piel, O. Arp, M. Klindworth, and A. Melzer, *Obliquely propagating-dust density waves*, Phys. Rev. E **77**, 026407 (2008).

[57] S. Zhdanov *et al.*, *Dissipative dark solitons in a dc complex plasma*, Europhys. Lett. **89**, 25001 (2010).

[58] S. Peters, A. Homann, A. Melzer, and A. Piel, *Measurement of dust particle shielding in a plasma from oscillations of a linear chain*, Phys. Lett. A **223**, 389 (1996).

[59] A. Homann *et al.*, *Determination of the dust screening length by laser-excited lattice waves*, Phys. Rev. E **56**, 7138 (1997).

[60] D. Samsonov *et al.*, *Mach Cones in a Coulomb Lattice and a Dusty Plasma*, Phys. Rev. Lett. **83**, 3649 (1999).

[61] D. Samsonov, J. Goree, H. M. Thomas, and G. E. Morfill, *Mach cone shocks in a two-dimensional Yukawa solid using a complex plasma*, Phys. Rev. E **61**, 5557 (2000).

[62] A. Melzer *et al.*, *Laser-excited Mach cones in a dusty plasma crystal*, Phys. Rev. E **62**, 4162 (2000).

[63] S. Nunomura, D. Samsonov, and J. Goree, *Transverse Waves in a Two-Dimensional Screened-Coulomb Crystal (Dusty Plasma)*, Phys. Rev. Lett. **84**, 5141 (2000).

[64] S. Nunomura *et al.*, *Dispersion relations of longitudinal and transverse waves in two-dimensional screened Coulomb crystals*, Phys. Rev. E **65**, 066402 (2002).

[65] V. Nosenko *et al.*, *Compressional and shear wakes in a two-dimensional dusty plasma crystal*, Phys. Rev. E **68**, 056409 (2003).

[66] V. Nosenko, J. Goree, and A. Piel, *Cutoff Wave Number for Shear Waves in a Two-Dimensional Yukawa System (Dusty Plasma)*, Phys. Rev. Lett. **97**, 115001 (2006).

[67] A. Piel, V. Nosenko, and J. Goree, *Laser-excited shear waves in solid and liquid two-dimensional dusty plasmas*, Phys. Plasmas **13**, 042104 (2006).

[68] M. Rosenberg, *Ion-dust streaming instability in processing plasmas*, J. Vac. Sci. Technol. A **14**, 631 (1996).

[69] R. L. Merlino, *Dust-acoustic waves driven by an ion-dust streaming instability in laboratory discharge dusty plasma experiments*, Phys. Plasmas **16**, 124501 (2009).

[70] N. N. Rao, P. K. Shukla, and M. Y. Yu, *Dust-acoustic waves in dusty plasmas*, Planet. Space Sci. **38**, 543 (1990).

[71] J. H. Chu, J.-B. Du, and L. I, *Coulomb solids and low-frequency fluctuations in RF dusty plasmas*, J. Phys. D: Appl. Phys. **27**, 296 (1994).

[72] A. Barkan, R. L. Merlino, and N. D'Angelo, *Laboratory observation of the dust-acoustic wave mode*, Phys. Plasmas **2**, 3563 (1995).

[73] C. Thompson, A. Barkan, N. D'Angelo, and R. L. Merlino, *Dust acoustic waves in a direct current glow discharge*, Phys. Plasmas **4**, 2331 (1997).

[74] V. E. Fortov *et al.*, *Mechanism of dust-acoustic instability in a direct current glow discharge plasma*, Phys. Plasmas **7**, 1374 (2000).

[75] S. V. Ratynskaia *et al.*, *Dust mode in collisionally dominated complex plasmas with particle drift*, IEEE Trans. Plasma Sci. **32**, 613 (2004).

[76] T. Trottenberg, D. Block, and A. Piel, *Dust confinement and dust-acoustic waves in weakly magnetized anodic plasmas*, Phys. Plasmas **13**, 042105 (2006).

[77] E. Thomas Jr., *Measurements of spatially growing dust acoustic waves in a dc glow discharge plasma*, Phys. Plasmas **13**, 042107 (2006).

[78] I. Pilch, T. Trottenberg, A. Piel, and M. E. Koepke, *Dynamics of small dust clouds trapped in a magnetized anodic plasma*, Phys. Plasmas **14**, 123704 (2007).

[79] C.-T. Liao *et al.*, *Lagrangian-Eulerian Micromotion and Wave Heating in Nonlinear Self-Excited Dust-Acoustic Waves*, Phys. Rev. Lett. **100**, 185004 (2008).

[80] T. M. Flanagan and J. Goree, *Observation of the spatial growth of self-excited dust-density waves*, Phys. Plasmas **17**, 123702 (2010).

[81] V. E. Fortov *et al.*, *Large-amplitude dust waves excited by the gas-dynamic impact in a dc glow discharge plasma*, Phys. Rev. E **69**, 016402 (2004).

[82] V. E. Fortov *et al.*, *Shock wave formation in a dc glow discharge dusty plasma*, Phys. Rev. E **71**, 036413 (2005).

[83] J. Heinrich, S.-H. Kim, and R. L. Merlino, *Laboratory Observations of Self-Excited Dust Acoustic Shocks*, Phys. Rev. Lett. **103**, 115002 (2009).

[84] P. Bandyopadhyay, G. Prasad, A. Sen, and P. K. Kaw, *Experimental Study of Nonlinear Dust Acoustic Solitary Waves in a Dusty Plasma*, Phys. Rev. Lett. **101**, 065006 (2008).

[85] R. Heidemann *et al.*, *Dissipative Dark Soliton in a Complex Plasma*, Phys. Rev. Lett. **102**, 135002 (2009).

[86] E. Thomas Jr. and R. L. Merlino, *Dust Particle Motion in the Vicinity of Dust Acoustic Waves*, IEEE Trans. Plasma Sci. **29**, 152 (2001).

[87] M. Schwabe *et al.*, *Highly Resolved Self-Excited Density Waves in a Complex Plasma*, Phys. Rev. Lett. **99**, 095002 (2007).

[88] L.-W. Teng, M.-C. Chang, Y.-P. Tseng, and L. I, *Wave-Particle Dynamics of Wave Breaking in the Self-Excited Dust Acoustic Wave*, Phys. Rev. Lett. **103**, 245005 (2009).

[89] T. M. Flanagan and J. Goree, *Development of nonlinearity in a growing self-excited dust-density wave*, Phys. Plasmas **18**, 013705 (2011).

[90] K. O. Menzel, O. Arp, D. Caliebe, and A. Piel, *The Structure of Self-Excited Dust-Density Waves Under Microgravity*, IEEE Trans. Plasma Sci. **38**, 838 (2010). (see Appendix B.1)

[91] K. O. Menzel, O. Arp, and A. Piel, *Spatial Frequency Clustering in Nonlinear Dust-Density Waves*, Phys. Rev. Lett. **104**, 235002 (2010). (see Appendix B.2)

[92] K. O. Menzel, O. Arp, and A. Piel, *Frequency clusters and defect structures in nonlinear dust-density waves under microgravity conditions*, Phys. Rev. E **83**, 016402 (2011). (see Appendix B.3)

[93] F. Verheest, *Waves In Dusty Space Plasmas* (Kluwer Academic Publishers, Dordrecht, 2000).

[94] P. K. Shukla and M. M. Mamun, *Introduction to dusty plasma physics* (IOP, New York, 2002).

[95] A. Piel, *Plasma Physics: An Introduction to Laboratory, Space, and Fusion Plasmas* (Springer, Berlin, 2010).

[96] M. Bonitz, N. Horing, and P. Ludwig, in *Introduction to Complex Plasmas*, edited by M. Bonitz, N. Horing, and P. Ludwig (Springer, Heidelberg, 2010), Vol. 59.

[97] T. Nitter, *Levitation of dust in rf and dc glow discharges*, Plasma Sources Sci. Technol. **5**, 93 (1996).

[98] A. Piel and A. Melzer, *Dynamical processes in complex plasmas*, Plasma Phys. Control. Fusion **44**, R1 (2002).

[99] V. E. Fortov *et al.*, *Complex (dusty) plasmas: Current status, open issues, perspectives*, Physics Reports **421**, 1 (2005).

[100] A. Piel *et al.*, *Complex plasmas: forces and dynamical behaviour*, Plasma Phys. Control. Fusion **50**, 124003 (2008).

[101] P. K. Shukla and B. Eliasson, *Colloquium: Fundamentals of dust-plasma interactions*, Rev. Mod. Phys. **81**, 25 (2009).

[102] G. E. Morfill and A. V. Ivlev, *Complex plasmas: An interdisciplinary research field*, Rev. Mod. Phys. **81**, 1353 (2009).

[103] E. C. Whipple, *Potentials of surfaces in space*, Rep. Prog. Phys. **44**, 1197 (1981).

[104] F. F. Chen, *Introduction to plasma physics and controlled fusion* (Plenum Press, New York, 1990).

[105] I. H. Hutchinson, *Principles of plasma diagnostics* (Cambridge Univ. Press, Camridge, 2002).

[106] H. M. Mott-Smith and I. Langmuir, *The Theory of Collectors in Gaseous Discharges*, Phys. Rev. **28**, 727 (1926).

[107] O. Arp, D. Block, A. Piel, and A. Melzer, *Dust Coulomb Balls: Three-Dimensional Plasma Crystals*, Phys. Rev. Lett. **93**, 165004 (2004).

[108] O. Arp, D. Block, M. Klindworth, and A. Piel, *Confinement of Coulomb balls*, Phys. Plasmas **12**, 2102 (2005).

[109] S. Käding *et al.*, *Shell transitions between metastable states of Yukawa balls*, Phys. Plasmas **15**, 073710 (2008).

[110] D. Block *et al.*, *Structural and dynamical properties of Yukawa balls*, Plasma Phys. and Control. Fusion **49**, B109 (2007).

[111] A. Melzer *et al.*, *Finite dust clusters in dusty plasmas*, Plasma Phys. Control. Fusion **52**, 124028 (2010).

[112] M. A. Liebermann and A. J. Lichtenberg, *Principles of plasma discharges and material processing.* (John Wiley and Sons Inc., New York, 1994).

[113] P. S. Epstein, *On the resistance experienced by spheres in their motion through gases*, Phys. Rev. **23**, 710 (1924).

[114] B. Liu, J. Goree, V. Nosenko, and L. Boufendi, *Radiation pressure and gas drag forces on a melamine-formaldehyde microsphere in a dusty plasma*, Phys. Plasmas **10**, 9 (2003).

[115] L. S. Frost, *Effect of Variable Ionic Mobility on Ambipolar Diffusion*, Phys. Rev. **105**, 354 (1957).

[116] M. S. Barnes *et al.*, *Transport of dust particles in glow-discharge plasmas*, Phys. Rev. Lett. **68**, 313 (1992).

[117] M. D. Kilgore, J. E. Daugherty, R. K. Porteous, and D. B. Graves, *Ion Drag on an isolated particulate in a low pressure discharge*, J. Appl. Phys. **73**, 7195 (1993).

[118] S. Khrapak, A. V. Ivlev, G. Morfill, and H. Thomas, *Ion drag in complex plasmas*, Phys. Rev. E **66**, 046414 (2002).

[119] S. A. Khrapak, A. V. Ivlev, G. E. Morfill, and S. K. Zhdanov, *Scattering in the attractive Yukawa potential in the limit of strong interaction*, Phys. Rev. Lett. **90**, 225002 (2003).

[120] S. A. Khrapak, A. V. Ivlev, and G. E. Morfill, *Momentum transfer in complex plasmas*, Phys. Rev. E **70**, 056405 (2004).

[121] I. H. Hutchinson, *Ion collection by a sphere in a flowing plasma: 3. Floating potential and drag force*, Plasma Phys. Control. Fusion **47**, 71 (2005).

[122] I. H. Hutchinson, *Collisionless ion drag force on a spherical grain*, Plasma Phys. Control. Fusion **48**, 185 (2006).

[123] C. Zafiu, A. Melzer, and A. Piel, *Ion drag and thermophoretic forces acting on free falling charged particles in an rf-driven complex plasma*, Phys. Plasmas **9**, 4794 (2002).

[124] C. Zafiu, A. Melzer, and A. Piel, *Measurement of the ion drag force on falling dust particles and its relation to the void formation in complex dusty plasmas*, Phys. Plasmas **10**, 1278 (2003).

[125] V. Schneider, T. Trottenberg, I. Teliban, and H. Kersten, *An experiment for the investigation of forces on microparticles in ion beams.*, Rev. Sci. Instrum. **81**, 013503 (2010).

[126] S. V. Vladimirov and M. Nambu, *Attraction of charged particulates in plasmas with finite flows*, Phys. Rev. E **52**, R2172 (1995).

[127] V. A. Schweigert *et al.*, *Alignment and instability of dust crystals in plasmas*, Phys. Rev. E **54**, 4155 (1996).

[128] J. B. Pieper, J. Goree, and R. A. Quinn, *Three-dimensional structure in a crystallized dusty plasma*, Phys. Rev. Lett. **54**, 5636 (1996).

[129] Y. Hayashi, *Structure of a Three-Dimensional Coulomb Crystal in a Fine-Particle Plasma*, Phys. Rev. Lett. **83**, 4764 (1999).

[130] A. Melzer, V. A. Schweigert, and A. Piel, *Transition from attractive to repulsive forces between dust molecules in a plasma sheath*, Phys. Rev. Lett. **83**, 3194 (1999).

[131] R. Kompaneets *et al.*, *Dust clusters with non-Hamiltonian particle dynamics*, Phys. Plasmas **13**, 072104 (2006).

[132] M. Lampe, G. Joyce, G. Ganguli, and V. Gavrishchaka, *Interactions between dust grains in a dusty plasma*, Phys. Plasmas **7**, 3851 (2000).

[133] G. Joyce, M. Lampe, and G. Ganguli, *Instability-Triggered Phase Transition to a Dusty-Plasma Condensate*, Phys. Rev. Lett. **88**, 095006 (2002).

[134] R. Kompaneets *et al.*, *Potential around a charged dust particle in a collisional sheath*, Phys. Plasmas **14**, 052108 (2007).

[135] A. V. Ivlev *et al.*, *First Observation of Electrorheological Plasmas*, Phys. Rev. Lett. **100**, 095003 (2008).

[136] M. Kroll, J. Schablinski, D. Block, and A. Piel, *On the influence of wakefields on three-dimensional particle arrangements*, Phys. Plasmas **17**, 013702 (2010).

[137] J. Goree, G. E. Morfill, V. N. Tsytovich, and S. V. Vladimirov, *Theory of dust voids in plasmas*, Phys. Rev. E **59**, 7055 (1999).

[138] K. Avinash, *"Voids" and phase separation in complex (dusty) plasmas*, Phys. Plasmas **8**, 2601 (2001).

[139] M. R. Akdim and W. J. Goedheer, *Modeling of voids in colloidal plasmas*, Phys. Rev. E **65**, 015401 (2001).

[140] K. Avinash, A. Bhattacharjee, and S. Hu, *Nonlinear Theory of Void Formation in Colloidal Plasmas*, Phys. Rev. Lett. **90**, 075001 (2003).

[141] V. Land and W. J. Goedheer, *Effect of large-angle scattering, ion flow speed and ion-neutral collisions on dust transport under microgravity conditions*, New J. Phys. **8**, 8 (2006).

[142] M. Klindworth, O. Arp, and A. Piel, *Langmuir probe diagnostics in the IMPF device and comparison with simulations and tracer particle experiments*, J. Phys. D: Appl. Phys. **39**, 1095 (2006).

[143] M. Kretschmer *et al.*, *Force field inside the void in complex plasmas under microgravity conditions*, Phys. Rev. E **71**, 056401 (2005).

[144] M. Wolter *et al.*, *Force measurements in dusty plasmas under microgravity by means of laser manipulation*, Phys. Plasmas **14**, 123707 (2007).

[145] H. M. Thomas *et al.*, *Complex Plasmas under Microgravity Conditions: Parabolic Flights*, Phys. Scripta **T89**, 16 (2001).

[146] L.-J. Hou, Y.-N. Wang, and Z. L. Mišković, *Theoretical study of laser-excited Mach cones in dusty plasmas*, Phys. Rev. E **70**, 056406 (2004).

[147] N. D'Angelo, *Coulomb solids and low-frequency fluctuations in RF dusty plasmas*, J. Phys. D: Appl. Phys. **28**, 1009 (1995).

[148] E. Thomas Jr., R. Fisher, and R. L. Merlino, *Observations of dust acoustic waves driven at high frequencies: Finite dust temperature effects and wave interference*, Phys. Plasmas **14**, 123701 (2007).

[149] J. D. Williams, E. Thomas Jr., and L. Marcus, *Observations of vertically propagating driven dust acoustic waves: Finite temperature effects*, Phys. Plasmas **15**, 043704 (2008).

[150] I. Pilch, T. Reichstein, and A. Piel, *Synchronization of dust density waves in anodic plasmas*, Phys. Plasmas **16**, 123709 (2009).

[151] E. Thomas Jr., *Driven dust acoustic waves with thermal effects: Comparison of experiment to fluid theory*, Phys. Plasmas **17**, 043701 (2010).

[152] C.-R. Du *et al.*, *Agglomeration of microparticles in complex plasmas*, Phys. Plasmas **17**, 113710 (2010).

[153] H. R. Prabhakara and V. L. Tanna, *Trapping of dust and dust acoustic waves in laboratory plasmas*, Phys. Plasmas **3**, 3176 (1996).

[154] V. E. Fortov *et al.*, *Dust-acoustic wave instability at the diffuse edge of radio frequency inductive low-pressure gas discharge plasma*, Phys. Plasmas **10**, 1199 (2003).

[155] E. Thomas Jr., *Dust Clouds in Dc-Generated Dusty Plasmas: Transport, Waves, and Three-Dimensional Effects*, Contrib. Plasma Phys. **49**, 316 (2009).

[156] A. Zobnin, A. Usachev, O. Petrov, and V. Fortov, *Dust-acoustic instability in an inductive gas-discharge plasma*, J. Exp. Theoret. Phys. **95**, 429 (2002).

[157] J. D. Williams and E. Thomas Jr., *Initial measurement of the kinetic dust temperature of a weakly coupled dusty plasma*, Phys. Plasmas **13**, 063509 (2006).

[158] O. Arp *et al.*, *Experimental Investigation of Dust Density Waves and Plasma Glow*, IEEE Trans. Plasma Sci. **38**, 842 (2010).

[159] S. V. Singh and N. N. Rao, *Linear and nonlinear dust-acoustic waves in inhomogeneous dusty plasmas*, Phys. Plasmas **5**, 94 (1998).

[160] P. K. Shukla and M. Rosenberg, *Boundary effects on dust-ion-acoustic and dust-acoustic waves in collisional dusty plasmas*, Phys. Plasmas **6**, 1038 (1999).

[161] V. Yaroshenko and G. E. Morfill, *Parametric excitation of low frequency waves in complex (dusty) plasmas*, Phys. Plasmas **9**, 4495 (2002).

[162] N.-X. Wei and J.-K. Xue, *Bounded dust-acoustic waves in a cylindrically bounded collisional dusty plasma with dust charge variation*, Phys. Plasmas **13**, 052101 (2006).

[163] V. V. Yaroshenko, M. H. Thoma, and G. E. Morfill, *Dust density waves in a complex plasma layer*, Phys. Plasmas **14**, 082104 (2007).

[164] M. Rosenberg, *A note on ion-dust streaming instability in a collisional dusty plasma.*, J. Plasma Phys. **67**, 235 (2002).

[165] M. Rosenberg and P. K. Shukla, *A note on dust-acoustic instability in an inductive gas discharge plasma.*, Plasma Phys. Control. Fusion **45**, L31 (2003).

[166] M. Rosenberg, E. Thomas Jr., and R. L. Merlino, *A note on dust wave excitation in a plasma with warm dust: Comparison with experiment.*, Phys. Plasmas **15**, 073701 (2008).

[167] P. Kaw and R. Singh, *Collisional Instabilities in a Dusty Plasma with Recombination and Ion-Drift Effects*, Phys. Rev. Lett. **79**, 423 (1997).

[168] M. R. Jana, A. Sen, and P. K. Kaw, *Collective effects due to charge-fluctuation dynamics in a dusty plasma*, Phys. Rev. E **48**, 3930 (1993).

[169] F. Melandsø, T. Aslaksen, and O. Havnes, *A new damping effect for the dust-acoustic wave*, Planet. Space Sci. **41**, 321 (1993).

[170] A. V. Ivlev and G. Morfill, *Acoustic modes in a collisional dusty plasma: Effect of the charge variation.*, Phys. Plasmas **7**, 1094 (2000).

[171] S. A. Khrapak and V. V. Yaroshenko, *Low-frequency waves in collisional complex plasmas with an ion drift*, Phys. Plasmas **10**, 4616 (2003).

[172] G.-J. He, W.-S. Duan, and D.-X. Tian, *Effects of dust size distribution on dust acoustic waves in two-dimensional unmagnetized dusty plasma*, Phys. Plasmas **15**, 043702 (2008).

[173] P. K. Shukla, *Nonlinear waves and structures in dusty plasmas*, Phys. Plasmas **10**, 1619 (2003).

[174] P. K. Shukla and A. A. Mamun, *Solitons, shocks and vortices in dusty plasmas*, New J. Phys. **5**, 17 (2003).

[175] S. Ratynskaia *et al.*, *Experimental Determination of Dust-Particle Charge in a Discharge Plasma at Elevated Pressures*, Phys. Rev. Lett. **93**, 085001 (2004).

[176] P. K. Kaw and A. Sen, *Low frequency modes in strongly coupled dusty plasmas*, Phys. Plasmas **5**, 3552 (1998).

[177] O. Buneman, Instability, *Turbulence, and Conductivity in Current-Carrying Plasma*, Phys. Rev. Lett. **1**, 8 (1958).

[178] M. Mikikian *et al.*, *Self-excited void instability in dusty plasmas: plasma and dust cloud dynamics during the heartbeat instability*, New J. Phys. **9**, 268 (2007).

[179] D. Winske and M. Rosenberg, *Nonlinear development of the dust acoustic instability in a collisional dusty plasma*, IEEE Trans. Plasma Sci. **26**, 92 (1998).

[180] J. Pramanik *et al.*, *Experimental observation of dust-acoustic wave turbulence*, Phys. Lett. A **312**, 84 (2003).

[181] S. Kyrkos, G. J. Kalman, and M. Rosenberg, *Beam-Plasma Instabilities in a 2D Yukawa Lattice*, Phys. Rev. Lett. **102**, 225006 (2009).

[182] M. Rosenberg and G. Kalman, *Dust acoustic waves in strongly coupled dusty plasmas*, Phys. Rev. E **56**, 7166 (1997).

[183] M. S. Murillo, *Longitudinal collective modes of strongly coupled dusty plasmas at finite frequencies and wavevectors*, Phys. Plasmas **7**, 33 (2000).

[184] V. V. Yaroshenko, V. Nosenko, and G. E. Morfill, *Effect of strong electrostatic interactions of microparticles on the dust acoustic waves*, Phys. Plasmas **17**, 103709 (2010).

[185] M. Klindworth, O. Arp, and A. Piel, *Langmuir probe system for dusty plasmas under microgravity*, Rev. Sci. Instrum. **78**, 033502 (2007).

[186] Siglo-2D, Version 1.1, Kinema Software.

[187] S. A. Khrapak *et al.*, *Particle charge in the bulk of gas discharges*, Phys. Rev. E **72**, 016406 (2005).

[188] M. R. Akdim and W. J. Goedheer, *Modeling the effect of dust on the plasma parameters in a dusty argon discharge under microgravity*, Phys. Rev. E **67**, 066407 (2003).

[189] V. Land and W. J. Goedheer, *The Plasma inside a dust free void: hotter, denser or both?*, New J. Phys. **9**, 0246 (2007).

[190] V. Nosenko *et al.*, *Measurements of the power spectrum and dispersion relation of self-excited dust acoustic waves*, Europhys. Lett. **88**, 65001 (2009).

[191] D. Gabor, *Theory of Communication*, J. Inst. Electr. Eng. **93**, 429 (1946).

[192] F. W. King, *Hilbert Transforms* (Cambridge Univ. Press, Cambridge, 2009).

[193] J. F. Nye and M. V. Berry, *Dislocations in Wave Trains*, Proc. R. Soc. Lond. A **336**, 165 (1974).

[194] M.-A. Bray and J. P. Wikswo, *Use of topological charge to determine filament location and dynamics in a numerical model of scroll wave activity*, IEEE Trans. Biomed. Eng. **47**, 1086 (2002).

[195] K. E. Daniels and E. Bodenschatz, *Statistics of defect motion in spatiotemporal chaos in inclined layer convection*, Chaos **13**, 55 (2003).

[196] M. R. Dennis, *Braided nodal lines in wave superpositions*, New J. Phys. **5**, 134 (2003).

[197] C. Giacovazzo *et al.*, in *Fundamentals of Crystallography*, edited by C. Giacovazzo (Oxford Univ. Press, Oxford, 2011).

[198] F. S. Roux, *Fluid dynamical enstrophy and the number of optical vortices in a paraxial beam*, Opt. Commun. **268**, 15 (2006).

[199] Y. Feng, J. Goree, and B. Liu, *Accurate particle position measurement from images*, Rev. Sci. Instrum. **78**, 053704 (2007).

[200] B. Boashash, *Estimating and interpreting the instantaneous frequency of a signal. Part I: Fundamentals*, Proc. IEEE **80**, 520 (1992).

[201] N. E. Huang *et al.*, *On Instantaneous Frequency*, Adv. Adap. Data Ana. **1**, 177 (2009).

[202] B. M. Annaratone *et al.*, *Complex-plasma manipulation by radiofrequency biasing*, Plasma Phys. Control. Fusion **46**, B495 (2004).

[203] S. Käding and A. Melzer, *Three-dimensional stereoscopy of Yukawa (Coulomb) balls in dusty plasmas*, Phys. Plasmas **13**, 090701 (2006).

[204] M. Kroll, S. Harms, D. Block, and A. Piel, *Digital in-line holography of dusty plasmas*, Phys. Plasmas **15**, 063703 (2008).

[205] D. Samsonov *et al.*, *High speed laser tomography system*, Rev. Sci. Instrum. **79**, 035102 (2008).

[206] B. Buttenschön, M. Himpel, and A. Melzer, *Spatially resolved three-dimensional particle dynamics in the void of dusty plasmas under microgravity using stereoscopy*, New J. Phys. **13**, 023042 (2011).

[207] M. Gaster, *Vortex shedding from circular cylinders at low Reynolds numbers*, J. Fluid Mech. **46**, 749 (1971).

[208] B. R. Noack, F. Ohle, and H. Eckelmann, *On Cell-Formation In Vortex Streets*, J. Fluid Mech. **227**, 293 (1991).

[209] N. E. Diamant and A. Bortoff, *Nature of the intestinal slow-wave frequency gradient*, Am. J. Physiol. **216**, 301 (1969).

[210] S. K. Sarna, E. E. Daniel, and Y. J. Kingma, *Simulation of slow-wave electrical activity of small intestine*, Am. J. Physiol. **221**, 166 (1971).

[211] T. E. Vadivasova, G. I. Strelkova, and V. S. Anishchenko, *Phase-frequency synchronization in a chain of periodic oscillators in the presence of noise and harmonic forcings*, Phys. Rev. E **63**, 036225 (2001).

[212] N. E. Diamant, P. K. Rose, and E. J. Davison, *Computer simulation of intestinal slow-wave frequency gradient*, Am. J. Physiol. **219**, 1684 (1970).

[213] B. Robertson-Dunn and D. A. Linkens, *A mathematical model of the slow-wave electrical activity of the human small intestine*, Med. Biol. Eng. Comp. **12**, 750 (1974).

[214] S. Balasubramanian and R. A. Skop, *A Nonlinear Oscillator Model For Vortex Shedding From Cylinders And Cones In Uniform And Shear Flows*, J. Fluids Structures **10**, 197 (1996).

[215] G. V. Osipov and J. Kurths, *Regular and chaotic phase synchronization of coupled circle maps*, Phys. Rev. E **65**, 016216 (2001).

[216] G. V. Osipov, A. S. Pikovsky, M. G. Rosenblum, and J. Kurths, *Phase synchronization effects in a lattice of nonidentical Rössler oscillators*, Phys. Rev. E **55**, 2353 (1997).

[217] G. V. Osipov and M. M. Sushchik, *Synchronized clusters and multistability in arrays of oscillators with different natural frequencies*, Phys. Rev. E **58**, 7198 (1998).

[218] L. L. Rubchinsky, M. M. Sushchik, and G. V. Osipov, *Patterns in networks of oscillators formed via synchronization and oscillator death*, Math. Comp. Sim. **58**, 443 (2002).

[219] A. Vilfan and T. Duke, *Frequency Clustering in Spontaneous Otoacoustic Emissions from a Lizard's Ear*, Biophys. J. **95**, 4622 (2008).

[220] O. I. Kanakov, G. V. Osipov, C.-K. Chan, and J. Kurths, *Cluster synchronization and spatio-temporal dynamics in networks of oscillatory and excitable Luo-Rudy cells*, Chaos **17**, 015111 (2007).

[221] G. V. Osipov, J. Kurths, and C. Zhou, *Synchronization in oscillatory networks* (Springer, Dordrecht, 2007).

[222] A. La Porta and C. M. Surko, *Predicting the motion of phase defects in a traveling-wave convection pattern*, Physica D **139**, 177 (2000).

[223] P. C. Bressloff and S. Coombes, *Traveling Waves in a Chain of Pulse-Coupled Oscillators*, Phys. Rev. Lett. **80**, 4815 (1998).

[224] M. E. Koepke and D. M. Hartley, *Experimental verification of periodic pulling in a nonlinear electronic oscillator*, Phys. Rev. A **44**, 6877 (1991).

[225] H. Haken, *Synergetics* (Springer, Berlin, 1983).

[226] T. Gyergyek, M. Čerček, and M. Stanojević, *Experimental Evidence of Periodic Pulling in a Weakly Magnetized Discharge Plasma Column*, Contrib. Plasma Phys. **37**, 399 (1997).

[227] H. Lashinsky, *Periodic pulling and the transition to turbulence in a system with discrete modes, in Proceedings of the Symposium on Turbulence of Fluids and Plasmas*, edited by J. Fox (Polytechnic Institute of Brooklyn, Brooklyn, 1969), pp. 24–46.

[228] B. E. Keen and W. H. W. Fletcher, *Measurement of growth rate, non-linear saturation coefficients, and mode-mode coupling coefficients of a 'Van der Pol' plasma instability*, J. Phys. D: Appl. Phys. **3**, 1868 (1970).

[229] F. Melandsø, *Lattice waves in dust plasma crystals*, Phys. Plasmas **3**, 3890 (1996).

[230] L. Pekárek, J. Beránek, and J. Krása, *Creation of discontinuities in a frequency-modulated ionisation wave*, J. Phys. D: Appl. Phys. **11**, 1731 (1978).

[231] M. E. Koepke, A. Dinklage, T. Klinger, and C. Wilke, *Spatiotemporal signatures of periodic pulling during ionization-wave-mode transitions*, Phys. Plasmas **8**, 1432 (2001).

B Reprints of Journal Papers

B.1

THE STRUCTURE OF SELF-EXCITED DUST-DENSITY WAVES UNDER MICROGRAVITY

K. O. Menzel, O. Arp, D. Caliebe, and A. Piel

The Structure of Self-Excited Dust-Density Waves Under Microgravity

Kristoffer Ole Menzel, Oliver Arp, David Caliebe, and Alexander Piel

Abstract—Dusty plasmas under microgravity conditions are a great opportunity to observe dynamical processes in strongly coupled systems. For example, in such systems, self-excited dust-density waves can occur at low gas pressures in extended regions of the discharge. Recently, we have performed a series of measurements in a parallel-plate RF reactor during parabolic flights. It reveals that the waves can appear in two completely different states. One of them yields a high spatial and temporal coherence of the density fluctuations. This feature allows us to utilize scanning video microscopy to obtain information on the structure of the 3-D wave field. Under different experimental conditions, we also found that a wave field with multiple different wavelengths can arise in the dust volume. This results in defects in the wave pattern due to merging wavefronts. We determine their temporal evolution, which can be derived accurately from the phase information.

Index Terms—Dust-density waves (DDWs), dusty plasma, microgravity, topological charge.

I. INTRODUCTION

EXPERIMENTAL studies of dust-density waves (DDWs) became a field of broad interest in the community of complex plasmas, since they were first observed by Barkan *et al.* [1]. The onset of the waves is triggered by streaming ions, and they emerge spontaneously at low gas pressures and high dust densities. Since no external excitation is required, i.e., by applying an additional modulated low-frequency bias, we call the waves self-excited. Nevertheless, other experiments used bias modulation of the electrodes to excite waves in an otherwise stable dust cloud [2], [3].

DDWs were studied extensively in the laboratory in dc plasmas [4]–[6] as well as in radio-frequency (RF) discharges [7]. Unfortunately, those measurements are influenced by the gravitational force which introduces an unwanted preferred direction to the system. This can lead to asymmetries in the dust clouds or even compress them in the plasma sheath. One method to avoid this problem is to establish a temperature gradient in the discharge to compensate for gravity [8]. However, this results in more forces acting on the dust particles, complicating the situation. Thus, a number of measurements were performed under microgravity conditions on parabolic flights [9]–[11] and
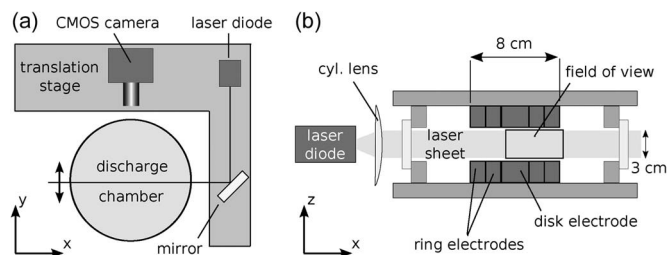
Fig. 1. Sketch of the IMPF-K chamber. (a) The top view shows the translation stage which allows scans in the y-direction. (b) The side view illustrates the vertical laser sheet illuminating a plane between the electrodes. The concrete field of view, seen by the camera, is also marked.

aboard the International Space Station [2], [3]. Here, the DDWs can be observed in extended large dust clouds. We showed earlier that these waves propagate in the direction of the local ion flow or at an oblique angle for ion velocities comparable with the Bohm velocity [9]–[11]. Recent investigations described the structure of externally driven DDWs in those situations qualitatively [12]. In this paper, we present complementary methods to study the structure and the wave dynamics in more detail.

II. EXPERIMENTAL SETUP AND OBSERVATIONS

All observations of DDWs presented in the following were carried out in the International Microgravity Plasma Facility–Kiel (IMPF-K) chamber on parabolic flights. The facility was already used for a number of measurements under microgravity and is described in detail elsewhere [13].

It consists of a symmetric capacitively coupled parallel RF discharge, operating at 13.56 MHz. A sketch of the device is shown in Fig. 1. In this configuration, the electrodes are segmented into a central disk and two concentric electrically connected rings. The vertical distance between the electrodes is 30 mm, and the outer ring has a diameter of 80 mm. Self-excited waves occur when RF amplitudes of typically $U_{\rm rf} = (40 \ldots 80)$ $V_{\rm PP}$ are applied to the center and ring electrodes, operating in push–pull mode. Argon is chosen as the working gas and waves could be observed at pressures of $(10 \ldots 30)$ Pa. Dust with a diameter of 6.8 μm is introduced to the reactor via the six dispensers situated at the chamber edges. Earlier investigations showed that the electron temperature is $T_e = (2.5 \ldots 4)$ eV, and the ion density $n_i \approx 1 \times 10^{15} {\rm m}^{-3}$ [14].

The primary diagnostics for measuring wave properties is a scanning video microscopy (SVM) system with a high-speed CMOS camera. It records the scattered light of the dust particles
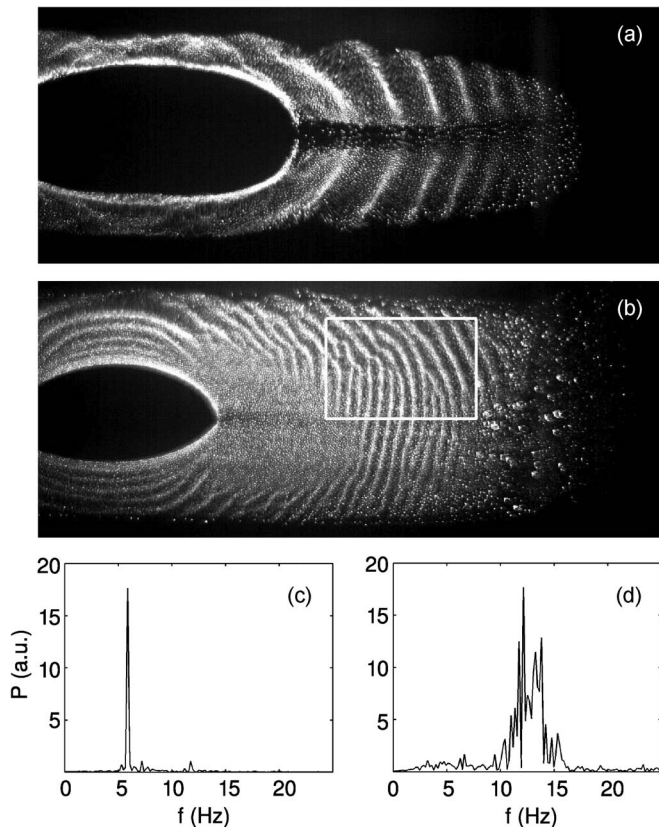
Fig. 2. Self-excited waves can be observed in two different specific states. The wave field can be either (a) coherent over a broad region or (b) it shows a high amount of topological defects. Another difference can be seen in the typical power spectra of the waves: (c) The coherent waves are highly monochromatic, whereas (d) states containing defects have several dominant peaks.

which are illuminated by a vertical laser sheet ($\lambda = 660$ nm). The frame rate of the camera (approximately 100 frames/s) guarantees that the measured wave frequencies of up to 10 Hz are not affected by aliasing effects. As the whole system is mounted on a translation stage, the observations are not limited to a fixed plane, but horizontal scans through the complete dust cloud are possible.

Typical images of self-excited DDWs are shown in Fig. 2(a) and (b), at a gas pressure of $p = 15$ Pa and $p = 30$ Pa, respectively. In both situations, RF amplitudes of 70 V_{pp} (center) and 50 V_{pp} (ring) were applied to the electrodes. The field of view has a resolution of 1200×500 pixels which corresponds to 67×28 mm^2. The observed intensity modulations indicate wave activity and—after being blurred with a Gaussian filter—can be used as an estimate for dust density n_d. The waves propagate at typical velocities of a few 10 mm $\cdot$ s^{-1} radially outward from the dust-free center of the discharge, the so-called void, to the discharge edges.

Our measurements at different pressures and RF voltages in the aforementioned ranges clearly depict that the waves can be found in two specific states. It is obvious that the first one has a strong spatial and temporal coherence. Typical Fourier spectra from the wave fields can be seen in Fig. 2(c) and (d). Their evaluation reveals an additional highly monochromatic nature of the coherent state. Its spectrum consists of only one sharp peak, except for the first harmonic, as a consequence of the
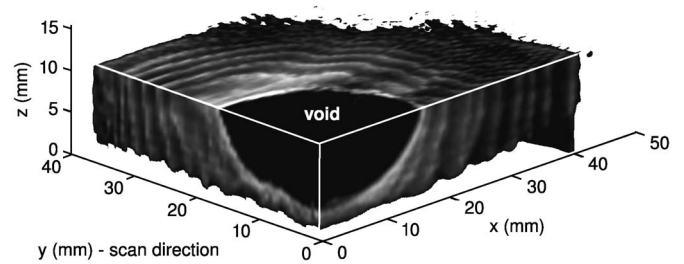

Fig. 3. Three-dimensional reconstruction of the wave field displayed in Fig. 2(a). The figure shows an octant of the complete dust cloud. The recorded images lie in the xz-plane, whereas the scan is done in the y-direction.

nonlinear wave character. Furthermore, the peak deviates only slightly from the mean over the complete wave field (only by a few tenths percent).

The second situation, however, looks quite different. It is characterized by a high amount of topological defects appearing as bifurcations in single-wavefronts. This structure is also reflected in a broad spectrum, implying that the number of wavefronts passing a fixed point in the wave field per time varies temporally.

III. THREE-DIMENSIONAL RECONSTRUCTION

The high spatial and temporal coherence of the waves in monochromatic states leads to the idea of reconstructing a still picture of the wave field in three dimensions. For this purpose, we recorded sequences of the images when the laser sheet was scanned through the discharge. As the dust-cloud geometry is assumed to be rotationally symmetric, we have chosen to limit the scan to one half-space, starting at the equatorial plane.

After data acquisition, a correlation analysis is performed to assure that the waves have a high degree of coherence. In the next step, from the whole bunch of images, only those with a constant phase relation to each other are fetched for the reconstruction. This criterion allows us to treat the images as if all of them were recorded at the same time, similar to stroboscopic sampling. The temporal gap between two selected frames is therefore $\Delta T = 1/f_{rec}$. The reconstruction frequency f_{rec} is identified as the dominant peak in a spectrum of time series taken during a scan. Note that because the speed of the translation stage ($v_{scan} = 3.15$ mm $\cdot$ s^{-1}) is on the order of the wave's phase velocity, the Doppler effect causes a difference between f_{rec} and the real wave frequency f_{DDW} here. After this preselection, the images are stored in a 3-D data set on the order of the given temporal evolution.

Applying the described algorithm offers a new kind of visualizing wave fields. Fig. 3 shows an octant of the same dust cloud recorded in Fig. 2(a). The recorded images lie in the xz-plane, and the scan goes along the y-axis. As the resolution in the xz-plane is usually up to ten times higher, a standard interpolation algorithm between data points in the y-direction is applied.

The reconstruction depicts the shape of single wavefronts. They lie concentrically around the void. Possible irregularities are attributed to fluctuations in the residual gravity during parabolas. Therefore, the reconstruction underlines the presumption of rotational symmetry.

IV. Topological Defects

In the preceding section, we described self-excited waves occurring in a monochromatic state. However, most of our observations did not show highly coherent or monochromatic waves. We rather found disordered structures with bifurcations in the wavefronts, resembling ripple marks in the sand at shores. Those bifurcations, where the wavefronts split or merge, are known as topological defects. Their appearance and number is mainly affected by the total amount of dust inside the plasma. Our measurements showed that a high dust amount leads in general to the formation of defect patterns. In contrast, the variation of typical discharge parameters, i.e., gas pressure, RF amplitudes, or particle size, affects the frequency and the wavelength of the DDWs.

As the coherence is a fundamental-wave attribute for a successful reconstruction, the described algorithm fails for the disordered states. However, a detailed analysis of the defect motion in two dimensions is possible and allows a deeper insight into the dynamics of self-excited DDWs.

We showed earlier that phase information in the wave field can be determined from the dominant frequency in the power spectrum [11]. This information was then used to get an estimate of the wavelength anywhere in the wave field. In the following, we will show that the resulting phase maps can also be utilized to detect the topological defects accurately.

Because the phase was so far projected on one spectral component, the derivation of wave properties from phase maps was restricted to time-averaged information. Nonetheless, in the present case, the temporal evolution of the defects is of interest and, hence, a new definition of the phase is necessary. This is possible by means of the analytic signal, where the original real time series of intensity $I(x, z, t)$ is expanded into the complex plane

$$A(x, z, t) = I(x, z, t) + i \cdot \tilde{I}(x, z, t). \tag{1}$$

Rewriting (1) in Euler's notation results in

$$A(x, z, t) = E(t) \cdot \exp\left[i \cdot \phi(x, z, t)\right] \tag{2}$$

with the envelope function $E(t)$ and the instantaneous phase

$$\phi(x, z, t) = \arctan\left(\frac{\tilde{I}(x, z, t)}{I(x, z, t)}\right). \tag{3}$$

The calculation of the complex part $\tilde{I}(t)$ is done by the Hilbert transform, a standard technique in digital signal processing

$$\tilde{I}(t) = H\left\{I(t)\right\} = \frac{1}{\pi} \int_{-\infty}^{\infty} \frac{I(\tau)}{t - \tau} \, d\tau. \tag{4}$$

The resulting phase map for the region of interest marked by the white rectangle in Fig. 2(b) is shown in Fig. 4. The phase information is mapped periodically between 0 and 2π. Note that both maps represent exactly the same time step in the recorded sequence. As can be seen, the phase map resembles the raw data
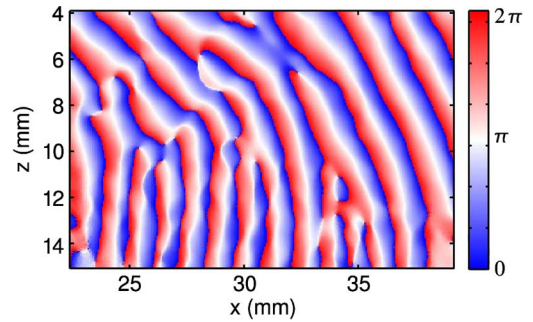

Fig. 4. Instantaneous phase can be calculated for any time step of a recorded sequence. The resulting phase map clearly resembles the original raw data (white box in Fig. 2).
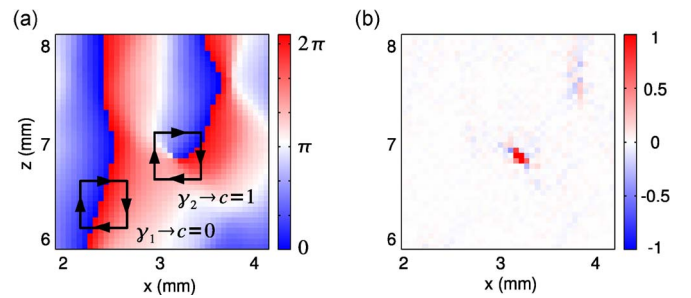

Fig. 5. (a) To detect singularities in a phase map, the integral in (5) is calculated for each pixel. (b) The resulting topological charge. Only paths encircling a singularity, like γ_2, contribute to the charge.

quite well; single wavefronts and, thus, also the defect positions can be recognized.

The next step to detect these singularities in a wave field is done by calculating the topological charge [15]. It is determined by the integral

$$c(x, z, t) = \frac{1}{2\pi} \oint_{\gamma} \vec{\nabla}\phi(x, z, t) \, d\vec{l} \tag{5}$$

over a closed path γ at any point in the phase map. Hence, only at those positions where γ encircles a singularity that the topological charge will differ from zero. In principle, $c(x, z, t)$ will be an integer multiple of 2π. For the measured data, it lies in between $+1$ and -1, depending on the sense of rotation of the phase at a defect position. To clarify the procedure, Fig. 5(a) shows a small region around a dislocation in the phase map. Two closed paths are drawn. One of them has its center on a wavefront (γ_1), whereas the other one encircles a singularity (γ_2). Obviously, only the second contributes to the topological charge. The result is shown in Fig. 5(b).

As the defect positions are now determined, their temporal evolution can be analyzed. We observed two different scenarios. On the one hand, the defects are locked in the wave field and, consequently, their velocities are comparable with the wave speed. The wave pattern moves as a whole. On the other hand, the defects can be fixed in space, resulting in a permanent splitting and merging of wavefronts.

V. Summary

In this paper, we have presented recently performed measurements under microgravity conditions. They comprise two

different states of self-excited DDWs. One of them, namely, a highly coherent and monochromatic one, is suitable to be fully reconstructed in three dimensions by SVM. It reveals a rotational symmetry of the wave field and gives first hints of the interplay of the bulk and surface modes of the waves.

The other state, observed in the majority of the measurements, is characterized by an extended defect structure. Bifurcations in the wavefront pattern are made responsible to match regions of different plasma parameters in the wave field. The extension of measured signals to the complex plane by means of the Hilbert transform allows us to extract the phase information of wave fields at any time step. The resulting phase maps are used to determine defect positions. Further investigations will have to analyze the defect trajectories in the wave field with emphasis on the relative motion to the wavefronts in more detail.

REFERENCES

[1] A. Barkan, R. L. Merlino, and N. D'Angelo, "Laboratory observation of the dust-acoustic wave mode," *Phys. Plasmas*, vol. 2, no. 10, pp. 3563–3565, Oct. 1995.

[2] S. Khrapak, D. Samsonov, G. Morfill, H. Thomas, V. Yaroshenko, H. Rothermel, T. Hagl, V. Fortov, A. Nefedov, V. Molotkov, O. Petrov, A. Lipaev, A. Ivanov, and Y. Baturin, "Compressional waves in complex (dusty) plasmas under microgravity conditions," *Phys. Plasmas*, vol. 10, no. 1, pp. 1–4, Jan. 2003.

[3] V. V. Yaroshenko, B. M. Annaratone, S. A. Khrapak, H. M. Thomas, G. E. Morfill, V. E. Fortov, A. M. Lipaev, V. I. Molotkov, O. F. Petrov, A. I. Ivanov, and M. V. Turin, "Electrostatic modes in collisional complex plasmas under microgravity conditions," *Phys. Rev. E, Stat. Phys. Plasmas Fluids Relat. Interdiscip. Top.*, vol. 69, no. 6, p. 066401, Jun. 2004.

[4] E. Thomas, Jr., "Measurements of spatially growing dust acoustic waves in a DC glow discharge plasma," *Phys. Plasmas*, vol. 13, no. 4, p. 042107, Apr. 2006.

[5] T. Trottenberg, D. Block, and A. Piel, "Dust confinement and dust-acoustic waves in weakly magnetized anodic plasmas," *Phys. Plasmas*, vol. 13, no. 4, p. 042105, Apr. 2006.

[6] I. Pilch, T. Trottenberg, A. Piel, and M. E. Koepke, "Dynamics of small dust clouds trapped in a magnetized anodic plasma," *Phys. Plasmas*, vol. 14, no. 12, p. 123704, Dec. 2007.

[7] C.-T. Liao, L.-W. Teng, C.-Y. Tsai, C.-W. Io, and I. Lin, "Lagrangian–Eulerian micromotion and wave heating in nonlinear self-excited dust-acoustic waves," *Phys. Rev. Lett.*, vol. 100, no. 18, p. 185 004, May 2008.

[8] M. Schwabe, M. Rubin-Zuzic, S. Zhdanov, H. M. Thomas, and G. E. Morfill, "Highly resolved self-excited density waves in a complex plasma," *Phys. Rev. Lett.*, vol. 99, no. 9, p. 095002, Aug. 2007.

[9] A. Piel, M. Klindworth, O. Arp, A. Melzer, and M. Wolter, "Obliquely propagating dust-density plasma waves in the presence of an ion beam," *Phys. Rev. Lett.*, vol. 97, no. 20, p. 205009, Nov. 2006.

[10] A. Piel, M. Klindworth, O. Arp, A. Melzer, and M. Wolter, "Erratum: Obliquely propagating dust-density plasma waves in the presence of an ion beam," *Phys. Rev. Lett.*, vol. 99, no. 20, p. 209903, Nov. 2007.

[11] A. Piel, O. Arp, M. Klindworth, and A. Melzer, "Obliquely propagating-dust density waves," *Phys. Rev. E, Stat. Phys. Plasmas Fluids Relat. Interdiscip. Top.*, vol. 77, no. 2, p. 026407, Feb. 2008.

[12] M. Schwabe, S. K. Zhdanov, H. M. Thomas, A. V. Ivlev, M. Rubin-Zuzic, G. E. Morfill, V. I. Molotkov, A. M. Lipaev, V. E. Fortov, and T. Reiter, "Nonlinear waves externally excited in a complex plasma under microgravity conditions," *New J. Phys.*, vol. 10, p. 033037, 2008.

[13] M. Klindworth, O. Arp, and A. Piel, "Langmuir probe diagnostics in the IMPF device and comparison with simulations and tracer particle experiments," *J. Phys. D, Appl. Phys.*, vol. 39, no. 6, pp. 1095–1104, Mar. 2006.

[14] M. Klindworth, O. Arp, and A. Piel, "Langmuir probe system for dusty plasmas under microgravity," *Rev. Sci. Instrum.*, vol. 78, no. 3, p. 033502, Mar. 2007.

[15] J. F. Nye and M. V. Berry, "Dislocations in wave trains," *Proc. R. Soc. Lond. A, Math. Phys. Sci.*, vol. 336, no. 1605, pp. 165–190, Jan. 1974.

Kristoffer Ole Menzel received the Diploma degree in physics from Christian-Albrechts-Universität (CAU) Kiel, Kiel, Germany, in 2008 where he is currently working toward the Ph.D. degree in the group of A. Piel.

He participated on several parabolic flight campaigns. His interests include the dynamics of density waves in dusty plasmas under microgravity.

Oliver Arp received the Ph.D. degree in physics from Christian-Albrechts-Universität (CAU) Kiel, Kiel, Germany, in 2006.

Currently, he is Postdoctoral Research Fellow with CAU Kiel and Coordinator of the microgravity experiment.

David Caliebe received the Diploma degree in physics from Christian-Albrechts-Universität (CAU) Kiel, Kiel, Germany, in 2008 where he is currently working toward the Ph.D. degree in the group of A. Piel.

He participated on several parabolic flight campaigns. His interests include transport phenomena in dusty plasmas under microgravity.

Alexander Piel was born in 1950. He received the Ph.D. degree and habilitation from Ruhr-University Bochum, Bochum, Germany, in 1977 and 1986, respectively.

Since 1989, he has been a Full Professor with Christian-Albrechts-Universität (CAU) Kiel, Kiel, Germany. His research interests cover dusty plasmas, plasma waves, and ionospheric research.

Dr. Piel is a Fellow of the APS.

B.2

SPATIAL FREQUENCY CLUSTERING IN NONLINEAR DUST-DENSITY WAVES

K. O. Menzel, O. Arp, and A. Piel

P H Y S I C A L   R E V I E W   L E T T E R S

Spatial Frequency Clustering in Nonlinear Dust-Density Waves

K. O. Menzel,* O. Arp, and A. Piel

Institut für Experimentelle und Angewandte Physik, Christian-Albrechts-Universiät, Kiel, Germany
(Received 26 February 2010; published 7 June 2010)

Self-excited density waves were studied in a strongly coupled dusty plasma of a radio-frequency discharge under microgravity conditions. The spatiotemporal evolution of the complicated three-dimensional wave field was investigated and analyzed for two different situations. The reconstructed instantaneous phase information of the wave field revealed a partial synchronization within multiple distinct domains. The boundaries of these regions coincide with the locations of topological defects.

　　　　　　　PACS numbers: 52.27.Lw, 05.45.Xt, 52.35.Fp, 52.35.Mw

Synchronization, the mutual adjustment of rhythms of coupled independent oscillators, has enjoyed great popularity among all fields of natural sciences [1], since its first observation by Huygens [2]. Popular examples are swarms of fireflies [3], neural networks [4], and the interaction between the human cardiovascular and respiratory systems [5]. Synchronization is also observed in spatially extended systems consisting of a large number of constituents such as plasma discharges, where the entrainment of global oscillations [6–8] or waves [9,10] by external drivers are well-known features.

A unique laboratory for studying dynamic processes in many-body systems is strongly coupled dusty plasmas. These systems contain highly charged micrometer-sized particles that interact via a screened Coulomb (Yukawa) potential. Dusty plasmas are highly transparent, and their dynamics is slow with typical time scales of the order of a few ten Hz. Therefore, it is possible to track the motion of individual particles by means of video cameras. Since gravity leads to particle sedimentation into flat dust clouds, the investigation of large three-dimensional systems is preferentially done under weightlessness [11] or by compensating gravity by means of an additional force [12]. Damping and coupling between the particles can be adjusted over a wide range by changing the gas friction and the plasma parameters. By these means it is possible to produce dusty plasmas in crystalline, liquid, or gaseous states.

Wavelike instabilities have been observed in each of these states as propagating dust-density fluctuations [13–16] in one-, two-, and three-dimensional geometry. Waves can either be externally excited in otherwise stable systems by an additional, periodic force [17] or they can be self-excited if internal sources of free energy exist [13]. The latter case is attributed to a Buneman-type instability that arises from streaming ions relative to the dust particles [18]. The natural oscillation frequency of the individual particles is determined by the local plasma parameters and their interaction with neighboring particles. The manipulation of self-excited waves by external drivers is a well-established technique to get insight into the dispersion

properties of the wave [19]. Further, the nonlinear interaction between the driver and the system was recently studied in detail [20]. Experiments on nonlinear phenomena concerned nonperiodic structures such as shock waves [21] and solitons [22], as well as wave breaking [23].

It is known from other fields of physics that nonlinear effects can significantly affect the macroscopic behavior of extended systems of coupled oscillators. A prominent example is the formation of so-called synchronization clusters or frequency plateaus, i.e., spatial regions in which the individual oscillators adjust to one collective frequency [24]. In such systems, distinct clusters of different oscillation frequencies may occur. This situation is called partial rather then global synchronization. This effect is well known from numerical calculations of chaotic Rössler oscillators [25], weakly nonlinear Ginzburg-Landau systems [26], Van der Pol oscillators [26,27], and the Luo-Rudy model for cardiac cells [28], when the natural frequencies of the individual oscillators have a spatial variation. Nevertheless, experimental observations of spatial frequency clustering are rare, especially in higher dimensions. In this Letter, we investigate self-excited dust-density waves (DDWs) in a nonuniform plasma background in order to study such nonlinear synchronization phenomena.

The experiments were performed in the IMPF-K2 parallel-plate radio-frequency (rf) reactor on parabolic flights under microgravity conditions. A vertical section through the device is shown in Fig. 1. It is identical to the chamber described in Ref. [15], except for a simplified electrode configuration. The discharge was operated with peak-to-peak voltages of $U_{rf} = (40$–$70)$ V_{pp} at 13.56 MHz in push-pull mode. Spherical monodisperse melamine-formaldehyde particles of (9.55 ± 0.13) μm diameter were injected into an argon plasma. Self-excited dust-density waves emerge spontaneously in large dust clouds at neutral gas pressures below a critical value of $p_{crit} \approx 30$ Pa.

A video microscope was used for the observation of the particle dynamics. A vertical sheet of light from a low-power laser diode illuminates a thin slice of the dust cloud
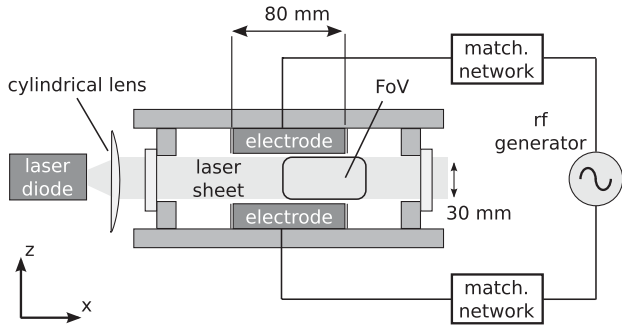
FIG. 1. Side view of the IMPF-K2 chamber. Particles are illuminated by laser diode. The camera's field of view (FoV) is marked with a rectangle. Both electrodes are fed by the same rf generator operating in push-pull mode via two matching networks.

inside the plasma. The scattered light of the particles is observed at a right angle by a camera operating at a frame rate of 100 frames per second. Aliasing effects can be excluded, since typical frequencies of the DDWs are below 20 Hz. The observed field of view has a spatial resolution of 400×910 pixels, which corresponds to an area of (21.6×47.3) mm^2 in the plane of the laser sheet.

A typical snapshot of a dust cloud at $U_{rf} = 48$ V$_{pp}$ and $p = 15$ Pa is shown in Fig. 2(a). Obviously, the dust density is periodically modulated by self-excited DDWs, which propagate from the boundary of the central dust-free region (void) outwards with a phase velocity of $v_{ph} = (10$–$30)$ mm s^{-1}. Although, the waves are driven by ions flowing from the center of the discharge outwards, the propagation direction of the wave is not necessarily parallel to the ion flow [15,16]. A first indication for a nonlinear character of the DDWs can be obtained directly from the snapshot: The wave has a strongly nonsinusoidal shape with very narrow crests and broad troughs, which contain a significantly reduced number of dust particles. The wavelength is not constant over the entire dust cloud. It varies from $\lambda_{DDW} \approx 1.5$ mm close to the void to $\lambda_{DDW} \approx 3$ mm in the outer regions of the cloud. Wave fronts are not strictly parallel, but they may split or merge. Such spots are known as topological defects, which are not fixed in the wave field, but move at $(70$–$90)\%$ of the local phase velocity of the wave.

The blurred intensity of a video frame yields direct information on the spatial dust-density distribution $n_d(x, z)$ as both quantities are assumed to be proportional to each other. For a detailed analysis of the temporal evolution of general wave parameters, n_d is transformed into its analytic signal $A(x, z, t) = n_d(x, z, t) + i \cdot \hat{n}_d(x, z, t)$ by means of a Hilbert transform, which is commonly used in digital signal processing. It allows us to define instantaneous wave properties such as the phase $\phi(t) = \arctan[\hat{n}_d(t)/n_d(t)]$ and the instantaneous frequency via $f_i = \partial\phi/\partial t$. With this method we have evaluated time series with a length of approximately 10 wave periods. In this way, it is possible to map the spatial phase
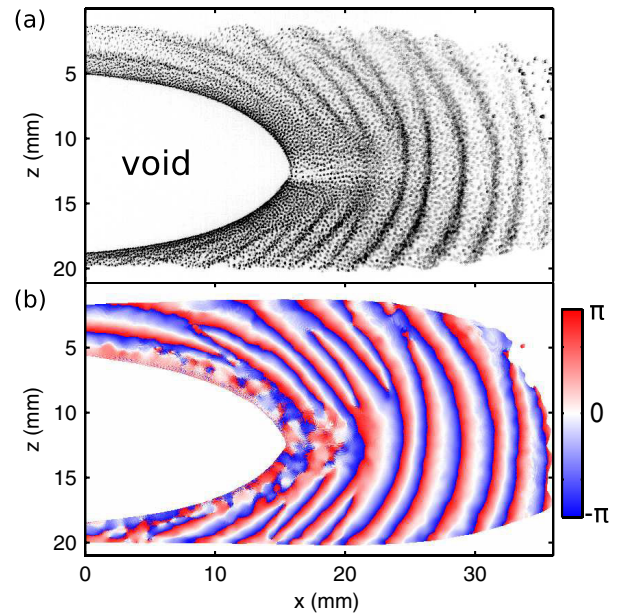

FIG. 2 (color online).   (a) Typical image of the wave field in the discharge for a distinct time step. To pronounce the dominant features the image was inverted. Topological defects are merging points of two wave fronts. They develop in the bulk region of the dust cloud. Vertical asymmetries are due to residual gravity. (b) Calculated instantaneous phase for the same time step. Pixels with no wave activity were neglected.

information of the wave for any recorded video frame. Figure 2(b) shows a phase map for the same time step as the snapshot of Fig. 2(a). It becomes evident that the topology of the phase map perfectly matches the amplitude map.

The time derivative of the phase evolution represents the instantaneous frequency. The mean frequency at an arbitrary position in the wave field is defined as the average over the complete time series, $f_m = \langle f_i \rangle$. This spatial information can also be compiled in a map; see Fig. 3(a). One immediately recognizes that the frequency is not constant over the dust cloud but rather decreases from the central void to the discharge edge by a factor of roughly 0.6. Furthermore, the observed decrease is not monotonic. Instead, clusters of nearly the same frequency are found, a key result of this Letter. For the three largest clusters (around positions 1–3) frequencies of $f_1 = 5.7$ Hz, $f_2 = 6.5$ Hz, and $f_3 = 7.6$ Hz were determined, each with a standard deviation of 0.2 Hz.

To give further evidence for the formation of clusters, we have calculated the standard deviation of the frequencies in the immediate vicinity of each pixel coordinate. The resulting topology, displayed in Fig. 3(b), reveals the formation of sharp boundaries whereas only small deviations are found within one cluster. In addition, the positions of the topological defects are also marked in the map. They are obtained from the spatial phase information by calculating the topological charge, which is proportional to the curl of $\nabla\phi$. It is seen that the defects occur exclusively at the

boundary between two clusters. The high amount of defects in the vicinity of the void is due to irregular wave motion. Note that the map shows all defects that appear in the evaluated time series. It does not give any information about their spatiotemporal evolution.

The described situation was exemplarily chosen from a set of measurements with nearly identical conditions and a similar clustering behavior. In order to examine the influence of external parameters on the cluster formation, we have inspected a dust cloud at a quite different set of discharge conditions ($p = 15$ Pa, $U_{\rm rf} = 70$ V$_{\rm pp}$, $d = 6.8$ μm), which was recorded in an earlier experiment [29]. The wave field had a much higher global coherence. The corresponding frequency map in Fig. 3(c) shows a
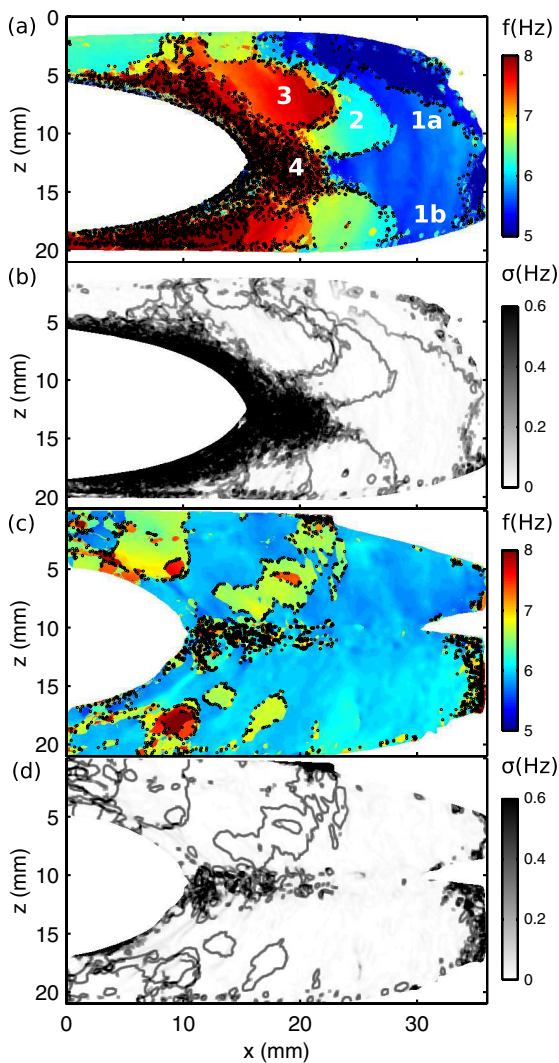
large plateau of the dominant frequency with only small embedded clusters of different frequencies, and the number of defects is reduced.

A second way of studying the frequency clusters is focused on the relative phase evolution inside a single cluster or between different clusters, respectively. This method was introduced in Ref. [30] to analyze the interaction of nonlinear, noisy oscillators with potential frequency mismatches. The generalized phase difference (GPD) $\psi_{nm}(t) = n\phi_1(t) - m\phi_2(t)$ of two unwrapped phase series is calculated, where $n{:}m$ is the ratio of their corresponding frequencies. This quantity should fulfill two conditions if synchronization is given: First, the GPD should be bounded, i.e., $|\psi_{nm}| <$ const. And second, the distribution of ψ_{nm} modulo 2π should be peaked. We have tested both conditions for four different situations: within one cluster (positions $1a/1b$), between clusters $1/2$ and $2/3$, and between $1a$ and position 4, which is located in a defect region. In order to get higher significance, we tested two groups of 16 pixels each, both located around the given positions.

It is found that within the selected cluster ($n{:}m = 1$) the GPD is bounded and its distribution is nearly Gaussian; see Fig. 4(a) and 4(b). For neighboring clusters the smallest rational frequency ratios within the measurement uncertainty are $n{:}m = 5{:}6$ [Figs. 4(c) and 4(d)] and $n{:}m = 4{:}5$ [Figs. 4(e) and 4(f)], respectively. The figures give no clear

FIG. 3 (color online). (a),(c) Spatial frequency distribution for the same field of view as in Fig. 2 at two different sets of experimental parameters. Multiple regions of nearly constant frequencies arise. The topological defects (black dots) encircle single frequency clusters. (b),(d) Standard deviation of the frequency distribution in a 5×5 pixel vicinity of each spot. Pixels with no wave activity were removed from all maps.
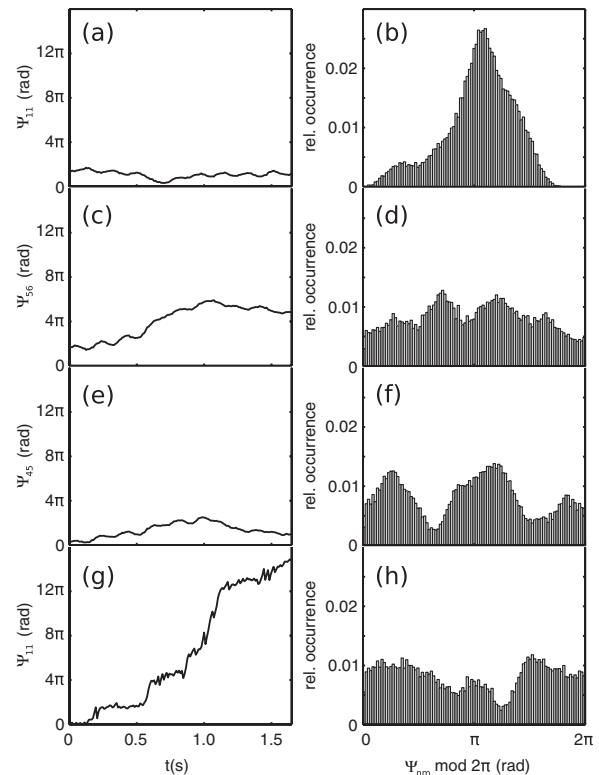

FIG. 4. Generalized phase difference ψ_{nm} mod2π and histograms of ψ_{nm} mod2π between positions $1a/1b$ (a),(b), between cluster $1/2$ (c),(d) and $2/3$ (e),(f), and for positions $1a$ and 4 (g), (h).

hint for synchronization. The GPDs behave similar to the unsynchronized situation of Figs. 4(g) and 4(h), where $n{:}m = 1$ was chosen. The temporal evolution is not bounded and the histogram is not unimodal but rather flat.

We explain the observed formation of spatial frequency clustering as follows: The high growth rate of the Buneman instability ensures that the fastest growing wave mode determines the local oscillation frequency in a small domain. Consequently, our dusty plasma can be considered as an ensemble of individual self-sustained oscillators with nonlinear damping. Such a system was often treated as Van der Pol-like, which is a well-known model for instabilities in plasma physics [9,31]. In our case the natural frequencies of the oscillators are defined by the local plasma parameters; i.e., they depend on the dust density n_d, particle charge q_d, and particle mass m_d, respectively. Because of nonuniform plasma conditions inside the discharge and a nonuniform dust distribution, that decreases from the void edge to the outer regions of the discharge, a gradient of natural frequencies is established in the ensemble.

Unlike linear waves excited by an external driver, which oscillate at the unique frequency of the driver, the present system can be understood as a multitude of individual oscillators which represent the most unstable wave mode at each position.

The situation in our experiment has similarities with the one-dimensional system described by Osipov and Sushchik [26]. It needs to be mentioned that the model in [26] assumes a diffusive, i.e., symmetric, coupling between the oscillators. In the present system, there is a unique wave propagation direction which may break this symmetry. Also, typical variations within one cluster and between different clusters are similar to those observed in Ref. [32]. The question of whether the system reaches a global synchronization or separates into clusters of different frequencies depends on the distribution of the natural oscillator frequencies, the coupling strength, and the degree of nonlinearity. The size of a frequency cluster increases with coupling strength and degree of nonlinearity and decreases for stronger frequency gradients. This is also true for our experiments. In the earlier experiment [29], the gradient of the particle density that determines the natural frequency within the system was approximately 0.7 times lower compared to the exposed experimental situation. In addition, the measured modulation depth, representing the degree of nonlinearity, was 1.4 times higher. Both trends would result in an increasing cluster size. The synchronization of the individual oscillators is not only limited to an adjustment of their frequencies but also of their phases.

In summary, we have observed the frequency clustering phenomenon in an extended field of self-excited waves. This behavior is known from systems of coupled oscillators [25,26], which also showed the formation of wave patterns [27,28]. Our experiments confirm that the degree of wave nonlinearity determines the cluster size. In future experiments this phenomenon will be studied for a large parameter set to explore this relationship in more detail and to identify the role of topological defects for frequency clustering.

*menzel@physik.uni-kiel.de

[1] A. Pikovsky, M. Rosenblum, and J. Kurths, *Synchronization: A Universal Concept in Nonlinear Science* (Cambridge University Press, Cambridge, England, 2001).

[2] C. Hugenii, *Horologium Oscillatorium* (Parisiis, France, 1673).

[3] S. H. Strogatz and I. Stewart, Sci. Am. **269**, 102 (1993).

[4] L. Glass, Nature (London) **410**, 277 (2001).

[5] C. Schäfer et al., Nature (London) **392**, 239 (1998).

[6] C. Wilke, H. Deutsch, and R. W. Leven, Contrib. Plasma Phys. **30**, 659 (1990).

[7] M. E. Koepke and D. M. Hartley, Phys. Rev. A **44**, 6877 (1991).

[8] R. Timm and A. Piel, Contrib. Plasma Phys. **32**, 599 (1992).

[9] D. Block et al., Phys. Rev. E **63**, 056401 (2001).

[10] M. E. Koepke et al., Phys. Plasmas **3**, 4421 (1996).

[11] G. E. Morfill et al., Phys. Rev. Lett. **83**, 1598 (1999).

[12] H. Rothermel et al., Phys. Rev. Lett. **89**, 175001 (2002).

[13] A. Barkan, R. L. Merlino, and N. D'Angelo, Phys. Plasmas **2**, 3563 (1995).

[14] J. B. Pieper and J. Goree, Phys. Rev. Lett. **77**, 3137 (1996).

[15] A. Piel et al., Phys. Rev. Lett. **97**, 205009 (2006); **99**, 209903 (2007).

[16] A. Piel et al., Phys. Rev. E **77**, 026407 (2008).

[17] S. A. Khrapak et al., Phys. Plasmas **10**, 1 (2003).

[18] M. Rosenberg, J. Vac. Sci. Technol. A **14**, 631 (1996).

[19] C. Thompson et al., Phys. Plasmas **4**, 2331 (1997).

[20] I. Pilch, T. Reichstein, and A. Piel, Phys. Plasmas **16**, 123709 (2009).

[21] J. Heinrich, S.-H. Kim, and R. L. Merlino, Phys. Rev. Lett. **103**, 115002 (2009).

[22] R. Heidemann et al., Phys. Rev. Lett. **102**, 135002 (2009).

[23] L.-W. Teng et al., Phys. Rev. Lett. **103**, 245005 (2009).

[24] G. B. Ermentrout and N. Kopell, SIAM J. Math. Anal. **15**, 215 (1984).

[25] G. V. Osipov et al., Phys. Rev. E **55**, 2353 (1997).

[26] G. V. Osipov and M. M. Sushchik, Phys. Rev. E **58**, 7198 (1998).

[27] A. K. Kryukov et al., Phys. Rev. E **79**, 046209 (2009).

[28] O. I. Kanakov et al., Chaos **17**, 015111 (2007).

[29] K. O. Menzel et al., IEEE Trans. Plasma Sci. **38**, 838 (2010).

[30] P. Tass et al., Phys. Rev. Lett. **81**, 3291 (1998).

[31] T. Klinger et al., Phys. Lett. A **182**, 312 (1993).

[32] B. R. Noack, F. Ohle, and H. Eckelmann, J. Fluid Mech. **227**, 293 (1991).

B.3

FREQUENCY CLUSTERS AND DEFECT STRUCTURES IN NONLINEAR DUST-DENSITY WAVES UNDER MICROGRAVITY CONDITIONS

K. O. Menzel, O. Arp, and A. Piel

Frequency clusters and defect structures in nonlinear dust-density waves under microgravity conditions

K. O. Menzel,[*] O. Arp, and A. Piel

Institut für Experimentelle und Angewandte Physik, Christian-Albrechts-Universiät, D-24098 Kiel, Germany
(Received 22 October 2010; revised manuscript received 24 November 2010; published 18 January 2011)

Density waves in a dusty plasma emerge spontaneously at low gas pressures and high dust densities. These acousticlike wave modes were studied in a radio-frequency discharge under microgravity conditions. The complex three-dimensional wave pattern shows a spatially varying wavelength that leads to bifurcations, i.e., topological defects, where wave fronts split or merge. The calculation of instantaneous wave attributes from the spatiotemporal evolution of the dust density allows a precise analysis of those structures. Investigations of the spatial frequency distribution inside the wave field revealed that the wave frequency decreases from the bulk to the edge of the cloud in terms of frequency jumps. Between those jumps, regions of almost constant frequency appear. The formation of frequency clusters is strongly correlated with defects that occur exclusively at the cluster boundaries. It is shown that the nonlinearity of the waves has a significant influence on the topology of the wave pattern.

I. INTRODUCTION

A dusty (complex) plasma contains—besides ions, electrons, and neutrals—micrometer sized particles. This fourth, heavy component shows various structures and dynamic phenomena that take place on comparably long time scales, since the characteristic dust-plasma frequency is of the order of only a few ten Hz. This makes the oscillatory motion of the particles easily accessible via standard video cameras in experiments. Since the first observation of a spontaneously emerging dust-acoustic-like wave mode in dusty plasmas [1], dust-density waves (DDWs) are of fundamental interest in this field of research. Experiments on DDWs were performed in direct current (dc) [2–7], as well as in radio-frequency (rf) discharges [8–11]. In laboratory experiments, the dust particles sediment into the plasma sheath because of gravity. Experiments with spatially extended dust clouds were carried out under microgravity conditions during parabolic flights [10,11] and aboard the International Space Station (ISS) [12,13]. As self-excited dust-density waves are attributed to a Buneman-type instability, where the input of free energy to the system is generated by streaming ions [14], its onset critically depends on three plasma parameters, namely the gas pressure, the discharge electric field, and the dust density [11].

In the last few years, experimental investigations with emphasis on nonlinear wave phenomena became of high interest [15]. Reports included the observation of nonlinear, periodic waves in the laboratory [16] and under microgravity [17]. In addition, the interaction of dust-acoustic shock waves was investigated in a glow discharge [18]. On the microscopic level, wave breaking inside DDWs was observed [9]. A recent investigation showed a strong modulation of the plasma glow by the DDWs in microgravity experiments, suggesting a nonlinear interaction between plasma and wave [19].

On the theoretical side, dust-acoustic waves were originally predicted in 1990 by Rao *et al.* [20]. A fluid model was used to explain a dust-acoustic instability, resulting in a linear dispersion relation and a Korteweg–de Vries equation for the nonlinear case. Through the years, several further approaches were introduced. They include fluid as well as kinetic models and take into account dust-ion collisions [14,21], dust-density inhomogeneities [22], and grain charge variations [23–25]. Those improvements allow reasonable predictions of wavelengths, frequencies, and growth rates. In addition, a two-dimensional treatment of streaming ions gives local growth rates with respect to the ion velocity and can therefore explain the existence of an oblique mode arising under microgravity conditions [10,11,14].

In order to measure the dispersion properties of DDWs, the temporal modulation of plasma parameters is a widely used approach. For example, Thompson *et al.* [2] applied an additional low-frequency electric field to the discharge, resulting in a synchronization of driving force and oscillating dust density. This method allowed the verification of most of the wave properties that were predicted from linear theories. The entrainment process itself was lately studied in detail [26].

Recently, we discovered under microgravity conditions [27] that regions of different but almost constant frequency occur in the dust-density wave fields, so-called frequency clusters. This feature is accompanied by the appearance of topological defects. In this paper, we refine the previous analysis and describe the observed features in more detail. Moreover, we address the role of defects on the formation of frequency clusters. A comparison of the findings with numerical simulations suggests a model for our system, which explicitly accounts for the nonlinear wave character.

II. EXPERIMENAL SETUP

The measurements were performed under microgravity conditions on parabolic flights provided by DLR (German Aerospace Center). The waves were generated in the IMPF-K2 chamber, which is an improved descendant of the chamber prototype for the International Plasma Microgravity Facility (IMPF). It is similar to the facility described in detail in Ref. [28], except for a simplified electrode configuration.

A side view of the experimental setup is shown in Fig. 1(a). An argon plasma is produced by a symmetric parallel
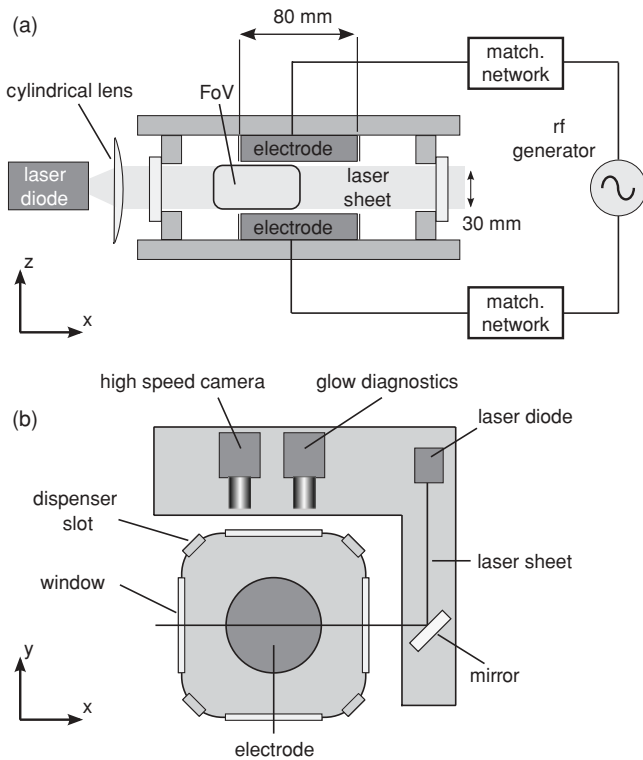
---
[*]menzel@physik.uni-kiel.de

FIG. 1. Sketch of the IMPF-K2 chamber. (a) Side view of the chamber. The field of view is marked with a rectangle. (b) The top view shows the basic video microscopy setup with illumination laser and high speed camera.

plate radio-frequency discharge operated at 13.56 MHz. Two transparent electrodes made of indium tin oxide (ITO) with a diameter of 80 mm form a discharge gap of 30 mm and are fed in push-pull mode via a symmetric matching network by an rf generator with typical peak-to-peak voltages of $U_{rf} = (40–70)$ V$_{pp}$.

Dust particles are injected into the plasma by eight independently operating dispensers. For the present investigations, this configuration ensures a high total amount of dust. The monodisperse and spherical melamin-formaldehyde particles have a diameter of $d = (6.84 \pm 0.07)$ μm.

In this setup, self-excited DDWs can be observed only when the energy gain of the ions is sufficiently higher than dissipation arising from neutral drag. Consequently, in our experiment the gas pressure $p = (15–30)$ Pa is chosen below a critical value of $p_{crit} \approx 35$ Pa to ensure the appearance of wave motion. To exclude the possibility that the observed instability is triggered by external mechanical forces, which may arise from residual gravity during the parabolic maneuver, an additional accelerometer was installed close to the plasma chamber that logs the acceleration in all three spatial directions at a sample rate of 1 kHz.

For the observation of the dust dynamics, a standard video microscope was used. The configuration, as seen in Fig. 1(b), comprises a low-power laser diode ($\lambda = 660$ nm, 50 mW) that illuminates the dust particles with a thin vertical sheet and a high speed camera. By choosing a frame rate of approximately 100 fps we can exclude any aliasing effects in the recorded wave motion as the frequency of the DDWs is typically only

of the order of a few Hz. The observed field of view (FOV) has a spatial resolution of (510×880) pixels, corresponding to an area of (25×43) mm^2 inside the laser sheet.

III. FUNDAMENTAL WAVE PROPERTIES

A characteristic snapshot of the dust cloud is shown in Fig. 2(a). It was recorded at $U_{rf} = 65$ V$_{pp}$ and $p = 30$ Pa. Typically, the dust fills a large volume of the discharge except for the central dust-free void region [29]. For the given set of parameters, the dust density is obviously periodically
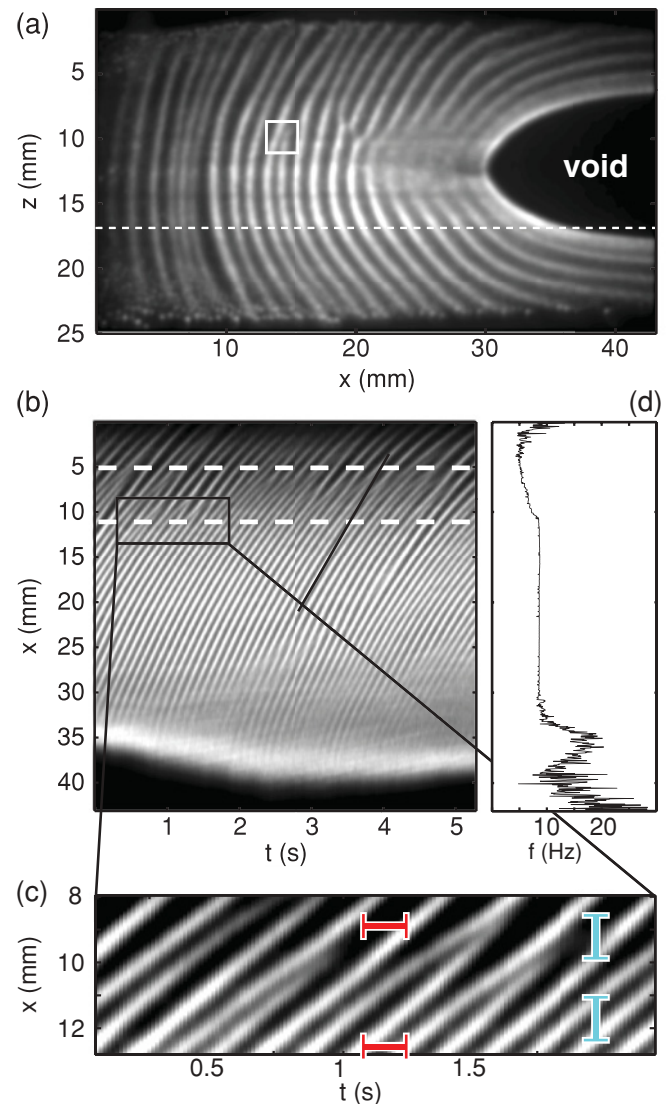

FIG. 2. (Color online) (a) Typical snapshot of the wave field in the rf discharge. Topological defects are merging points of two wave fronts (square). They develop in the bulk region of the dust cloud. (b) Space-time diagram for the dashed line in (a). The added black line demonstrates that waves with different phase velocity exist. Wave fronts merge at distinct bifurcation points in a region between the dashed lines. (c) A closeup shows the vicinity of several defects. The red (horizontal) and blue (vertical) bars of equal length match the wave field in the lower part but deviate in the upper part. (d) Spatial frequency distribution along the dashed line, determined from the maxima and minima of the space-time diagram.

modulated by self-excited DDWs. The waves are not generated by a periodically expanding and collapsing void boundary, associated with the heartbeat instability [30]. This can be concluded since the waves initially emerge at the outer parts of the dust clouds near the discharge edges when the gas pressure is lowered successively and falls below the critical pressure. For a further decrease, the wave field then expands over the entire cloud. Moreover, by checking the recorded acceleration, we can exclude any correlation between residual acceleration inside the aircraft and the dust-density fluctuations. The waves propagate radially outward from the boundary of the void. Although the waves gain energy from streaming ions, it is known from earlier experiments [10,11] that the waves do not necessarily propagate parallel to the local ion flow and the electric field, respectively.

Because the electric field is perpendicular to the plasma edge, one would expect that the waves strike the discharge edges at right angles. This is only true in the vicinity of the void, but may be different in the outer regions [10,11]. The snapshot further reveals the nonlinear character of the DDWs: The waves consist of very narrow crests and wide troughs, which contain a significantly reduced number of dust particles. Furthermore, it becomes obvious that the wavelength varies over the entire dust cloud with typical values of $\lambda_{DDW} \approx 1.5$ mm close to the void and $\lambda_{DDW} \approx 3$ mm in the outer regions of the cloud. We also observed that wave fronts are not strictly parallel, but they may split or merge spontaneously. Such spots are known as topological defects.

A first impression of the temporal behavior of the waves can be obtained from a space-time diagram as displayed in Fig. 2(b). It transforms the intensity evolution along a chosen horizontal section [dashed line in Fig. 2(a)] into a two-dimensional map, where the abscissa represents time and the ordinate represents the horizontal position. This method was already established in the context of DDW analysis [16,17,26] and allows us to determine several wave properties, e.g., phase velocity, wavelength, and wave period, as it is possible to track single wave fronts over time.

The local phase velocity of the DDW is represented by the slope of a wave front. In the diagram of Fig. 2(b) the black line of constant slope indicates that the velocity is decreasing toward the dust cloud edge, since the wave slope bends away from the line in the upper part of the diagram. Velocities of 15 mms^{-1} in the dust volume and 8 mms^{-1} near the boundary were obtained.

A change in frequency and wavelength can be seen by the red (horizontal) and blue (vertical) bars of identical length in Fig. 2(c), which match the wave field in the lower region but reveal a mismatch in the upper region. One generally finds higher frequencies near the void. This is an important finding, since it cannot be understood within the context of linear wave theory that would require a fixed frequency and would only allow a spatial variation of the wavelength.

The closeup view in Fig. 2(c) presents a case where pairs of wave fronts merge, resulting in one single wave front. This demonstrates that a topological defect is not only a spatial phenomenon but must be treated also in the time domain. Figure 2(b) clearly shows that such events are not equally distributed along the chosen axis. Rather, the defects occur inside a band that is marked by dashed lines.
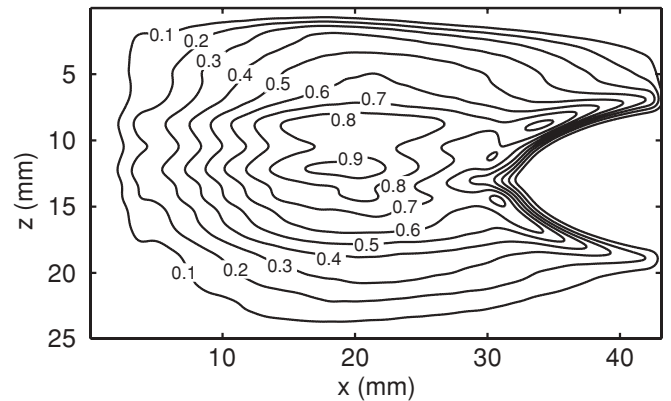

FIG. 3. Dust-density distribution for the wave field of Fig. 2(a). The density is given in arbitrary units, normalized to the maximum of the distribution. A strong gradient from the void boundary toward the discharge edges is established. Ripples in the density contours are caused by inhomogeneous illumination.

Since the distance between two wave fronts determines the wave period and frequency, respectively, it is possible to estimate a spatial frequency distribution along the axis by averaging over the distance between neighboring maxima and minima, respectively. The resulting distribution for a time series of 200 frames at constant plasma parameters is displayed in Fig. 2(d). It reveals a constant frequency over a broad region (11–30 mm) and the expected decrease toward the discharge edge. In the region of low wave activity (30–35 mm), the frequency estimation yields spurious values.

A qualitative picture of the dust-density distribution inside the dust cloud can be obtained by averaging the recorded intensity over an appropriate time interval. The result for the measurement of Fig. 2(a) is displayed in Fig. 3. It is found that the density is not constant over the entire cloud but decreases gradually from the void to the discharge edges.

IV. FREQUENCY CLUSTERS

As mentioned earlier, the spatial frequency variation of the DDW is not a trivial finding. It is rather associated to the complicated topology of the nonlinear wave field. Hence it is important to determine the spatial frequency distribution for the entire wave field.

A. Data processing

This is done by evaluating the time series of the dust-density evolution everywhere in the wave field. It is common to use the recorded intensity of the video frames as a direct measure of the density. All effects that may result from the granularity of particles are suppressed by blurring single frames with a Gaussian low-pass filter. This yields the individual time series $n_d(x,z,t)$ for the dust density at an arbitrary pixel position, denoted by spatial coordinates (x,z). The time series have a length of 512 time steps and are made zero mean by subtracting a moving average. After such data preprocessing, the typical evolution of the dust density can be found in Fig. 4(a). The envelope function, defined from the instantaneous wave amplitude (see below), decreases between two maxima, which hints at interference phenomena. When investigating the
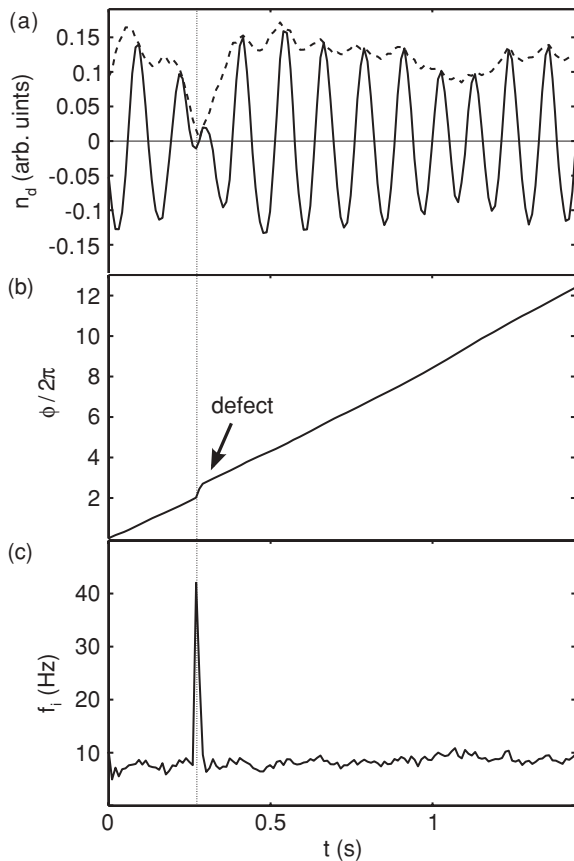
FIG. 4. (a) Measured zero-mean time series of the dust-density fluctuations for one distinct position in the dust cloud. The instantaneous amplitude is marked with a dashed line. Its sudden drop to zero indicates the occurrence of a topological defect. (b) Unwrapped phase information for the same position in the wave field shows an abrupt jump by π at the defect. (c) Instantaneous frequency for the same position, determined by the slope of the phase evolution. The dotted vertical line in the three graphs indicates the moment of defect occurrence.

envelope over several wave periods, it becomes obvious that the system is nonstationary.

The next step of the analysis is to determine the instantaneous frequency of the wave from a given time series. For this purpose, we expand the measured real time series into the complex plane via

$$A(x,z,t) = n_d(x,z,t) + i\hat{n}_d(x,z,t). \tag{1}$$

The resulting time series $A(t)$ is known as the "analytic signal," first introduced by Gabor [31], and represents a standard technique in digital signal processing. It consists of the original time series and an additional imaginary part, which is calculated by the Hilbert transform $H\{n_d(t)\}$, defined as

$$\hat{n}_d(t) = H\{n_d(t)\} = \frac{1}{\pi} \int_{-\infty}^{\infty} \frac{n_d(\tau)}{t-\tau} d\tau. \tag{2}$$

Transferring Eq. (1) into Euler's notation clearly shows the advantage of this expression, since $A(x,z,t) = E(x,z,t) \cdot$
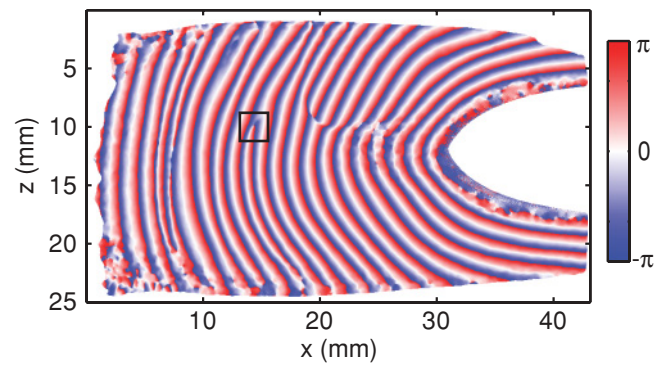

FIG. 5. (Color online) Calculated instantaneous phase for the same time step as in Fig. 2(a). Pixels with no wave activity were neglected and set to zero. Although the raw image shows almost no wave activity at the left edge of the void, phase fronts can be reconstructed in this area, indicating a correlation between upper and lower parts of the dust cloud.

$\exp[i \cdot \phi(x,z,t)]$ with the envelope function $E(x,z,t) = (n_d^2 + \hat{n}_d^2)^{1/2}$ gives rise to the definition of an instantaneous phase,

$$\phi(x,z,t) = \text{atan2}\left[\hat{n}_d(x,z,t), n_d(x,z,t)\right]. \tag{3}$$

The spatial phase distribution for the snapshot of Fig. 2(a) is illustrated in Fig. 5. It clearly reproduces the shape of the wave fronts. Moreover, it reveals wave motion in a region, where no waves could be visually detected in the raw data. The representation further demonstrates that the parts above and below the void show correlation, although the wave fronts between them are not connected.

The described methodological approach is widely used in numerous different research areas, as, for example, in biological, medical, and nonlinear physical systems [32], mainly due to the fact that $\phi(x,z,t)$ can be utilized to generate two more physical quantities that are of interest, namely the instantaneous frequency, defined as $f_i(t_0) = (1/2\pi) \cdot \partial\phi/\partial t|_{t=t_0}$, and the local wave vector, defined as $\vec{k}_l(\vec{r}_0) = \partial\phi/\partial\vec{r}|_{\vec{r}=\vec{r}_0}$.

Usually the phase lies between 0 and 2π. In contrast, Fig. 4(b) displays the temporal evolution of the unwrapped phase where all eventual phase jumps $2\pi \to 0$ are unfolded. It was determined at the same position as the time series of Fig. 4(a). One can see that $\phi(t)$ is in general a monotonically increasing function. Exceptions are at some distinct time steps. They are clear hints for the appearance of a defect, as will be seen in Sec. V. The slope of the phase evolution at a selected time step t_0, representing the instantaneous frequency, can be seen in Fig. 4(c). It varies only slightly, except for defect positions. We thus define the time-averaged frequency $f_m = \langle f_i(t) \rangle_T$. The averaging time T is chosen according to the specific purpose of the data analysis. No averaging yields instantaneous properties. Averaging over one wave period ($\approx$10–20 frames) improves the signal-to-noise ratio. Averaging over several wave periods ($>$100 frames) is used to evaluate global wave properties when the plasma conditions are constant and the system parameters are not affected by residual gravity.
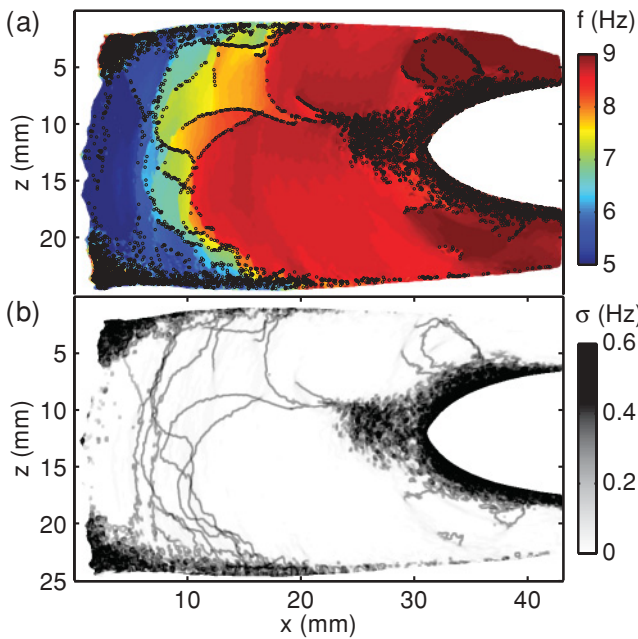
FIG. 6. (Color online) (a) Spatial frequency distribution for the same field of view as in Fig. 2(a), calculated via Hilbert transform. Different regions of nearly constant frequencies established in the wave field. The topological defects that encircle single frequency clusters are marked with black dots. (b) Standard deviation of the frequency distribution in a (5×5) pixel vicinity of each spot. Pixels with no wave activity were removed from both maps.

B. Frequency distributions

If the described procedure is carried out for all positions of the recorded two-dimensional dust volume sections, a spatial frequency distribution $f_m(x,z)$ can be constructed. The map in Fig. 6(a) results from the evaluation of time series of about 10–20 wave periods (200 frames). As immediately seen, the frequency is not constant in the dust cloud. It rather decreases from 8.6 Hz at the void edge to 5.2 Hz at the plasma boundary by roughly 40%. The waves always propagate in the direction of lower frequencies. In addition, the frequency decays nonmonotonically. Moreover, we find regions of almost constant frequency that are separated by significant frequency jumps. These regions are called frequency clusters. For the largest clusters, average frequencies of $f_1 = 5.2$ Hz, $f_2 = 7.8$ Hz, and $f_3 = 8.6$ Hz were determined. Inside those regions the frequency stays nearly constant with maximum deviations of about 4%. The mentioned features are even more pronounced in a horizontal section through the frequency distribution (Fig. 7) where the distributions obtained from the space-time diagram (fine black line) are compared with the Hilbert transform (bold red line) for the axis marked in Fig. 2(a). Obviously, the latter method discloses a substructure of several frequency steps at the discharge edge facing side of the wave field (0–10 mm), whereas the the former only shows a decrease of the frequency.

To support the idea of cluster formation, the standard deviation of the frequency for all positions in the wave field was calculated using (5×5) pixel blocks. The corresponding map is displayed in Fig. 6(b) and reveals sharply defined boundaries
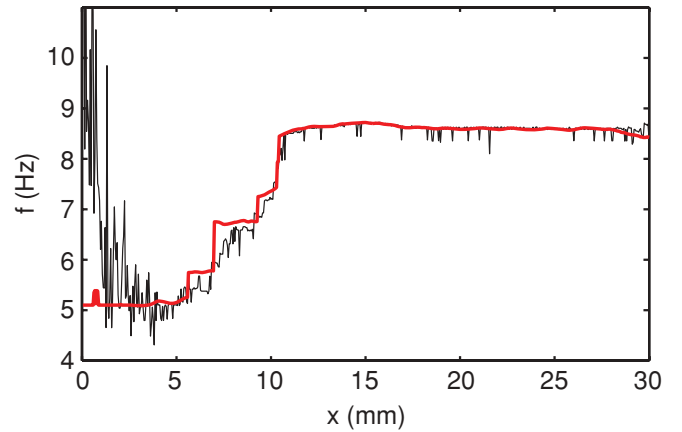

FIG. 7. (Color online) Frequency distribution determined from space-time diagram (fine black line) and from the temporal average of the instantaneous frequency (bold red line). The chosen horizontal axis is the same as in Fig. 2(a). The methods differ in the region of varying frequency (0–10 mm). The instantaneous frequencies disclose frequency steps in the intermediate region and a constant frequency at the discharge edge (0–5 mm).

between the clusters. Inside the clusters only small frequency variations are found.

C. Parameter variation

In order to investigate the behavior of frequency clusters under the influence of different plasma parameters, we compiled frequency maps for two more data sets. The first one was recorded at lower gas pressure and rf voltage compared to the exposed situation ($p = 15$ Pa, $U_{\rm rf} = 48$ V$_{\rm pp}$, $d = 9.55$ μm) and is described in detail in Ref. [27]. The second data set was recorded at the same voltage but different pressure ($p = 15$ Pa, $U_{\rm rf} = 70$ V$_{\rm pp}$, $d = 6.8$ μm), described in Ref. [33]. At first glance the former wave field is comparable to the exposed situation; the latter corresponds to a highly coherent wave state. The determined frequency maps with marked defect positions are shown in Fig. 8. Obviously, the first map has similarities with the exposed situation. In contrast, the map in Fig. 8(b) comprises just one large cluster. For each situation we calculated the modulation depth, defined as the ratio of signal maxima to signal minima, at those positions in the dust cloud where a sufficiently high wave activity was detected. We found an average ratio of 1.42 for the exposed situation of this paper, 1.52 for the measurement at low pressure and voltage, and 1.62 for the highly coherent state. In addition, the dust-density distribution for both states were estimated as described above. Since the profile of the first data set is qualitatively similar to the above exposed situation, only the distribution for the coherent state is shown in Fig. 9. Obviously, the estimated frequency gradients are 2–3 times lower compared to the other situations. Nevertheless, it is important to mention that the averaged intensity is only a rough estimate of the dust density, since inhomogeneous illumination may cause artifacts.

V. DEFECT STRUCTURES

Due to the fact that the wavelength of the DDWs varies significantly, the wave pattern is very complex. This results
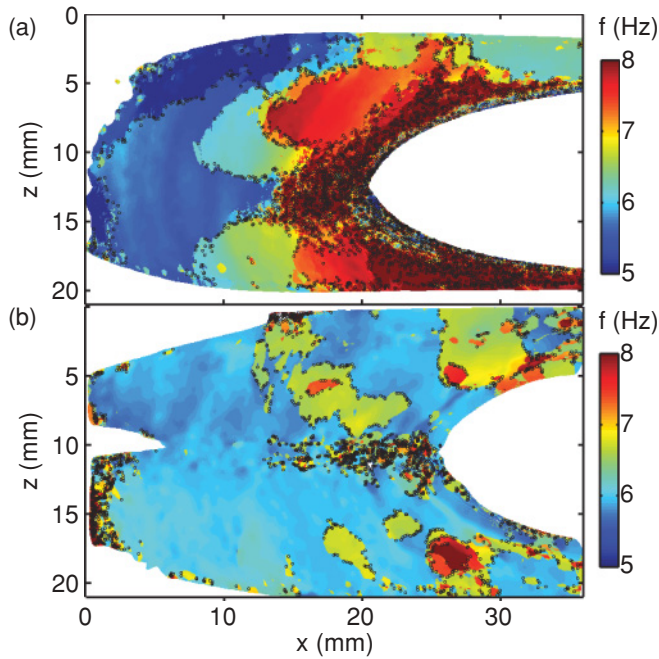
FIG. 8. (Color online) Frequency distributions for wave fields with modulation depths of (a) 1.52 and (b) 1.62. For the lower modulation depth the corresponding map reveals comparably small clusters and a high amount of topological defects. For the higher modulation depth one large cluster has formed.

in the occurrence of bifurcation points at positions where two wave fronts merge or split. Hence the conservation of wave number is not satisfied in the present system. As already seen in the space-time diagram, wave fronts are added to or removed from the system at the bifurcation. These particular points are called topological defects. To examine their relationship with the polychrome wave field, the defects are analyzed by utilizing the above compiled phase map (Fig. 5) that perfectly resembles the raw data.
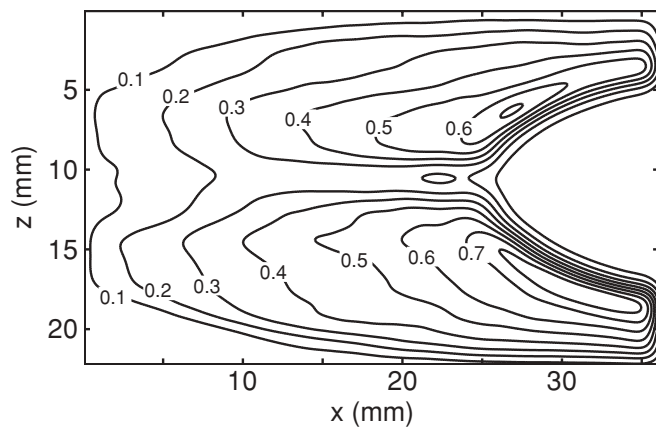

FIG. 9. Dust-density distribution for the wave field of Fig. 8(b) in arbitrary units, normalized to the maximum of the distribution. In comparison to the distribution of Fig. 3 only small gradients were found.

A. Defect analysis

In the unwrapped phase evolution, defects appear as abrupt jumps. One example occurs in the time series of Fig. 4(b). The detection of the spatial defect positions is based on the property that a defect can be regarded as a singularity in the phase map, i.e., the phase becomes undefined. To detect these phase defects, we derive from the instantaneous phase maps the so-called topological charge,

$$c(x,z,t) = \frac{1}{2\pi} \oint_\Gamma \vec{\nabla}\phi(x,z,t) \cdot d\vec{l}, \quad (4)$$

which was established by Nye [34] to evaluate singularities in ultrasonic waves. Since then it was applied in numerous works; see, e.g., Refs. [35,36]. The integral in Eq. (4) sums up infinitesimal phase differences $\vec{\nabla}\phi$ along a closed path Γ. Consequently, only those paths can contribute to the charge, which encircle a defect. This is illustrated in Fig. 10(a). It shows a closeup of the spatial phase information as determined by Eq. (3) at the vicinity of a defect. Two examples are given: path Γ_1 has its center on a wave front, whereas Γ_2 completely surrounds the defect. Only the charge of path Γ_2 differs from zero.

Applying the Stokes theorem, Eq. (4) allows us to define a topological charge density as [37]

$$c_d(x,z,t) = \frac{1}{2\pi} \cdot [\vec{\nabla} \times \vec{\nabla}\phi(x,z,t)]. \quad (5)$$

Using Eq. (5) is a more convenient way for determining the topological charge, as it reduces the computation time. The result is shown in Fig. 10(b). Since the vector field $\vec{\nabla}\phi$ was initially blurred with a Gaussian filter, the curl calculation yields a very smooth topological charge distribution. The charge that is assigned to the complete defect (integral over all pixels) takes values of $+1$ (white) or -1 (black), depending on the sense of rotation of the phase. In principle, also defects of higher orders, i.e., higher integers, are possible but do not appear in the evaluated data sets.

In a consecutive step, the defect positions can be determined with standard particle detection algorithms, like those introduced in Refs. [38,39]. The detection works with high accuracy because the topological charge of a defect has a Gaussian shape. In order to examine the relationship between frequency clusters and topological defects in the wave field, the positions of all defects are plotted on top of the frequency distribution of Fig. 6(a). This includes all defects that were found in the time series used for the frequency determination. It becomes evident that the defects appear almost exclusively at the boundaries between the frequency domains that were determined using the instantaneous frequency. The high amount of defects found near the void and in the outer regions of the wave field is due to irregular wave activity.

B. Defect dynamics

Since we have calculated the temporal evolution of the phase, it is also possible to track defect positions for a desired time interval, and thus an analysis of the dynamics of the defects could be performed. For this purpose, a sequence of successive frames of the topological charge is studied. The time step between two frames is given by the frame rate of
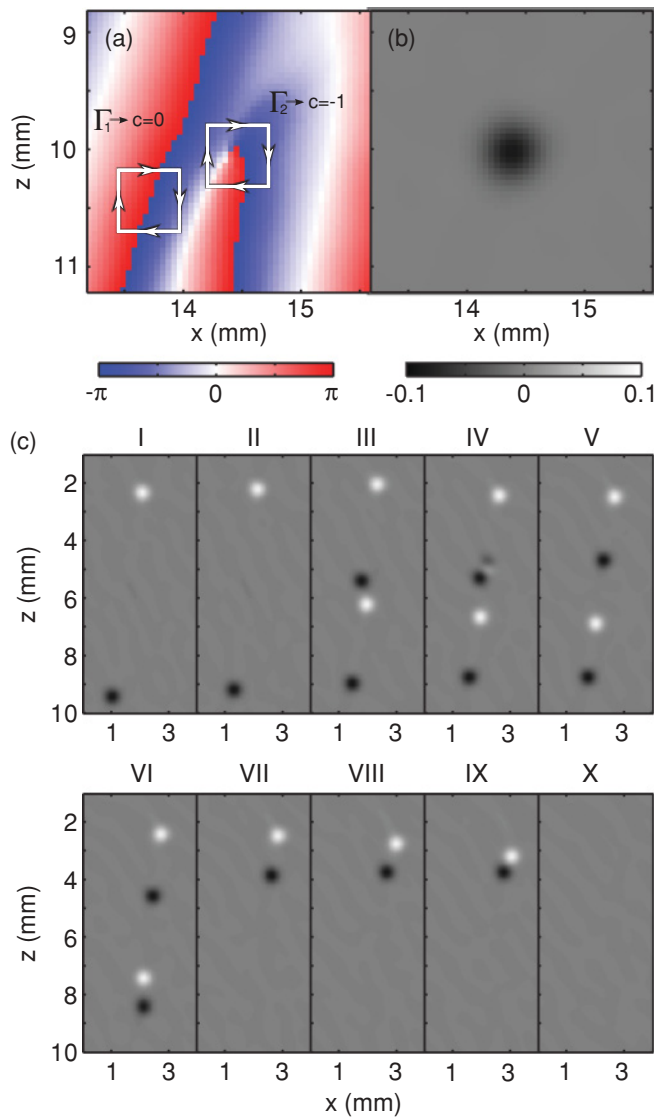
FIG. 10. (Color online) (a) The spatial phase information in the vicinity of a defect for the white square in Fig. 2(a). It marks the positions where two wave fronts merge into one. (b) Calculated topological charge density of the same region using Eq. (5). The charge of the defect results from the sum of all corresponding pixels and equals approximately −1. (c) Evolution of a defect pair with opposite charge in the wave field. In frame III a new pair of defects is created. In frame VII the lower neighboring defects are annihilated; in frame X the upper pair is annihilated. The color bar is the same as in (b).

the camera as approximately 0.01μs. Since the defects are characterized by their charge, they can be treated as "particles." Therefore the underlying pattern need not to be considered. An example for the motion of defect pairs with opposite charge is shown in Fig. 10(c). One remarkable feature of their motion is seen in frame III, where a second pair of defects between the original defects is created, resulting in four defects of alternating charge. Afterward, the two lower defects annihilate each other in frame VII; the upper pair vanishes in the last frame.

The observed events are in agreement with other experiments [40,41], which showed that defects are suddenly

occurring and disappearing objects. In addition, the defects are not fixed in the wave field and are consequently not moving with the local phase velocity. Instead, the wave front at a bifurcation that is located closer to the void is ruptured and caught up by the subsequent front, triggering a new rapture. In accordance to previous investigations [41,42], the defect motion can be separated into a "glide" motion (along the local wave velocity) and a "climb" motion (perpendicular to the local wave velocity). In our measurements the glide motion is dominant.

The defects represent events of vanishing amplitude as shown in Fig. 4(a), i.e., they are a consequence of destructively interfering waves and it is reasonable to assume that they move at the group velocity rather than the phase velocity. Unfortunately, the DDWs are characterized by their three-dimensional topology, so that defects may move out of the plane of observation. Consequently, a reliable estimation of all velocity components is not yet possible. This problem also implies that a detection of defect pairs of opposite topological charge, as seen in Fig. 10(c), at the ends of a wave front that is generated in the system is difficult. In principle, in three dimensions the defects will most probably occur along so-called "nodal lines" [43]. Nevertheless, the evaluation of long defect trajectories showed that they move with (70–90)% of the local phase velocity of the wave, which is in agreement with the above considerations.
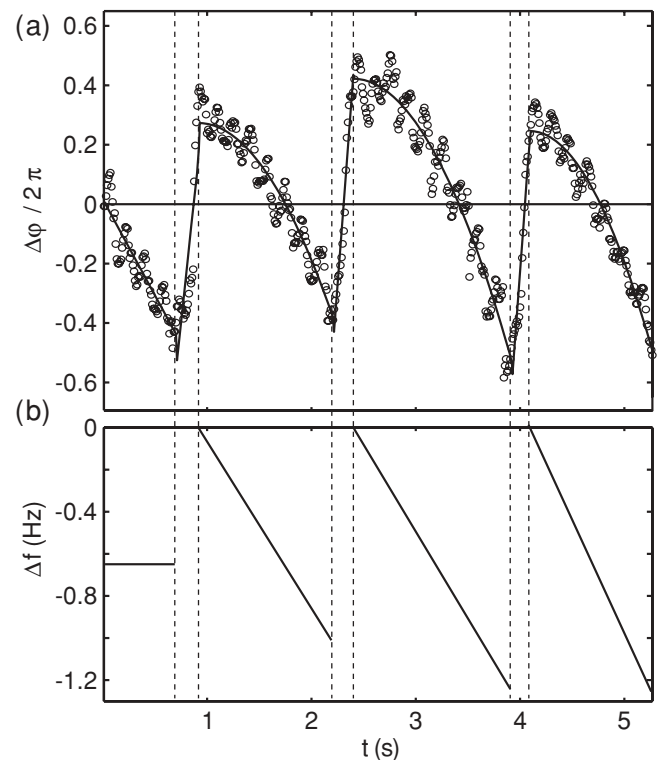

FIG. 11. (a) Evolution of $\Delta\phi(t) = \phi(t) - \bar{\phi}(t)$ (circles). The straight line corresponds to sectionwise parabolic fits between defects. (b) The derivative of the fitted curve in (a) transforms the phase differences into frequency differences. It shows a linear decrease between two defect events and is therefore a hint for a nonlinear interference.

C. Role of topological defects

The map of Fig. 6(b) illustrated that the frequency varies significantly only at the boundary between two adjacent clusters. These spatial variations are also seen as temporal fluctuations, which can be seen in Fig. 11(a). It shows a typical evolution of phase differences $\Delta\phi(t) = \phi(t) - \bar{\phi}(t)$ between instantaneous phase $\phi(t)$ and a time-averaged phase evolution $\bar{\phi}(t)$ that is determined by a linear fit on the unwrapped phase data. Due to the correction by a mean phase, $\Delta\phi(t)$ elucidates the behavior of the phase on a smaller time scale. In this particular example, a periodic pattern of defects appears, indicated by abrupt phase changes. Between these events the phase difference can be approximately described by a parabolic law. This evolution can be interpreted in terms of frequency differences by the temporal derivative of $\Delta\phi(t)$. Since this time series is affected by additional fluctuations due to the nonlinear character of the waves, a parabolic function is piecewise fitted to the data and differentiated afterwards. Figure 11(b) shows the resulting sawtoothlike deviation from instantaneous to mean frequency. This asymmetric evolution shows that the interference phenomenon that leads to the appearance of topological defects has a nonlinear character that is typical of relaxation oscillators. For a linear superposition of waves a sinusoidal variation would be expected. We have also observed defects with the opposite slope of the frequency evolution and an opposite sign of the phase jump.

VI. DISCUSSION

The observed dust-density waves show a very complicated wave pattern. The measured strong modulation depth proves the nonlinear character of the wave. The wave fronts are not strictly parallel but merge or split. These transient phenomena are known as topological defects. In principle, simple analysis methods, like the Fourier transform of the entire time series, allow us to determine a variety of wave properties. Nevertheless, the Fourier transform is an integrating method and thus has a time-averaging character with a frequency resolution determined by the length of the transform time series. Hence it is not capable to perform a suitable spatiotemporal analysis of the DDWs that includes the mentioned transient effects. Refined data analysis techniques adopted from digital signal processing, namely the Hilbert transform, made instantaneous physical quantities accessible. This means that the phase and amplitude of a wave can be determined with a resolution corresponding to the frame rate of the camera. The Hilbert transform allows a complete reconstruction of the spatiotemporal evolution of the wave field. We further defined an instantaneous frequency that makes it possible to study the frequency content of the waves in detail on different time scales. For example, one can evaluate the instantaneous frequency itself. Since the nonlinearity modulates the shape of the wave within one wave period, it is also possible to average the frequency over one wave period to remove such features. This allows a look at the specific behavior of the defects, as illustrated in Fig. 11(a). To get insight into the spatial frequency distribution of the waves, the frequency can further be averaged over several wave periods (at constant experimental conditions). The frequency analysis

based on the Hilbert transform is therefore similar to the wavelet transform, which also allows an adaptive control of the temporal resolution, but it is complementary to spectral methods like the Fourier transform.

The experimental data reveal the formation of frequency clusters that are separated by sharp boundaries. Besides a sharp transition in the frequency, the wave fronts show the aforementioned topological defects at boundaries between the clusters. This behavior was not expected because the system parameters inside the dust cloud, e.g., gas pressure, plasma potential, and particle charge, have smooth spatial variations with no abrupt changes. This suggests that the system undergoes synchronization processes within the clusters. The defects occur periodically in the wave field. Their repetition rate is proportional to the frequency step between two clusters. In our measurements, this periodicity cannot be determined at every position for two reasons. Since the cluster boundaries have a three-dimensional shape and the defects do not occur everywhere along a boundary [see Fig. 6(a)], the detection of defect events can be missed with the two-dimensional diagnostics. Furthermore, the defect boundaries in experimental situations are not sharp. They are broadened due to varying experimental parameters and noise [44]. Thus defects do not appear repeatedly at the same position, but fluctuate.

The formation of frequency clusters is known from other dynamical systems. There are a few experimental observations for purely one-dimensional systems. For example, spatially extended sections along the intestine of mammalians were found to oscillate at a unique frequency [45]. In addition, frequency clustering was reported for the vortex shedding frequency in a flow behind cone-shaped bodies [46]. Our inspection of the existing literature on plasma waves has shown that, except for our recent investigations [27], the frequency clustering effect has not yet been reported in this field. Nevertheless, a number of numerical studies also showed this remarkable feature in the wave field. These simulations investigated the synchronization of arrays of mutually coupled nonlinear oscillators. The oscillators are subjected to a gradient of the natural frequency. The simulations cover chaotic Rössler oscillators [47], weakly nonlinear Ginzburg-Landau systems [48], and the Luo-Rudy model for cardiac cells [49].

It is important to mention that the synchronization of the individual oscillators is not only limited to an adjustment of their frequencies, but also of their phases. Otherwise a wave motion of oscillators, as found in our dusty plasma, would not be observable. Different simulations [49,50] showed that this leads to the formation of propagating wave patterns. In particular, it was shown that a system of integrate-and-fire oscillators exhibits wave motion [51], where the wave propagates from higher to lower frequencies, as observed in our experiment.

Our system of dust-density waves shows a similarity with the coupled oscillator models in that the size of the frequency clusters grows for increasing nonlinearity. This conclusion can be drawn since the modulation depth, which was determined for three different sets of parameters, can be interpreted as a measure for the degree of nonlinearity. Furthermore, the cluster size depends on the gradient of one of the system parameters, namely the dust-density distribution. This is also similar to

the models, where a gradient of the natural frequencies of the oscillators is included. The simulations reveal the appearance of topological defects at cluster boundaries [46,48] as was found in our experiments. It is found that the instantaneous frequency between two defect events decreases or increases linearly, which is similar to the periodic pulling effect of a driven van der Pol oscillator and describes a process where the oscillator frequency drifts toward the frequency of the driver, entrains for a short moment, and then changes abruptly [52].

Since the defect positions can be accurately determined with the applied analysis techniques, the investigation of the defect dynamics is possible. We observed the creation and annihilation of defect pairs with opposite topological charge, which might be a consequence of the complex three-dimensional defect motion.

Frequency clustering cannot be understood from linear wave properties. There, a wave maintains its frequency but matches the varying propagation speed by adjusting the wavelength. Rather, linear instability analysis shows that for the present wave phenomenon a range of wave modes becomes unstable, which suggests that the frequency clusters are associated with mutual synchronization of these modes.

VII. CONCLUSION

We explain the formation of frequency clusters as follows: Due to the high gas pressure in our experiment the damping rates are so strong that any disturbance of the dust density will be damped within a few millimeters. Consequently, the observed wave phenomena cannot be interpreted as propagating waves that are excited at one specific point in the dust volume. In fact, the system must gain energy everywhere in the wave field. This is true for DDWs since they are excited by streaming ions as a Buneman-type instability. They are therefore dominated by the local plasma parameters at an arbitrary position, as, e.g., by particle mass, particle charge, and dust density. Hence the dust volume may not be interpreted as a passive medium in which an externally excited wave propagates, but rather as an ensemble of oscillators with different dust-plasma frequencies, similar to an amplifying laser medium. Nevertheless, most other wave phenomena in the context of dusty plasmas are generated by an external driver, as, for example, Mach cone shocks [38] or shear waves [53], which are mediated by the force of a laser beam. These experiments were carried out in other parameter regimes, where the lower gas pressure allows a regular wave propagation. They are consequently not comparable to the present situation.

Due to nonuniform plasma conditions inside the discharge and a nonuniform dust distribution that decreases from the void edge to the outer regions of the discharge (see Fig. 3), a gradient of natural frequencies is established in the ensemble. It is not yet possible to identify the "oscillator" precisely. We conjecture that not a single particle but a bunch of particles with an extension in the order of a wavelength, which may penetrate each other, represent such individual oscillators. These oscillators interact mutually. Since the dust-density fluctuations show a high degree of modulation, we expect a strongly varying dust charge between wave crests and troughs, which causes the interaction to be nonlinear. Earlier investigations [54–57] showed that the van der Pol oscillator has a paradigmatic character for nonlinear plasma waves and may also be a suitable model for the observed DDWs.

As for the numerical simulations of Refs. [44,48], we expect the group of oscillators to synchronize each other over a certain distance, resulting in a common oscillation frequency. If the stress inside the ensemble becomes too strong, the synchronization breaks up and another cluster is formed. At the interface between two clusters, the occurrence of a topological defect is necessary to match the subgroups. The coherence length of the oscillators will then be given by the degree of nonlinearity and the dispersion of natural frequencies in the system. We could show that our dusty plasma revealed the same tendencies as the simulations.

It needs to be mentioned that the model in [48] assumes a diffusive, i.e., symmetric, coupling between the oscillators. However, in the present system, there is a unique wave propagation direction that may break this symmetry. Additionally, the authors modeled the oscillators via a complex Ginzburg-Landau equation, i.e., a weakly nonlinear version of the van der Pol equation, which might also be more suitable for our system.

In conclusion, our investigations lead to a different view on dust-density waves where the wave field is treated as an ensemble of mutually coupled self-excited nonlinear oscillators. This is a possible explanation for the observed formation of frequency clusters and the occurrence of topological defects at the cluster boundaries.

[1] A. Barkan, R. L. Merlino, and N. D'Angelo, Phys. Plasmas **2**, 3563 (1995).

[2] C. Thompson, A. Barkan, N. D'Angelo, and R. L. Merlino, Phys. Plasmas **4**, 2331 (1997).

[3] S. V. Ratynskaia, M. Kretschmer, S. A. Khrapak, R. A. Quinn, G. E. Morfill, M. H. Thoma, A. V. Zobnin, A. D. Usachev, O. Petrov, and V. E. Fortov, IEEE Trans. Plasma Sci. **32**, 613 (2004).

[4] T. Trottenberg, D. Block, and A. Piel, Phys. Plasmas **13**, 042105 (2006).

[5] E. Thomas Jr., Phys. Plasmas **13**, 042107 (2006).

[6] J. D. Williams, E. Thomas Jr., and L. Marcus, Phys. Plasmas **15**, 043704 (2008).

[7] E. Thomas Jr., Phys. Plasmas **17**, 043701 (2010).

[8] J. B. Pieper and J. Goree, Phys. Rev. Lett. **77**, 3137 (1996).

[9] L.-W. Teng, M.-C. Chang, Y.-P. Tseng, and L. I, Phys. Rev. Lett. **103**, 245005 (2009).

[10] A. Piel, M. Klindworth, O. Arp, A. Melzer, and M. Wolter, Phys. Rev. Lett. **97**, 205009 (2006); **99**, 209903(E) (2007).

[11] A. Piel, O. Arp, M. Klindworth, and A. Melzer, Phys. Rev. E **77**, 026407 (2008).

[12] S. A. Khrapak, D. Samsonov, G. E. Morfill, H. Thomas, V. Yaroshenko, H. Rothermel, V. Fortov, A. Nefedov, V. Molotkov, O. Petrov, A. Lipaev, A. Ivanov, and Y. M. Baturin, Phys. Plasmas **10**, 1 (2003).

[13] V. V. Yaroshenko, B. M. Annaratone, S. A. Khrapak, H. M. Thomas, G. E. Morfill, V. E. Fortov, A. M. Lipaev, V. I. Molotkov, O. F. Petrov, A. I. Ivanov, and M. V. Turin, Phys. Rev. E **69**, 066401 (2004).

[14] M. Rosenberg, J. Vac. Sci. Technol. A **14**, 631 (1996).

[15] P. K. Shukla, Phys. Plasmas **10**, 1619 (2003).

[16] M. Schwabe, M. Rubin-Zuzic, S. Zhdanov, H. M. Thomas, and G. E. Morfill, Phys. Rev. Lett. **99**, 095002 (2007).

[17] M. Schwabe, S. K. Zhdanov, H. M. Thomas, A. V. Ivlev, M. Rubin-Zuzic, G. E. Morfill, V. I. Molotkov, A. M. Lipaev, V. E. Fortov, and T. Reiter, New J. Phys. **10**, 033037 (2008).

[18] J. Heinrich, S.-H. Kim, and R. L. Merlino, Phys. Rev. Lett. **103**, 115002 (2009).

[19] O. Arp, D. Caliebe, K. Menzel, A. Piel, and J. Goree, IEEE Trans. Plasma Sci. **38**, 842 (2010).

[20] N. N. Rao, P. K. Shukla, and M. Y. Yu, Planet. Space Sci. **38**, 543 (1990).

[21] P. Kaw and R. Singh, Phys. Rev. Lett. **79**, 423 (1997).

[22] S. V. Singh and N. N. Rao, Phys. Plasmas **5**, 94 (1998).

[23] V. E. Fortov, A. G. Khrapak, S. A. Khrapak, V. I. Molotkov, A. P. Nefedov, O. F. Petrov, and V. M. Torchinsky, Phys. Plasmas **7**, 1374 (2000).

[24] A. Zobnin, A. Usachev, O. Petrov, and V. Fortov, J. Exp. Theor. Phys. **95**, 429 (2002).

[25] S. A. Khrapak and V. V. Yaroshenko, Phys. Plasmas **10**, 4616 (2003).

[26] I. Pilch, T. Reichstein, and A. Piel, Phys. Plasmas **16**, 123709 (2009).

[27] K. O. Menzel, O. Arp, and A. Piel, Phys. Rev. Lett. **104**, 235002 (2010).

[28] M. Klindworth, O. Arp, and A. Piel, J. Phys. D **39**, 1095 (2006).

[29] G. E. Morfill, H. M. Thomas, U. Konopka, H. Rothermel, M. Zuzic, A. Ivlev, and J. Goree, Phys. Rev. Lett. **83**, 1598 (1999).

[30] M. Mikikian, L. Coudel, M. Cavarroc, Y. Tessier, and L. Boufendi, New J. Phys. **9**, 268 (2007).

[31] D. Gabor, J. Inst. Electr. Eng. **93**, 429 (1946).

[32] A. S. Pikovsky, M. Rosenblum, and J. Kurths, *Synchronization: A Universal Concept in Nonlinear Science* (Cambridge University Press, Cambridge, England, 2001).

[33] K. Menzel, O. Arp, D. Caliebe, and A. Piel, IEEE Trans. Plasma Sci. **38**, 838 (2010).

[34] J. F. Nye and M. V. Berry, Proc. R. Soc. London, Ser. A **336**, 165 (1974).

[35] A. La Porta and C. M. Surko, Phys. Rev. E **53**, 5916 (1996).

[36] M.-A. Bray and J. P. Wikswo, IEEE Trans. Biomed. Eng. **47**, 1086 (2002).

[37] F. S. Roux, Opt. Commun. **268**, 15 (2006).

[38] D. Samsonov, J. Goree, H. M. Thomas, and G. E. Morfill, Phys. Rev. E **61**, 5557 (2000).

[39] Y. Feng, J. Goree, and B. Liu, Rev. Sci. Instrum. **78**, 053704 (2007).

[40] A. La Porta and C. M. Surko, Phys. Rev. Lett. **77**, 2678 (1996).

[41] K. E. Daniels and E. Bodenschatz, Chaos **13**, 55 (2003).

[42] A. La Porta and C. M. Surko, Physica D **139**, 177 (2000).

[43] M. R. Dennis, New J. Phys. **5**, 134 (2003).

[44] T. E. Vadivasova, G. I. Strelkova, and V. S. Anishchenko, Phys. Rev. E **63**, 036225 (2001).

[45] N. E. Diamant and A. Bortoff, Am. J. Physiol.**216**, 301 (1969).

[46] B. R. Noack, F. Ohle, H. Eckelmann, J. Fluid Mech. **227**, 293 (1991).

[47] G. V. Osipov, A. S. Pikovsky, M. G. Rosenblum, and J. Kurths, Phys. Rev. E **55**, 2353 (1997).

[48] G. V. Osipov and M. M. Sushchik, Phys. Rev. E **58**, 7198 (1998).

[49] O. I. Kanakov, G. V. Osipov, C.-K. Chan, and J. Kurths, Chaos **17**, 015111 (2007).

[50] A. K. Kryukov, G. V. Osipov, A. V. Polovinkin, and J. Kurths, Phys. Rev. E **79**, 046209 (2009).

[51] P. C. Bressloff and S. Coombes, Phys. Rev. Lett. **80**, 4815 (1998).

[52] M. E. Koepke and D. M. Hartley, Phys. Rev. A **44**, 6877 (1991).

[53] V. Nosenko, J. Goree, and A. Piel, Phys. Rev. Lett. **97**, 115001 (2006).

[54] T. Klinger, A. Piel, F. Seddighi, and C. Wilke, Phys. Lett. A **182**, 312 (1993).

[55] M. E. Koepke, T. Klinger, F. Seddighi, and A. Piel, Phys. Plasmas **3**, 4421 (1996).

[56] H. Klostermann, A. Rohde, and A. Piel, Phys. Plasmas **4**, 2406 (1997).

[57] D. Block, A. Piel, C. Schröder, and T. Klinger, Phys. Rev. E **63**, 056401 (2001).

List of Publications

Publications in Peer-Reviewed Journals

<u>Part of this thesis</u>

[B.1] K. O. Menzel, O. Arp, D. Caliebe, and A. Piel.
The Structure of Self-Excited Dust-Density Waves Under Microgravity.
IEEE Trans. Plasma Sci. **38**, 838 (2010).

[B.2] K. O. Menzel, O. Arp, and A. Piel.
Spatial Frequency Clustering in Nonlinear Dust-Density Waves.
Phys. Rev. Lett. **104**, 235002 (2010).

[B.3] K. O. Menzel, O. Arp, and A. Piel.
Frequency clusters and defect structures in nonlinear dust-density waves under microgravity conditions.
Phys. Rev. E **83**, 016402 (2011).

<u>Further Publications</u>

1. O. Arp, D. Caliebe, K. O. Menzel, A. Piel, and J. A. Goree.
Experimental Investigation of Dust Density Waves and Plasma Glow.
IEEE Trans. Plasma Sci. **38**, 842 (2010).

Selected Contributions to International Conferences:

1. O. Arp, K. Menzel, and A. Piel.
Three-dimensional structure of self-excited dust density waves under microgravity conditions.
AIP Conference Proceedings **1041**, 159 (2008).

2. O. Arp, K. O. Menzel, A. Piel.
Frequency clustering in self-excited dust density waves under microgravity conditions.
Europhysics Conference Abstracts, O-3.310 (2010).

Danksagung

An erster Stelle gilt mein Dank Herrn Prof. Dr. Alexander Piel für die Möglichkeit in seiner Arbeitsgruppe zu promovieren. Insbesondere hat er mich in zahlreichen Diskussionen ermutigt, etablierte Denkweisen zu hinterfragen und andere Forschungszweige für meine Arbeit zu berücksichtigen.

Dr. Oliver Arp danke ich für seine Unterstützung während dieser Arbeit. Was ich in den letzten Jahren alles von Oliver gelernt habe, lässt sich hier nicht im Detail aufführen. Neben wesentlichen wissenschaftlichen Grundlagen gehören dazu unzählige Tipps für die Arbeit im Labor und am PC. Und auch wenn wir so manchen Kampf beim Verfassen von Artikeln ausgefochten haben, sind wir letztlich doch immer auf einen gemeinsamen Nenner gekommen.

Weiterhin möchte ich mich bei David Caliebe bedanken. Wer hätte schon vor eineinhalb Jahrzehnten gedacht, dass wir nach unserer gemeinsamen Schulzeit auch noch eine Wohnung und später ein Büro miteinander teilen würden. In all den Jahren konnte ich mich stets auf Davids freundschaftlichen Rat verlassen. Außerdem könnte ich ohne seine Hilfe wohl bis heute nicht programmieren.

Für die zahlreichen spannenden und teils amüsanten Diskussionen rund um die Welle als solche und die Staubdichtewelle im Besonderen danke ich Dr. Iris Pilch. Außerdem danke ich Dr. Franko Greiner und Dr. Dietmar Block, deren Türen immer für mich offen standen. Bei Tim Bockwoldt bedanke ich mich für die gemeinsame Forschung an den Staubdichtewellen im Labor und unter Schwerelosigkeit und außerdem für Tipps und Anmerkungen zu dieser Arbeit. Michael Poser danke ich natürlich für die tatkräftige Hilfe rund ums Parabelflugprojekt. Aber neben diesem dienstlichen Teil freue ich mich darüber, dass wir in den letzten Jahren so häufig Zeit für einen gemeinsamen Kaffee am frühen Morgen gefunden haben, bei dem man sich auch mal über private Dinge austauschen konnte. Volker Rohwer und Mario Knüppel danke ich für ihre Hilfe in allen technischen Belangen. Philipp Freese, Sonja Lepper, Christian Schmidt und Jochen Wilms sei für die Zeit gedankt, die sie im Rahmen ihrer Hilfstätigkeit in das Projekt gesteckt haben. Bei den Mitgliedern der AG Plasmadynamik bedanke ich mich für die schöne Arbeitsatmosphäre, die ich trotz allzu vieler verlorener Kuchenwetten stets genossen habe. Herrn Hohmann danke ich für seine teils sehr zeitintensive Literaturrecherche, die ich so häufig in Anspruch genommen habe. Frau Thiedemann, Frau Seeger und Frau Sommer danke ich für die Überwindung aller bürokratischer Hürden, von denen es nicht wenige gab. Für die gute Zusammenarbeit und die angenehme abendliche Unterhaltung auf den Kampagnen danke ich den Mitgliedern der AG Melzer in Greifswald. Marc Schmenner danke ich für die Durchsicht dieser Arbeit und den Feinschliff an meinem Englisch.

Meinen Eltern möchte ich dafür danken, dass sie mich in letzten 29 Jahren ausnahmslos, bei allem was ich gemacht habe und egal welche Entscheidung ich getroffen habe, unterstützt haben.

Meinen Schwiegereltern danke ich für ihre Hilfe, zu welcher Tag- oder Nachtzeit ich sie auch benötigt habe.

Ganz besonders danke ich Euch, Tine und Jonte. Dass Ihr mir in den letzten Monaten jeden Tag den Rücken freigehalten habt, ist für mich schon Hilfe genug gewesen. Aber Ihr habt es zudem immer wieder geschafft, mich zu motivieren und aufzubauen, wenn es mal wieder nicht so lief. Mit Eurer Liebe konntet Ihr mich immer wieder aufs Neue in eine ganz andere Welt entführen.

Lebenslauf

Persönliche Daten

Name:	Kristoffer Ole Menzel
Geburtsdatum:	29.01.1982
Geburtsort:	Kiel
Staatsangehörigkeit:	deutsch
Familienstand:	verheiratet, ein Sohn

Schulbildung

1988 - 1992	Hardenberg Grundschule in Kiel
1992 - 2001	Gymnasium Hebbelschule in Kiel
Juni 2001	Abitur mit den Prüfungsfächern Mathematik, Physik, Deutsch und Geschichte

Studium

Okt. 2002	Immatrikulation im Fach Physik an der Christian-Albrechts-Universität zu Kiel
Okt. 2004	Vordiplom mit Nebenfach Chemie
Juli - Aug. 2005	DESY Summer Student Programme
Nov. 2006	Abschluss der mündlichen Diplomprüfungen (Nebenfach Astrophysik)
Dez. 2006 - Dez. 2007	Anfertigung der Diplomarbeit "Lasermanipulation und Staubdichtewellen in einem komplexen Plasma" in der Arbeitsgruppe "Plasmadynamik" am Institut für Experimentelle und Angewandte Physik der Christian-Albrechts-Universität zu Kiel
Jan. 2008	Beendigung des Studiums der Physik mit Abschluss Diplom
seit März 2008	Promotion in der Arbeitsgruppe "Plasmadynamik" am Institut für Experimentelle und Angewandte Physik der Christian-Albrechts-Universität zu Kiel

Eidesstattliche Erklärung

Hiermit versichere ich an Eides Statt, dass die vorliegende Dissertation - abgesehen von der Beratung durch meinen wissenschaftlichen Lehrer und der Verwendung der angegebenen Hilfsmittel - nach Inhalt und Form meine eigene ist. Sie hat weder ganz noch teilweise an einer anderen Stelle im Rahmen eines Prüfungsverfahrens vorgelegen.

Kiel, den